CODIGEM

CORPORACIÓN DE DESARROLLO E INVESTIGACIÓN GEOLÓGICO-MINERO-METALÚRGICA

MINISTERIO DE ENERGÍA Y MINAS

DFID

DEPARTMENT FOR INTERNATIONAL DEVELOPMENT

BGS 1835

BRITISH GEOLOGICAL SURVEY

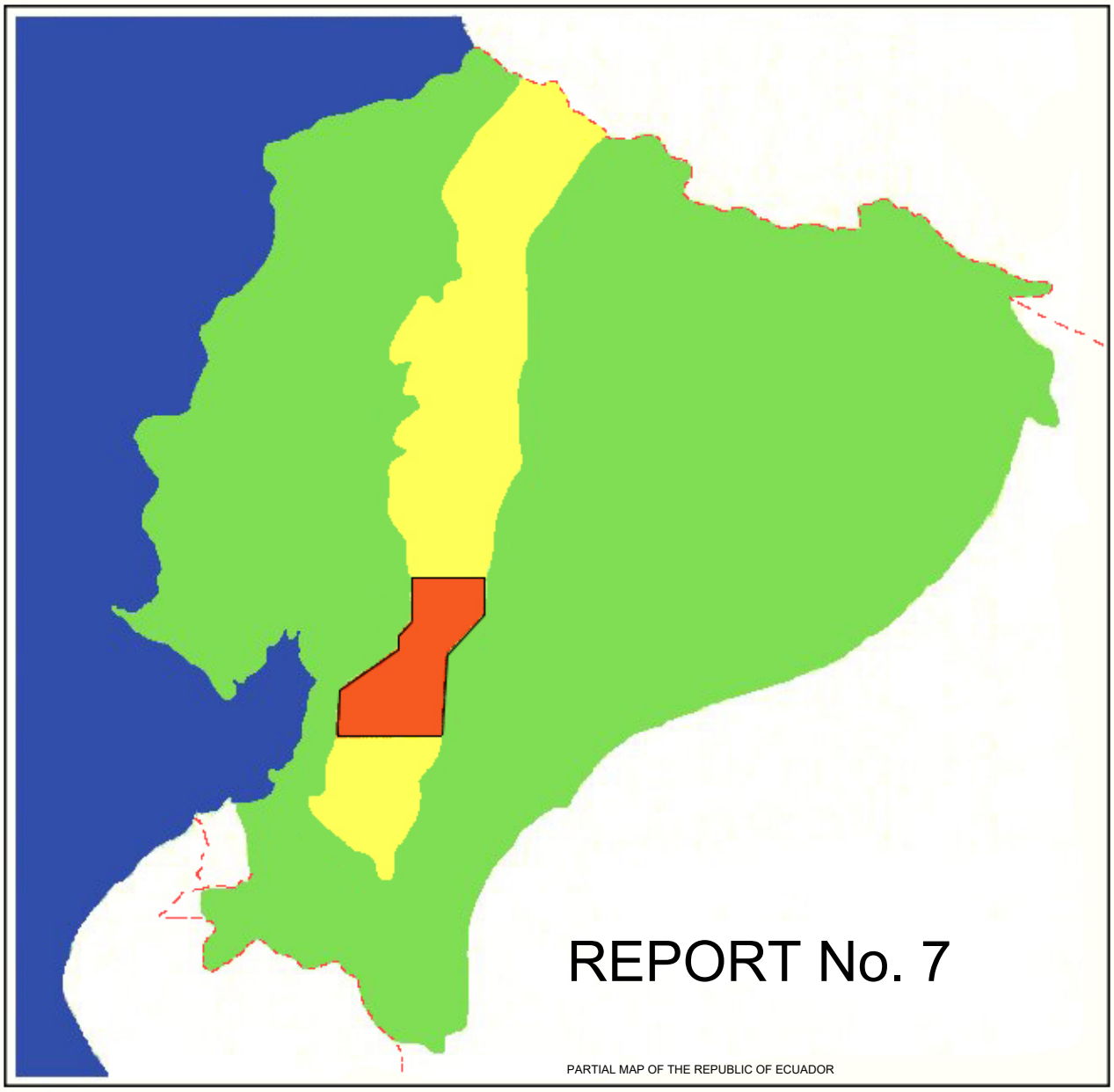

REPORT No. 7

PARTIAL MAP OF THE REPUBLIC OF ECUADOR

WORLD BANK MINING DEVELOPMENT AND ENVIRONMENTAL CONTROL PROJECT

GEOLOGICAL INFORMATION MAPPING PROGRAMME (WESTERN CORDILLERA)

PATRI MATRIQUE

CODIGEM

BGS 1835

MINING DEVELOPMENT AND ENVIRONMENTAL CONTROL PROJECT

GEOLOGICAL INFORMATION MAPPING PROGRAMME

Report Number 7

GEOCHEMICAL RECONNAISSANCE SURVEY OF THE WESTERN CORDILLERA OF ECUADOR BETWEEN 2°00' AND 3°00'S

T. M. Williams

A. Gaibor

P. N. Dunkley

CODIGEM-BRITISH GEOLOGICAL SURVEY

Quito-Ecuador

1997

Stalyn Paucar

2024 edition

GIMP GEOCHEMICAL SURVEY PROGRAMME
PARTICIPATING STAFF

Principal geochemists
Dr. T. M. Williams
Dr. P. N. Dunkley

British mission manager
Dr. J. A. Aspden

CODIGEM
Ing. A. Gaibor
Mr. E. Cruz
Arq. V. Acitimbay

FIELD OPERATIONS

Group supervisor	**Group supervisor**	**Group supervisor**
Ing. N. Báez	Ing. J. Bolaños	Ing. E. López
Samplers	**Samplers**	**Samplers**
R. Brito	J. Galarza	W. Castillo
H. Durazno	L. Saltos	M. Cruz
J. Galarza	R. Toco	E. Hinojosa
F. Núñez		E. Romero
H. Núñez		R. Rosales
J. Segovia		J. Solis

Reference

Williams, T., Gaibor, A. & Dunkley, P. (1997). *Geochemical Reconnaissance of the Western Cordillera of Ecuador between 2°00' and 3°00'S* (Stalyn Paucar, Ed., 2024). Report Number 7. Geological Information Mapping Programme. BGS-CODIGEM/MEM.

CONTENTS

FIGURES

TABLES

APPENDICES

1. INTRODUCTION

1.1. Background and objectives

The Geological Information Mapping Programme (GIMP) of the Misión Geológica Británica incorporates sub-components 3.3 and 3.4 of a wider Mining Development and Environmental Control Project (PRODEMINCA) initiated in Ecuador in 1995 under funding from the World Bank and the governments of the UK (through the Department for International Development), Sweden and Ecuador. The central aim of the GIMP is the provision of Geological maps and thematic geoscientific data for the Western Cordillera of Ecuador for subsequent use by the Ecuadorian Corporación de Desarrollo e Investigación Geológico-Minero-Metalúrgica (CODIGEM) in the promotion of sustainable investment in the metalliferous minerals sector.

The GIMP geological and thematic survey encompasses a 36000 km^2 area of the Western Cordillera between latitudes 1°N and 4°S. This zone, corresponding to approximately 40% of the (metalliferous) mineral prospective terrain of Ecuador, has been subdivided under the GIMP into five discrete 1:200000 scale map units (Fig. 1) each corresponding to one degree of latitude. All geological, geochemical and related thematic data for these areas are to be held by CODIGEM in an Oracle database and Microstation GIS environment, facilitating integrated data interrogation or publication at any desired scale. In accordance with the terms of sub-components 3.3. and 3.4 of the PRODEMINCA, a schedule of data release has been agreed by the Misión Geológica Británica and CODIGEM commencing with the 2°-3°S and 3°-4°S quadrangles in 1998.

1.2 Function

This report summarises the methodology and results of a drainage geochemical reconnaissance survey of the Western Cordillera between 2°S and 3°S, sampling of which was undertaken during the period May-December 1996. The area corresponds exactly to that of the 2°-3°S sheet of the GIMP 1:200000 geological map series, upon which all lithogeochemical normalization and anomaly validation have been based.

The data described in this report have been compiled for release in 1.44 MB diskette and CD-ROM digital formats in accordance with the requirement of prospective users (primarily exploration companies) to undertake independent data interpretation using a wide range of software applications. The function of this document is therefore solely to provide a data overview with reference to mineral exploration and broader environmental applications.

2. AREA OF COVERAGE

2.1 Physiography

The GIMP 1:200000 2°-3°S area encompasses a NE-trending tract of the Western Cordillera with a south-western extremity of 0642-9669 and a north-eastern extremity of 0750-9780 (UTM-SAD69 coordinates). The approximate area of coverage is 6300 km^2.

The regional physiography is dominated by high páramo terrain exceeding 3400 m. Cerro de Cajas, the highest peak, has an altitude of 4550 m. Sub-radial drainage in the central sector of the study area feeds the systems of the Río Paute to the south-east and the Río Chaucha to the west (Fig. 1).

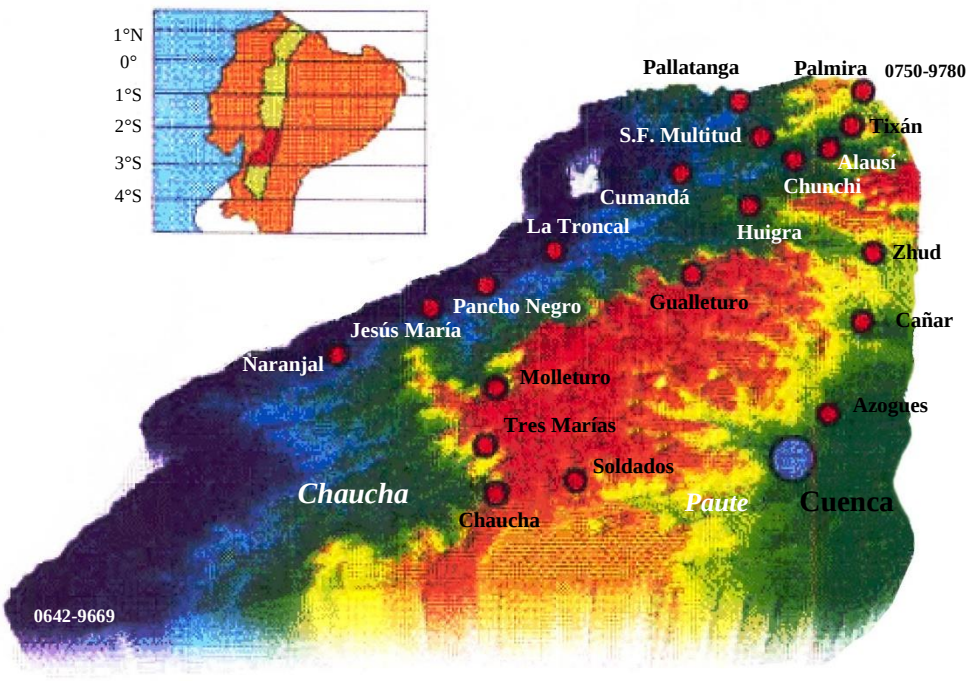

Figure 1. Physiography of the GIMP 2°-3°S area and regional position within the GIMP zone of coverage

Climatic information for four stations within, or marginal to, the zone of coverage is summarised in Table 1. The Cañar-Alausí sector is cool, with temperatures rarely exceeding 15°C. To the west of the Cordillera the foothills and coastal plains (Naranjal) are warm and humid, with a median temperature of ca. 25° C. Annual precipitation levels within and to the west of the Cordillera lie within the range of 1000-1200 mm.

Table 1. Climatic data for four stations within the Cuenca region

Station	Ave. Temp (°C)	Max. Temp (°C)	Rainfall (mm)
El Labrado	8.7	15.1	1193
Manuel Calle	24.5	32.5	1354
Naranjal	25.0	33.4	1092
San Carlos	24.7	32.8	1141

Human settlement and economic activity are dominated by Cuenca, Ecuador's third city, with a population in excess of 250000. Most other significant settlements are located along the Panamerican Highway which extends northward through the provincial centres of Cañar and Alausí. The principal east-west routes are the Cañar-La Troncal road to the western foothills of the Cordillera, the Cuenca-Molleturo road, and eastward routes from Azogues.

2.2 Geological setting

Geological mapping of GIMP 1:200000 2°-3°S area was undertaken by Misión Geológica Británica and CODIGEM staff during the period November 1995-August 1997. A synopsis of the geology, based on the sheet description of Dunkley and Gaibor (1997b), is provided below. Figures 2-3 outline the principal lithological units and their lithostratigraphic relations.

The geological evolution and tectonostratigraphy of the region have been summarised by Dunkley and Gaibor (1997b). Metamorphic rocks of pre-Cretaceous age form a basement onto which ocean floor basalts of the Pallatanga Unit were accreted during the Late Cretaceous. Turbiditic sediments of the Yunguilla Unit were deposited at least in part upon the accreted Pallatanga Unit during the Maastrichtian and show some evidence of derivation from a metamorphic source area. In the Early Tertiary, the ensimatic island arc terrain of the Macuchi Unit developed to the west, and siliciclastic basin-fill sequences of the Angamarca Group were deposited in a marginal sea between the arc and the continental margin. In the Late Eocene the arc terrane was accreted obliquely onto the continental margin and translocated northward. The two major accretionary events described are tectonically delineated within the mapped area by the Bulubulu and Chimbo-Cañi faults respectively.

Subduction-related continental margin calc-alkaline volcanism of the Saraguro Group commenced in the uppermost Middle Eocene and continued until the Miocene, generating extensive volcanic units of intermediate to acid composition which now dominate the central and eastern sectors of the region. The intercalation of acid ash-flow tuffs of latest Middle Eocene age within the turbiditic sediments of the Angamarca Group implies that this continental margin volcanic activity commenced shortly before the final docking of the Macuchi Arc (Dunkley and Gaibor, 1997b). In the Early Miocene E-W tension resulted in the formation of inter-montane basins (including the Cuenca Basin) within which fluvio-marine sediments were deposited. Late Miocene andesite lavas were erupted from the Quimsacocha stratovolcano immediately to the south of the 3°S line (the southern limit of the mapped area).

During the Quaternary the higher terrain in the central-southern sector of the area was glaciated. In the north, Pleistocene to recent volcanic ashes blanket the terrain. In the extreme northeast (between Tixán and Palmira) pumiceous deposits, ashes and diatomites were deposited in a fluvio-lacustrine basin.

2.2.1 Metamorphic basement

Pre-Cretaceous basement metamorphic rocks of the Western Cordillera outcrop over a strike-length of 40 km in a north-east trending belt which is bounded to the north-west by the Bulubulu Fault. Smaller outcrops occur in the north-east around Guasuntos, and as a series of inliers delineated by north-east trending structures within the Chaucha Batholith. The lithologies are predominantly metasedimentary phyllites and schists with interbedded psammites and conglomerates, although gneissic rocks of probable igneous origin occur locally. The metamorphic grade is generally low, but in some places garnet, sillimanite and andalusite have been recognized.

2.2.2 Pallatanga Unit

Fine-grained massive and pillowed basaltic lavas of the Pallatanga Unit form a virtually continuous NNE-trending belt along the western foothills of the region. To the south-east they are faulted against the metamorphic basement and volcanic rocks of the Saraguro Group along the Bulubulu Fault. Along the northwestern margin the basalts are bounded by the Multitud Fault. Zones of intense shearing occur and in places the basalts are tectonically interleaved with bounding lithological units. The basalts are tholeiitic in composition and have trace element characteristics very similar to ocean floor basalts. The age of the Pallatanga Unit is uncertain, but a tentative correlation with the Piñón Formation of the coast implies a Mid-Cretaceous origin.

2.2.3 Yunguilla Unit

The marine turbidite fan sequence of the Yunguilla Unit outcrops in the far north of the area and in the south-west. In both areas it is faulted against and tectonically interleaved with the Pallatanga Unit. Lithologies comprise dark grey, thin-bedded mudstones, siltstones and fine sandstones. The latter contains strained quartz and some detrital muscovite, possibly indicating a metamorphic source. Palaeontological age determinations for the Yunguilla Unit indicate a Maastrichtian age.

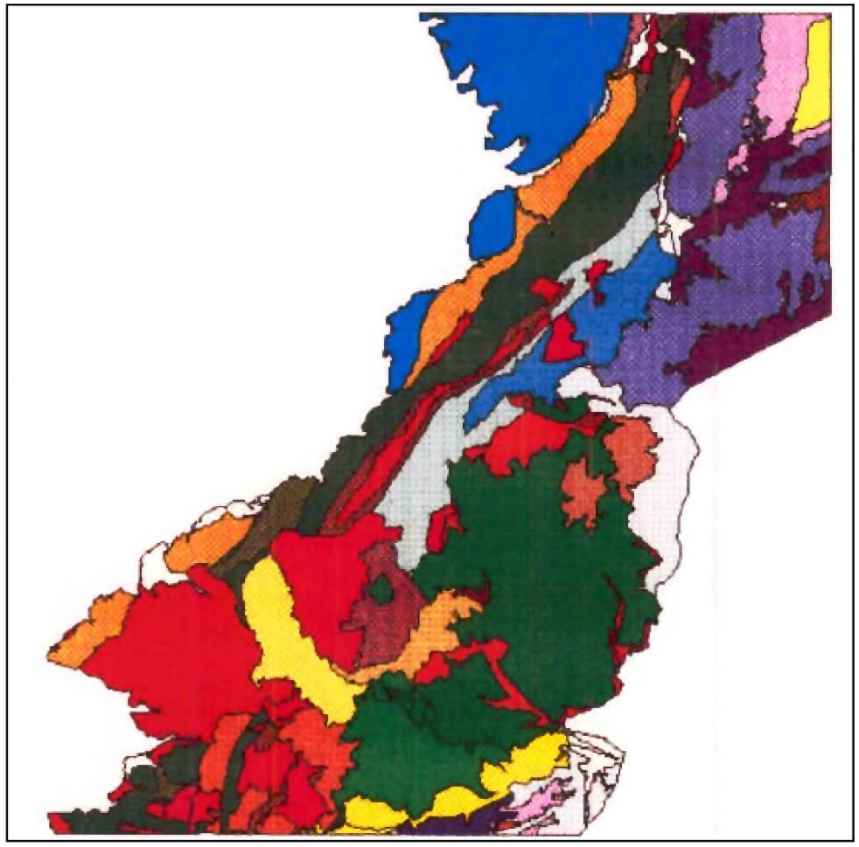

Figure 2. Simplified lithological outline of the Western Cordillera between 2°-3°S (after Dunkley and Gaibor, 1997b)

Note: Uncoded polygons = landslip or Quaternary cover

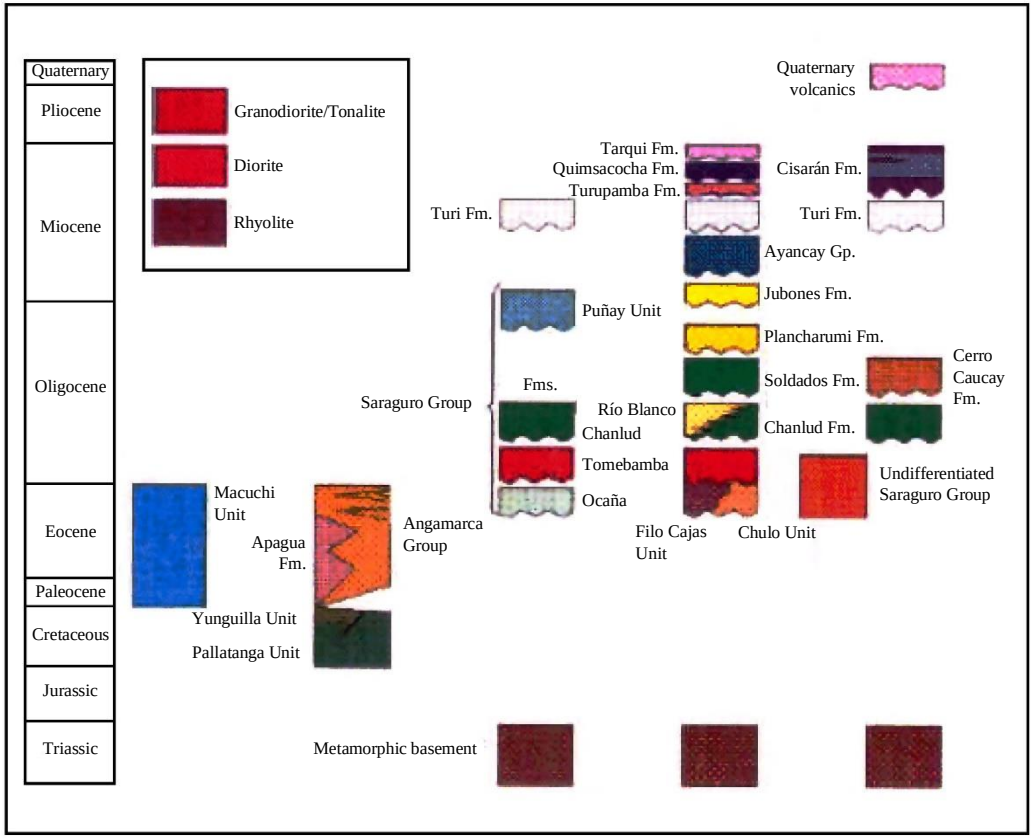

Figure 3. Simplified lithostratigraphy of the Western Cordillera between 2°-3°S (after Dunkley and Gaibor, 1997b)

Note: The position of intrusive rocks has no chronological significance

2.2.4 Macuchi Unit

The Macuchi Unit outcrops extensively in the north-west of the area in a number of blocks faulted to the east against the Angamarca Group. It consists predominantly of subaqueous basaltic and andesitic volcaniclastic rocks with some lavas and fine-grained high-level intrusions. The dominant lithologies are volcanic sandstones, basaltic tuffs and hyaloclastites. Pillow lavas and pillow breccias also occur. The rocks show extensive evidence of reworking and emplacement by mass-flow processes. Many of the sandstones were deposited by turbidity currents. Chemical analyses of lavas within the unit to the north of the study area indicate basaltic and andesitic compositions of tholeiitic to calc-alkaline affinity with island-arc trace-element characteristics. Egüez (1986) has reported Early to Middle Eocene radiolaria and Early Eocene foraminifera from the type area at Macuchi, in addition to two K-Ar ages of 41.6 ± 2.1 Ma and 35.8 ± 1.8 Ma.

2.2.5 Angamarca Group

The siliciclastic basin-fill sequence of the Angamarca Group, broadly contemporaneous with the Macuchi Unit, outcrops as a sequence of thin to medium-bedded turbiditic sandstones, siltstones and mudstones along a fault-bounded tract, approximately 50 km in strike-length, between the Macuchi and Pallatanga units in the north-west of the area. A differentiated Formation within the group, the Apagua Formation, forms an additional outcrop abutting the Macuchi Unit close to the 2°S line. Intercalations of primary and secondary dacitic tuffs occur within the turbiditic sandstones and siltstones. A fission track age of 37.8 ± 3.5 Ma was obtained from a dacitic ash-flow tuff intercalated within turbiditic sediments at Guamampata.

2.2.6 Saraguro Group

The Saraguro Group is the most expansive Geological unit of the area, occupying the high ground south of the Río Cañar and extending as far north as Huigra. It has been defined by Dunkley and Gaibor (1997b) as a sequence of intermediate to acid calc-alkaline subaerial volcanic rocks of late Middle Eocene to Early Miocene age. The group rests unconformably upon, or is faulted against, the Pallatanga Unit and metamorphic basement rocks. Andesitic and dacitic compositions predominate but rhyolitic rocks are also common and basaltic andesite compositions are present in very minor amounts. Eleven discrete lithological units have been mapped by Dunkley and Gaibor (1997b) spanning the Mid-Eocene to Early Miocene:

2.2.6.1 The Ocaña Formation is the oldest recognised unit of the Saraguro Group. Its outcrop forms a northeast-trending belt which is bounded in part to the north-west by the Bulubulu Fault. It consists mainly of massive, welded dacitic ash-flow tuffs with minor amounts of breccia and reworked volcaniclastic sediment. The unit is of upper Middle to Late Eocene age. Fission track ages of 37 ± 1.5 Ma and 38.6 ± 1.3 Ma are reported by Dunkley and Gaibor (1997b), while Egüez et al. (1992) report a K-Ar age of 35.9 ± 0.9 Ma for rocks near Huigra which have subsequently been included in the Formation.

2.2.6.2 The Chulo Unit outcrops in the Cajas area to the south-east of Molleturo. Its stratigraphy and structure are poorly understood. It consists of a diverse sequence of rhyodacitic and rhyolitic tuffs, breccias, sediments and rhyolites. The unit outcrops in the core of a broadly domal structure. To the west it is overlain by the Filo Cajas Unit and, to the north, east and south by the Tomebamba Tuffs and the Chanlud Formation. The age of the unit is uncertain, but it has been assigned a Late Eocene age on the basis of field relations with overlying units.

2.2.6.3 The Filo Cajas Unit forms the prominent escarpment of Filo Cajas. Dacitic lavas outcrop at the base of the escarpment and are overlain by a dark green-grey welded crystal-rich dacitic ash-flow tuff more than 100 metres thick which forms the columnar jointed summit of the ridge and outcrops throughout the area of Lagunas Playas Encantadas. The tuff contains abundant quartz crystals and numerous large blocks of andesite and dacite lava which in places account for up to 50% of the rock. This distinctive tuff is overlain by a well-stratified sequence of flaggy dacitic and rhyolitic tuffs. The age of the unit is uncertain. It unconformably overlies the Chulo Unit and is overlain by lavas and intruded by dykes of the Chanlud Formation. It is therefore assumed to be of Late Eocene or Early Oligocene age.

2.2.6.4 The Tomebamba Unit consists of ash-flow tuffs of intermediate composition. They occur in the southeastern part of Cajas in the Tomebamba valley, and around Gualleturo on the south side of the Cañar valley. In both areas they consist mainly of pale to mid-green massive lithic-lapilli ash-flow tuffs of high-silica andesite to low-silica dacite composition. They contain crystals of feldspar and amphibole which are usually chloritised. Unlike other pyroclastic units within the Saraguro Group, quartz crystals are uncommon or absent. Welding and eutaxitic fabrics are common. The Tomebamba Unit rests on older acid volcanic rocks of the Ocaña Formation and the Chulo Unit, and is overlain by andesite lavas of the Chanlud Formation. A zircon fission-track age of 34.1 ± 1.3 Ma is reported by Dunkley and Gaibor (1997b) from a tuff near the base of the unit in the Cajas area.

2.2.6.5 The Chanlud Formation crops out over an area of about 1200 km^2 in the high ground north and west of Cuenca and reaches a thickness of 1000 m. Subhorizontal to gently dipping andesitic lavas with associated breccias and minor intercalations of arenaceous volcanic sediments and tuffs predominate. Andesite dykes, mostly trending ESE, are common and acted as feeders to the lavas. While predominantly andesitic in composition, the uppermost flows are dacitic or rhyodacitic at a number of localities, and some of the dykes are basaltic. The Chanlud Formation rests unconformably on folded and tilted rocks of the Ocaña Formation, the Chulo, Filo Cajas and Tomebamba units. It is overlain unconformably by the Soldados and Cerro Caucay Formations. An early Oligocene age is assigned to the formation by inference with the age of overlying and underlying units.

2.2.6.6 The Río Blanco Formation outcrops in a broad NW-striking ridge extending southeast and northwest of Molleturo. It consists mainly of strongly feldspathic hypersthene- and hornblende-bearing andesitic lavas, ash-flow tuffs and breccias with intercalations of arenaceous volcaniclastic sediments, intruded throughout by small bodies of fine-grained meladiorite. Although andesitic compositions predominate, some tuffs are dacitic. At least part of the Formation was deposited subaqueously. Near Río Blanco the Formation overlies folded rocks of the Chulo Unit with angular unconformity. To the west of Hierba Buena it rests unconformably on highly sheared basalts of the Pallatanga Unit. At the eastern end of the outcrop the Formation is overlain by the Soldados Formation. By inference the Río Blanco Formation is assigned an early Oligocene age.

2.2.6.7 The Cerro Caucay Formation outcrops on the high ground west of Cañar and in small outliers as far southwest as Laguna Machángara. It consists of rhyolitic ash-flow tuffs up to 450 m thick, resting unconformably upon lavas of the Chanlud Formation. The tuffs display well-preserved vitroclastic textures and contain abundant crystals of feldspar, biotite, amphibole and quartz. Eutaxitic textures occur throughout and ultra-welded zones show evidence of rheomorphism in the form of flow-folding. The tuffs are glassy or finely recrystallised, and in a number of places strongly welded zones are preserved as original obsidian. Two zircon fission-track dates of 30.2 ± 1.1 and 27 ± 1.0 have been reported by Dunkley and Gaibor (1997b).

2.2.6.8 The Soldados Formation consists of subhorizontal to gently dipping crystal-rich dacitic ash-flow tuffs which outcrop in the central southern part of the mapped area. Northeast of Soldados it rests unconformably upon lavas of the Chanlud Formation. In the west it overlies the Río Blanco Formation. Immediately south of Soldados it is overlain unconformably by the Plancharumi Formation. The Formation reaches a thickness of more than 300 metres around Soldados, consisting of three massive, columnar jointed ash-flow tuff units overlain by several thinner units. The tuffs contain abundant feldspars and rounded quartz crystals, lesser amounts of amphibole, and at a few localities traces of biotite. A characteristic feature is the ubiquitous presence of abundant green chloritic lapilli with diffuse margins, interpreted to have been poorly vesicular magmatic clots within the original pyroclastic flows. The Formation is of Late Oligocene age. Rivera et al. (1992) report two biotite K/Ar ages of 26 ± 0.8 Ma and 27 ± 0.7 Ma from tuffs near Soldados. A zircon fission track age of 29.8 ± 1.2 Ma has also been obtained (Dunkley and Gaibor, 1997b).

2.2.6.9 The Plancharumi Formation consists of a fluvio-lacustrine sequence of poorly lithified rhyolitic volcaniclastic deposits, sediments and lavas which outcrop along the southern margin of the area around Soldados and extend westwards to Pimo. It rests unconformably upon the Soldados Formation. The Formation is characterised by pyroclastic flow deposits that are very rich in pumice lapilli and by well-bedded fine-grained primary air-fall tuffs with accretionary lapilli. Rhyolitic lavas are intercalated with the volcaniclastic rocks in the west, and rhyolitic breccias of autoclastic and mass-flow origin occur throughout the Formation. A zircon fission-track date of 25.7 ± 1.1 Ma has been obtained from a primary air-fall tuff (Dunkley and Gaibor, 1997b).

2.2.6.10 The Puñay Unit crops out in a northeasterly trending belt in the central sector of the study area. It is composed mainly of amphibole-bearing andesitic lavas, breccias, sandstones and siltstones (including red beds). It rests upon, and is faulted against the Ocaña Formation to the north-west and the Chanlud Formation to the south. At Cerro Puñay it dips uniformly to the southwest at about 45° and has a thickness of ca. 3000 m. Farther east between Huigra and Chanchán the unit contains a higher proportion of sedimentary material and consists of steeply dipping volcanic sandstones, andesitic lithic tuffs, breccias, purple-red siltstones and subordinate lavas. The sandstones show Bouma sequences indicative of deposition from turbidity currents. Whole-rock and plagioclase K/Ar ages of 21.0 ± 1.0 Ma and 27 ± 0.9 Ma respectively are reported from this section (Egüez et al., 1992).

2.2.6.11 The Jubones Tuff Formation outcrops along the southern margin of the area in the high páramo. It rests with angular unconformity on the Plancharumi and Soldados Formations and is overlain with strong discordance by the Quimsacocha Formation. The Formation comprises a very thick welded rhyolitic ash-flow tuff with very abundant feldspar, quartz and biotite crystals. Pratt et al. (1997) report a K/Ar age of 22.76 ± 0.97 Ma.

2.2.7 Ayancay Group

The Ayancay Group of the Cuenca Basin extends northward from Cuenca towards Azogues and Cañar. The group comprises sediments of fluvial origin consisting predominantly of sandstones, green and red mudstones and siltstones, rare tuffs, coaliferous beds and conglomerates. The group rests unconformably on the Saraguro Group and is overlain by the Turi Formation. Deposition of the group began some time after 18 Ma and was completed at about 10 Ma.

2.2.8 Turi Formation

Sedimentary rocks of the Turi Formation are confined to the Cuenca Basin and its extensions, outcropping in the extreme east and southeast of the study area, and in the area between Cañar and Suscal. It consists principally of poorly lithified coarse conglomerates and breccio-conglomerates of andesitic composition intercalated with pale-coloured tuffaceous sandstones and tuffaceous siltstones. The Turi Formation rests unconformably upon the Saraguro Group and is overlain by the Quimsacocha Formation. It was previously considered to be of Pliocene age (Bristow and Parodiz, 1982), but more recent fission-track dates indicate a Late Miocene age of 8-9 Ma.

2.2.9 Turupamba Formation

The Turupamba Formation occurs in two very small areas in the extreme south of the study area. It consists of acid pumice-lapilli tuffs with quartz crystals and carbon fragments. It overlies the Turi Formation and appears to be post-dated by the Quimsacocha Formation.

2.2.10 Quimsacocha Formation

The Quimsacocha Formation outcrops along the southern margin of the study area, extending southward to the eroded volcanic edifice of Quimsacocha. It consists of andesite lavas and associated breccias which dip radially away from Quimsacocha. The rocks are dark green-grey and porphyritic with acicular microphenocrysts of amphibole. The Formation unconformably overlies the Saraguro Group and the Turi Formation. Its age is uncertain, but its contact relationships with the Turi and Tarqui Formations indicate a Late Miocene age.

2.2.11 Tarqui Formation

The Tarqui Formation is preserved only along the interfluves southwest of Cuenca. It consists of white and red kaolinized acid tuffs which mantle all older lithological units. It is equated with the Tambo Viejo Formation, of uppermost Miocene age (Hungerbühler and Steinmann, 1996). The Quimsacocha caldera may have acted as a source for some of the Tarqui Formation tuffs (Pérez, 1990).

2.2.12 Cisarán Formation

The Cisarán Formation outcrops over much of the north-eastern sector of the area. Between Zhud and Alausí it reaches a thickness of 2200 m, comprising stratified intermediate lavas and extremely coarse and poorly sorted volcaniclastic rocks. The basal part is dominated by andesitic and dacitic lavas which pass up into a thick sequence of coarse to very coarse, poorly sorted andesite breccias with intercalations of cream-coloured volcanic sandstones, tuffs and lavas. The sediments are capped by andesitic and dacitic lavas which form a series of high plateaus culminating in the summit of Cerro Cisarán. The Formation rests upon the Turi Formation. Fission track ages of 6.8 ± 0.8 Ma have been obtained from tuffaceous sediments low in the sequence, and of 6.9 ± 0.7 Ma from andesite lavas southeast of Pallatanga. A K/Ar date of 7.15 ± 0.38 Ma has also been obtained from a lava intercalated in the uppermost sediments near the summit of Cerro Cisarán.

2.2.13 Quaternary Deposits

Alluvium occurs in all river valleys and forms extensive expanses along the margins of the cordillera and in the Cuenca Basin. Large alluvial fans exist where the main rivers disgorge onto the coastal plain, and colluvial fans occur in mountainous areas prone to landslips. Alluvial terraces occur in some of the larger valleys, for example in the Chimbo Valley south of Pallatanga. Quaternary volcanic deposits mainly consist of ashes which mantle large areas in the northeast, extending as far south as the Huigra area. Young unconsolidated dacitic pumice-flow deposits (ignimbrites) are also preserved on the valley sides near Alausí. A sedimentary basin of relatively thick fluvio-lacustrine volcanic sediments occurs on either side of the PanAmerican highway extending north of Tixán as far as Palmira. These deposits were previously mapped as the Formación Palmira and consist of poorly consolidated pumiceous volcanic deposits, tuffs, sandstones and diatomites. Young lacustrine deposits including sands, conglomerates and fine tuffs occur near Chanchán where the valley appears to have previously been dammed by a large colluvial fan.

2.2.14 Intrusive rocks

The largest intrusion of the region is the Chaucha Batholith, exposed in the southwest around Chaucha, Naranjal and Carmen de Pijilí. It consists mainly of biotite-hornblende granodiorite and tonalite. Two K/Ar ages of 9.77 ± 0.29 Ma (Müller-Kahle and Damon, 1970) and 12 ± 0.6 Ma (Snelling, 1969) have been reported. Linear intrusions of biotite-hornblende granodioritic rocks occur along the contact between the Pallatanga Unit and the basement along a 40 km strike-length trending north-east from the Chaucha Batholith. Medium to coarse grained hornblende diorites, with little or no quartz, occur in a line to the southeast of the granodiorites, the largest of which outcrops around Molleturo and extends northwards to the Río Patul. Stocks and large sill-like intrusions of hornblende diorite occur in the north, one of which has yielded a K/Ar date of 7.59 ± 0.35 Ma. High-level intrusive rhyolite domes and sills are common throughout the crop of the Saraguro Group. A group of such domes occurs around Laguna Totoras and several others are present in the Cañar Valley. Large meladiorite sills and andesite dykes intrude the Chanlud Formation, with which they were broadly coeval, and fine-grained meladiorites intrude the Río Blanco Formation with which they were also probably comagmatic.

2.2.15 Structure

Faults dominate the structure of the area. Regional trends are predominantly NE-SW to NNE-SSW, although in the south of the area NW-SE and to a lesser extent E-W trends are evident. An important NE-trending zone of parallel and anastomosing faults extends along the western margin of the area. The main faults within this zone mark the boundaries between several fundamental and contrasting litho-tectonic units. The most northwesterly of these major faults is the Chimbo-Cañi Fault situated along the Chimbo Valley, which marks the eastern limit of island arc rocks of the Macuchi Unit and the western limit of turbiditic sediments of the Angamarca Group. The Multitud Fault to the southeast marks the boundary between the Angamarca group and ocean floor basalts of the Pallatanga Unit to the east. Farther southeast, the Bulubulu Fault marks the eastern limit of the Pallatanga Unit and the western limit of the metamorphic basement which underlies the younger volcanic cover of the cordillera to the east. The Bulubulu and Multitud faults converge northwards and together they form a southern extension to the Pallatanga Fault System. The displacement patterns of lithological units together with limited evidence from S-C structures indicate dextral-slip movement along these fault zones. In the high ground west of Cuenca, the Saraguro Group is intensely fractured by NW-SE faults and intruded by a dyke swarm of the same orientation. This fracture trend may be a relatively superficial feature, representing Reidel shears formed in the cover in response to dextral strike-slip movement along the more fundamental NE-SW faults. Folds are present in the Angamarca Group and in the Puñay Unit. These have axes trending NNE-SSW to NE-SW.

2.3 Mineralisation

The most extensively documented prospect within the region is the porphyry system at Chaucha, first recorded in 1968 during a UNDP reconnaissance programme (UNDP, 1969). Mineralisation at the margin of the batholith occurs as hydrothermal breccias, veinlets and disseminations associated with zones of potassic, phyllic, argillic, silicic and propylitic alteration. Five zones of mineralisation have been delimited by surface exploration, the largest of which has proven ore reserves of 55 million tons grading 0.57% Cu and 0.3% Mo.

Several other prospects exist within or close to the margins of major intrusions. In the Carmen de Pijilí area Au mineralisation occurs in polymetallic quartz veins within the Pallatanga and Yunguilla units at the margin of the Chaucha batholith. A large zone of intense silicification carrying Au mineralisation occurs in the south-eastern sector of the Río Blanco Formation in the roof zone of the Chaucha Batholith. In the north-western sector of the Soldados Formation outcrop. Ag-Cu-Pb-Zn-Bi-Sb mineralisation is associated with zones of silicification and breccia pipe emplacement. Polymetallic quartz veins with Cu-Pb-Zn sulphides occur near the margin of the Molleturo diorite. Polymetallic (Au-Ag-Pb-Zn-Cu) assemblages, reportedly of epithermal character, occur in a number of areas in the Gualleturo-Ger-Purubín region.

3. SAMPLING AND ANALYTICAL PROCEDURES

The sampling and analytical methods employed by the project and procedures used for monitoring and controlling the quality of chemical analysis are described in detail by Dunkley et al. (1997) and Dunkley and Gaibor (1997a). The salient features of these methods are given in the following sections.

3.1 Numbering system

Throughout the GIMP geochemical survey samples were numbered randomly using a system based on that of Plant (1973) and Garrett (1983), in order to preclude analytically-induced campaign boundaries (within or between sheet areas) and/or the generation of spurious multiple-sample anomalies. Prior to sampling of the GIMP area between 4°-1°S ten thousand sample bags were sequentially numbered, randomized and issued to sampling teams. On return to the CODIGEM laboratory, all filled sample bags were re-ordered numerically and forwarded for analysis in sequential batches of about 120 samples each. Through this procedure short-term analytical fluctuations (affecting one or more sample batches) are manifested as analytical noise across the entire project area, rather than as discrete local or sub-regional trends.

3.2 Field sampling procedure

Drainage sediment samples were collected by three sampling teams each comprising between four and eight trained geologists and field assistants. Samples were collected during five commissions, each lasting three weeks, during dry season conditions (May-December). A total of 2456 samples were collected from an area of about 6300 km^2, representing an average sampling density of 1 sample per 2.56 km^2 (Sleeve Insert 1). In all instances emphasis was placed on the recovery of samples from first or second order streams, thus contrasting relatively small provenance areas.

The sampling methodology employed throughout the GIMP geochemical survey was derived from that of Plant and Moore (1979), and is compliant with the global IGCP 259/360 protocol for International Geochemical Mapping (Darnley et al., 1995). Sampling stations were routinely located upstream of potential sources of perturbation (habitation, industrial activity, agricultural discharges or bridging structures). At each site several kilograms of active channel sediment were collected following the removal of the hydrous-oxide enriched surface horizon. The sediment was then wet-screened through an 80 BSI mesh (177 μm) sieve using a minimal volume of water so as to avoid the loss of fine silt and clay fractions. Following a settling period of about 20 minutes, the clear water overlying the sediment was decanted and approximately 100 g of the remaining sediment was transferred to a pre-numbered kraft bag for transport and storage.

The selection of an 80 BSI sediment fraction for use throughout the GIMP survey was based on an orientation study by Dunkley et al. (1995) in the Río Junín basin. This survey studied the anomaly related to the Junín porphyry Cu-Mo deposit using four different sample size fractions and a variety of analytical techniques, in order to decide which methods would be most suitable for use in the routine survey. The study indicated that for several elements of economic interest the 80 BSI mesh fraction gave the best anomaly to background contrast, although for a few elements the 100 mesh gave a slightly better contrast. The 80 mesh fraction was selected for the routine survey because problems were envisaged in collecting sufficient 100 mesh material in many of the high-energy rivers of the project area. The 80 mesh fraction effectively reflects both mechanical and hydromorphic geochemical dispersion (e.g. Williams et al., 1992).

3.3 Sample preparation

On return from the field samples were air-dried at <40°C thus preventing any loss of Hg or other volatile elements. Samples were then disaggregated using a pre-washed pestle and mortar to yield a fine homogeneous powder. This was sub-sampled using a cone-and-quarter technique to produce a ca. 50 g aliquot for chemical analysis.

3.4 Analysis

Chemical analyses of samples were performed in the Vancouver laboratories of Bondar Clegg Ltd. using four methods.

3.4.1 Gold

Samples of 30 g mass were analysed for Au by a combination of fire assays followed by determination by atomic absorption spectrophotometry (AAS).

3.4.2 Major and trace cations

A suite of 34 major and trace cations (Ag, Cu, Pb, Zn, Mo, Ni, Co, Cd, Bi, As, Sb, Fe, Mn, Te, Ba, Cr, V, Sn, W, La, Al, Mg, Ca, Na, K, Sr, Y, Ga, Li, Nb, Sc, Ta, Ti, Zr) was simultaneously determined by inductively-coupled plasma emission spectroscopy (ICP-ES) following the digestion of 1.0 g aliquots of 100 ml of aqua-regia (ARISTAR). It is well-known that aqua regia only provides a partial dissolution technique and is particularly inefficient for many elements held in resistate minerals (e.g. Sn, Cr, W, Zr). However, a total dissolution technique would have been too expensive, and more importantly during the orientation survey was found to give extremely erratic results for several important elements (As, Sb). On the basis of this information, the aqua-regia technique was chosen as the best all-round technique.

3.4.3 Metalloids

On account of the low sensitivity (5 mg/kg in solid) of metalloid analyses by ICP-AES, the metalloid elements As and Sb were also determined by hydride-generation AAS on the same aqua-regia solution described in the previous section. A flow-injection (FIA) introduction system by Nakashima (1979) facilitated the reduction of As to arsine and injection into the aspiration chamber simultaneously by merging a flow of 0.2% $NaBH_2$, with the sample carrier.

3.4.4 Mercury

Total mercury was determined by cold-vapour AAS (CV-AAS) on the same aqua-regia solution prepared for multi-element determination by ICP-AES (see above).

4. QUALITY CONTROL

4.1 Sampling variance

For 31 elements the statistical variance attributable to at-site sediment heterogeneity and/or sampling bias was calculated for the entire GIMP survey area using a modified analysis of variance (ANOVA) technique (Plant et al., 1975). Duplicate sediment samples acquired through repeat sampling of selected drainage sites (at a maximum frequency of 2 per 100) were analysed, and the results were used to determine sampling variance using the sums of squares technique (Bolviken and Sinding-Larsen, 1973).

In instances where both duplicates from a single site yielded sub-detection limit values, the record was excluded from the calculation. Summary statistics are provided in Table 2. Statistical F-tests are not quoted, as the data do not fully satisfy the assumptions of conventional ANOVA analysis. It requires emphasis that the sampling variance data are themselves derived from the *analytical* determination of field duplicates. The values therefore assume interpretative significance only when in excess of the corresponding analytical precision threshold (section 4.2).

Table 2: Sampling variance data, based on ANOVA analysis of duplicate samples from selected field stations within the GIMP survey area.

Element	%variance	Element	%variance	Element	%variance	Element	%variance
Ag	7.1	**Sn**	15.2	**As**	3.1	**Ga**	11.6
Cu	3.1	**W**	21.7	**Sb**	6.9	**Y**	21.2
Pb	7.1	**La**	4.3	**Fe**	6.6	**Nb**	15.4
Zn	4.7	**Al**	3.6	**Mn**	7.1	**Sc**	16.0
Mo	25.0	**Mg**	7.1	**Bi**	17.5	**Ti**	4.4
Ni	12.4	**Ca**	12.5	**Ba**	3.2	**Zr**	12.1
Co	3.5	**Na**	12.2	**Cr**	9.3	**Hg**	21.7
Cd	4.2	**K**	9.4	**V**	4.9		

4.2 Analytical precision

Precision (p) is an index of the reproducibility of analytical determinations conventionally defined as:

$$p = \left(\frac{2s}{x}\right) * 100\%$$

The term is distinguishable from accuracy, which reflects the relationship between an individual determination or group of determinations and the true matrix composition. In exploration, indices of analytical precision are critical as they provide an insight into inter-comparability of data for individual samples or sample batches.

Analytical precision data for GIMP areas 3-4°S and 2-3°S were derived from a series of statistical exercises based on the duplicate analysis of aliquots of homogenized sediment (Plant et al., 1975; Thompson and Howarth, 1978). During the analytical run, qualitative assessment was carried out using an X-Y scatterplot (Fig. 4), on which precision is proportional to the scatter of coordinates for duplicate analyses around a line of 100% covariance.

Quantitative precision indices were subsequently calculated using the two methods of Thompson and Howarth (1976, 1978). The first entailed a calculation of the variation of the standard deviation (s_c) across an empirically-defined concentration range (c) in accordance with the linear function:

$$s_c = s_0 + kc$$

where s_0 is the standard deviation at zero concentration and k is the gradient of the straight line. Values for s_0 and k were obtained by:

(i) Determination of mean $\frac{x^1+y^1}{2}$ and absolute difference (x^1-y^1) values for all duplicate pairs.

(ii) Ranking of duplicate pairs by ascending mean.

(iii) Calculation for the 'mean of means' and 'median of differences' for discrete groups of 11 duplicate pairs (8 groups = 88, with 3 discarded).

(iv) Regression of median against mean values determined in (iii) to yield s_0 (intercept) and k (gradient).

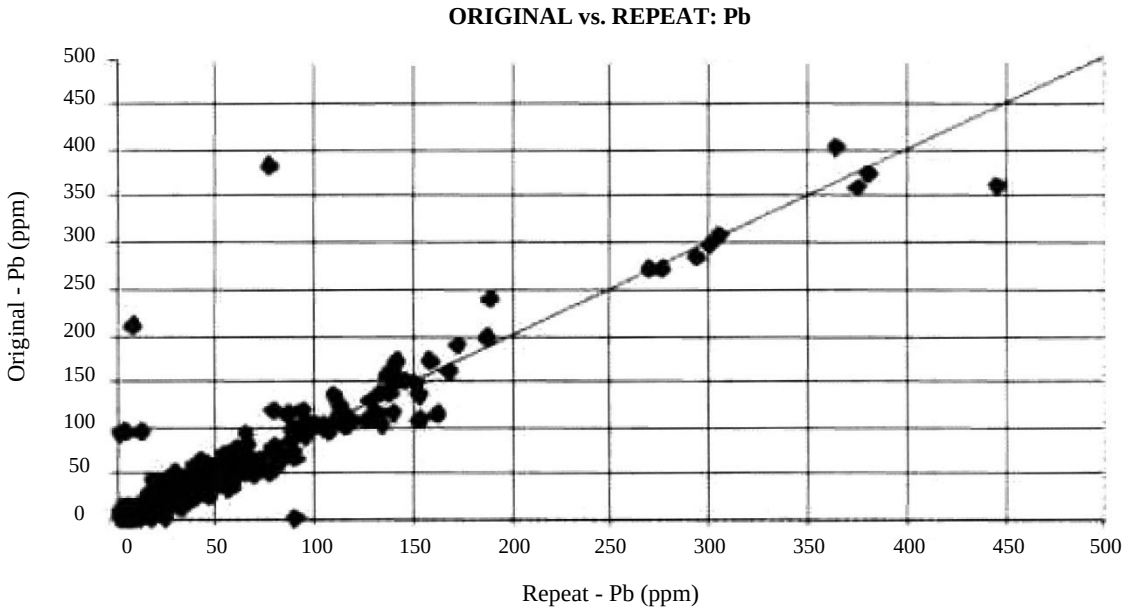

Figure 4**.** Typical X-Y scatterplot of analytical duplicates, utilised for the rapid semi-quantitative examination of precision for all elements determined under the GIMP geochemical survey programme

The second method utilised a series of precision control charts on which 90th and 99th percentile concordance lines were plotted for one or more pre-determined precision levels (Appendix 1). Practically acceptable precision thresholds defined by the latter method, and systematically applied to quality control of the analytical output for the GIMP 2°-3°S area, have been reported by Dunkley and Gaibor (1997a) and are summarised in Table 3.

Table 3. Precision thresholds for selected elements applied for quality-control of analytical data for the GIMP 2°-3°S area (from Dunkley and Gaibor, 1997a)

Element	%Est. precision	Element	%Est. precision
Ag	25	**As**	5
Cu	20	**Sb**	10
Pb	40	**Mn**	15
Zn	20	**Fe**	15
Mo	25	**V**	40
Ni	10	**Sr**	25
Co	15	**Cd**	15
Ba	20	**Li**	15
Cr	10	**Bi**	20

4.3 Control standards

4.3.1 GIMP control standards

Six control standards derived from stream sediments within the GIMP area were used to monitor the quality of chemical analyses during the analytical programme.

Three control samples were used in the first year of the project (J-1, Junín River; COR-1, Angamarca River; M-1, a mixture of J-1 and COR-1 in equal proportions). With the exception of J-1 which contains anomalous concentrations of Cu (equivalent of the 97th percentile value of the 2°-3°S), moderately high As (70th percentile) and Sb (90th percentile), these standards contain background concentrations of most elements of economic interest. Three additional control standards were therefore introduced during the second year of the project. These included PE (Ponce Enríquez), CN (Cerro Negro) and M-2 (a mixture of PE, CN and COR-1 in the proportions 1:1:2). These latter three standards contain moderately to strongly anomalous concentrations of most of Au, Ag, Cu, Mo, Pb, Zn, Cd, As, Sb and Hg.

The control standards J-1, COR-1 and M-1 were analysed at the UK laboratories of the British Geological Survey by a combination of ICP-AES, ICP mass spectrometry (ICP-MS) and X-ray fluorescence (XRF) methods at the outset of the GIMP survey (Table 4).

Table 4. BGS certification of GIMP control standards J1, COR1, and M1 based on the mean analysis by multiple techniques.

Element	BGS value (ppm)			Element	BGS value (ppm)		
	J-1	COR-1	M-1		J-1	COR-1	M-1
Ag	<0.2	<0.2	<0.2	**As**	12.5	5.0	7.0
Cu	175	23	79.5	**Sb**	3.3	0.6	1.4
Pb	3.5	5.0	7.0	**Mn**	468	375	413
Zn	61	43	50.5	**Fe (%)**	4.9	8.1	7.0
Mo	1.6	0.5	1.0	**V**	150	293	226
Ni	10.5	18.5	14.0	**Sr**	28.5	61.0	48.0
Co	10.7	14.8	12.9	**Cd**	ND	1.0	0.5
Ba	74	64.5	73	**Li**	5.9	6.0	5.5
Cr	44.5	82.0	65.0				

Two sub-samples of three or more control standards were submitted to the Bondar Clegg laboratories in blind fashion with each batch of 120 field samples. The resultant data provided a mechanism for evaluating (i) instrumental accuracy and (ii) temporal analytical drift. The latter was evaluated independently of precision (4.2 above) as it commonly involves a systematic adjustment, thus amenable to correction.

Results of replicate analyses of control standards conducted during the analysis of field samples from the GIMP 2°-3°S area are given in Appendix 2. Accuracy quotients obtained by dividing the mean of control standard analyses by the corresponding BGS certified value (standards J-1, COR-1 and M-1 only) are also shown. For elements such as Pb and Hg, relatively large discrepancies between laboratories reflect low Bondar Clegg precision at concentrations close to the ICP-AES/CV-AAS detection limits. Higher precision at analogous concentrations was achieved by BGS by using alternative (ICP-MS and CV-AFS) techniques. Low recovery quotients (<0.7) for the major cations K, Mg, Ca (not quoted) were also observed. This is probably due to the more efficient dissolution achieved at BGS using a hot-reflux technique.

The impact of systematic instrumental drift on the GIMP 2°-3°S dataset was evaluated using conventional time-series plots, as exemplified in Figs. 5-6. In rare instances in which control-standard values concurrently deviated by more than 2 standard deviations from the mean, an appropriate correction was applied. Examples exist in the time-series data shown for Zn, in which the values for standards submitted with analytical batches 22-24 are systematically depressed.

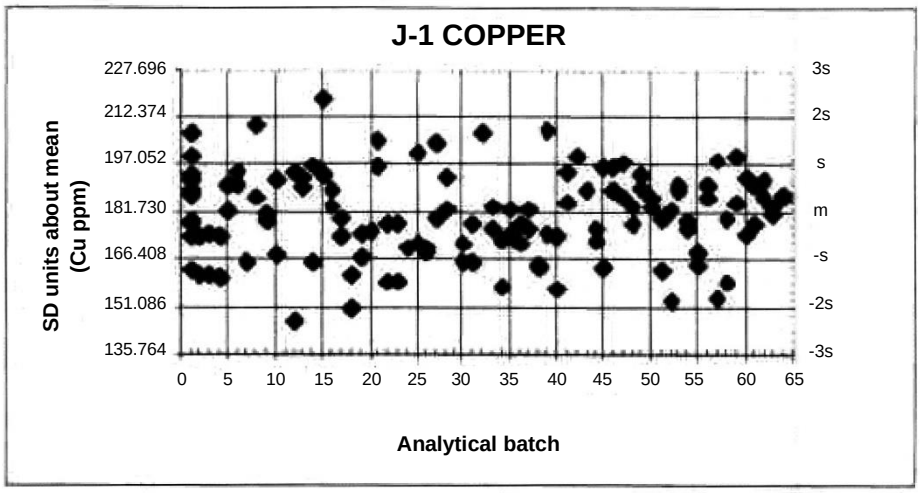

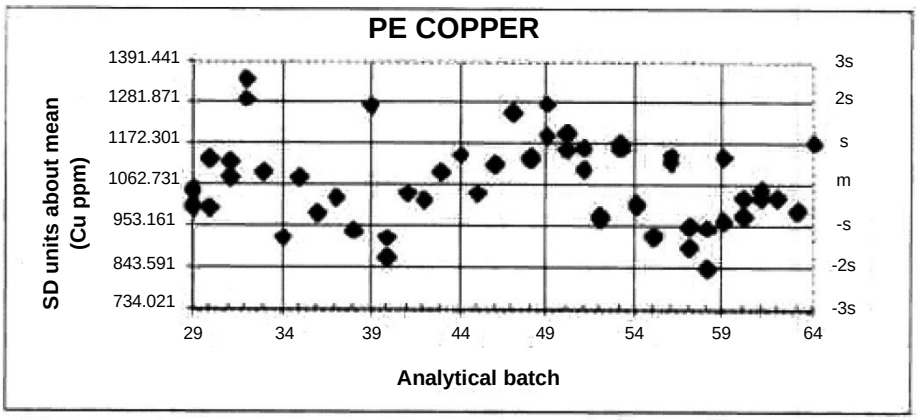

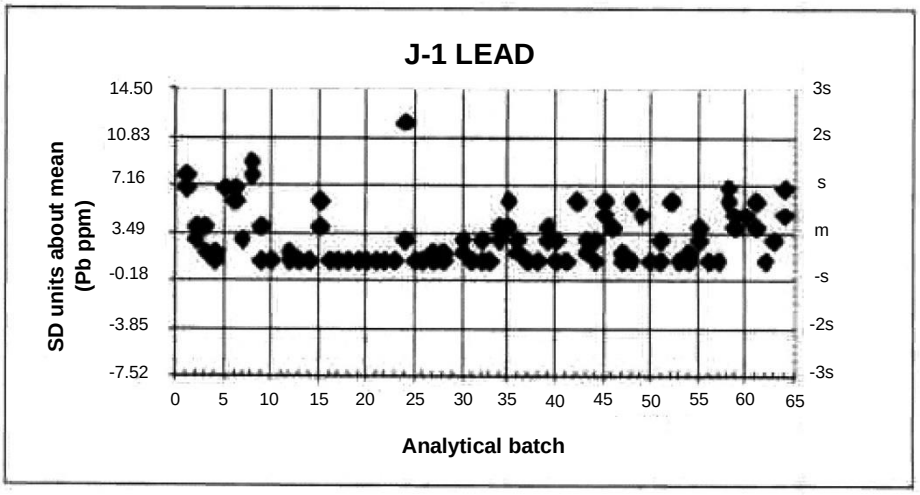

Figure 5. Copper and lead time-series control plots showing the results of replicate analyses of simultaneous duplicate pairs of Ecuadorian reference sediments. Correction of the empirical dataset is applied under the GIMP only in instances where BOTH samples within a duplicate pair deviate from the mean by >2 SD for any individual sample batch.

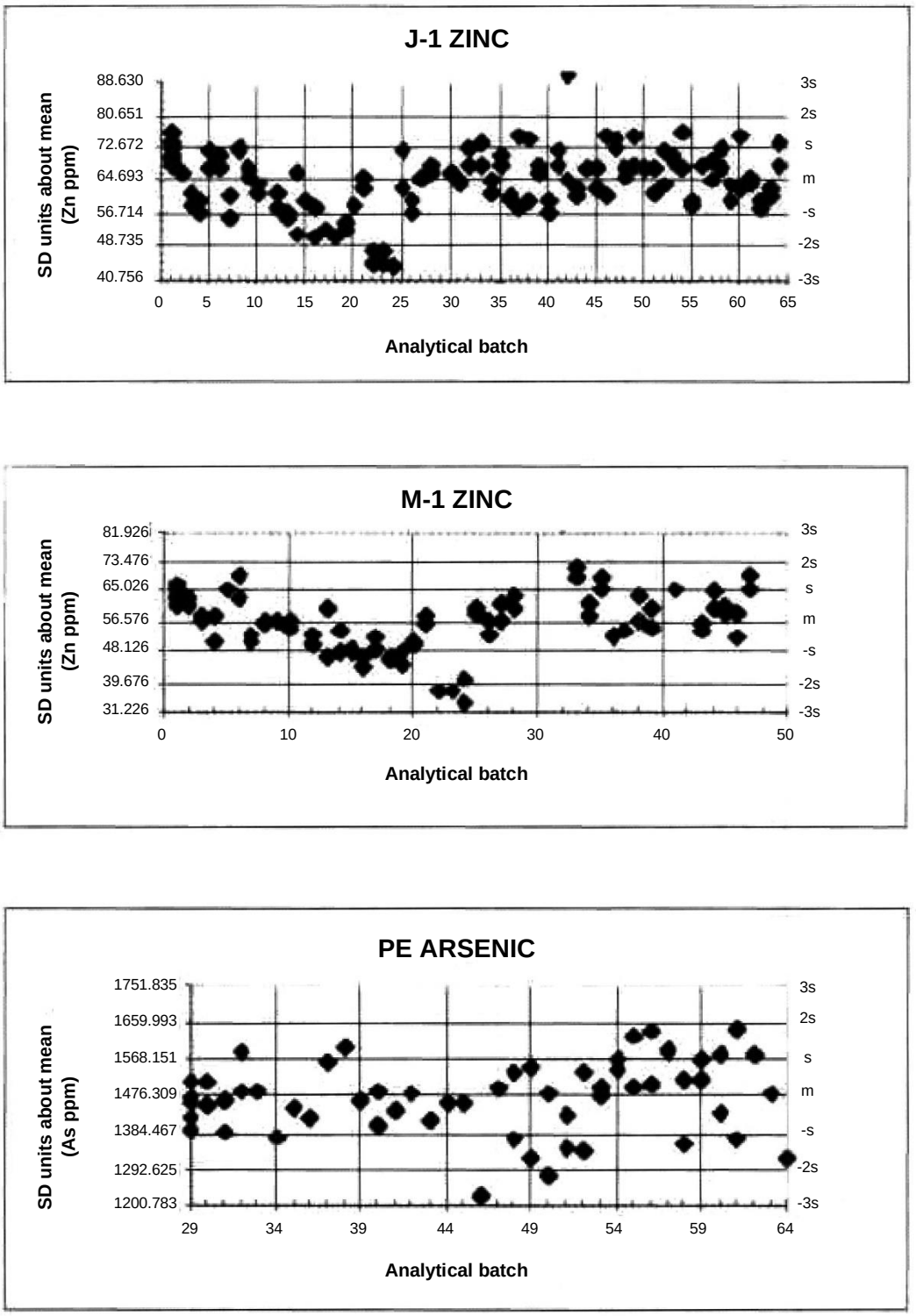

Figure 6. Zinc and arsenic time-series control plots showing the results of replicate analyses of simultaneous duplicate pairs of Ecuadorian reference sediments. Correction of the empirical dataset is applied under the GIMP only in instances where BOTH samples within a duplicate pair deviate from the mean by >2 SD for any individual sample batch. An example is provided by the Zn data for batches 22-24.

4.3.2 BGS control standards

In addition to the GIMP control standards described above, four BGS reference standards (S13, S15, S24, S3B) were submitted 'blindly' for analysis by Bondar Clegg. The BGS standards were derived from 100 BSI mesh stream sediments from granitic, sedimentary and metasedimentary terrains of northern Britain. All have been subjected to analysis in several European laboratories by a combination of XRF, AAS, ICP-AES, ICP-MS and direct-reader emission spectroscopy (DRES) methods. An inter-laboratory comparison of selected data for these samples is provided in Table 5. Relatively high values for elements such as Pb (notably in S3B) reflect the use by BGS of a total analytical technique (XRF) rather than the partial (aqua-regia digestion) method of Bondar Clegg.

Table 5. Inter-laboratory comparison of BGS reference standards

Element	BGS (ppm)				Bondar Clegg (ppm)			
	S24	S13	S15	S3B	S24	S13	S15	S3B
Ag	4.0	-	-	-	1.2	-	-	-
Cu	60	16.1	4.9	48.4	60	16.5	4.0	39.0
Pb	1114	112.4	24.7	1770	847	99	17.0	1464
Zn	385	113.8	28.5	786	379	114	29.0	563
Mo	3.7	1.5	1.9	148	<1	<1	<1	128
Ni	43.2	36.5	11.5	30.4	37.5	24	9.5	18.5
Co	84.6	-	-	-	70.5	-	-	-
Cd	3.8	-	-	-	1.4	-	-	-
As	126.0	15.8	8.8	<2	122.2	16.9	5.2	3.8
Sb	6.0	-	-	-	9.0	-	-	-
Ba	1060	-	-	-	504	-	-	-

4.4 Practical detection limits

With the exception of Au, analytical detection limits (LODs) provided by Bondar Clegg were not adopted for use in the validation of GIMP geochemical data as they do not account for the matrix influences typically encountered during the analysis of geological materials. Practical LODs for each element were instead determined by Dunkley and Gaibor (1997a) using two methods. The first involved the replicated analysis of reference samples over a range of concentrations, and the regression of the standard deviation against the mean concentration for each value to yield a value of standard deviation at zero concentration (s_0). A LOD of $3s_0$ was then calculated in accordance with UIPAC (1978). The second method involved the derivation of s_0 using the method of Thompson and Howarth (1978) as outlined in section 4.2. Details of practical LOD's obtained using both techniques are given in Table 6, with the adopted value highlighted in each case.

Table 6. Bondar Clegg and GIMP analytical detection limits (adopted values highlighted). All values are in mg/kg unless otherwise indicated.

Element	Bondar Clegg	Extrapolation Method	Thompson and Howarth
Ag	0.2	**1.0**	0.9
Au	0.05	-	-
As	1	6.1	**4.5**
Ba	1	**5.4**	2.4
Bi	5	**6.0**	-
Cd	0.2	**0.7**	1.4
Cr	1	**3.7**	4.7
Co	1	**2.6**	1.9
Cu	1	**4.5**	11.0
Fe	0.01%	**0.3%**	0.6%
Hg	0.01	**0.04**	0.04
Li	1	**1.2**	1.0
Mn	1	**34.0**	-
Mo	1	**1.35**	5.0
Ni	1	**3.3**	2.4
Pb	2	**4.0**	12.0
Sb	0.2	1.9	**0.74**
Zn	1	**5.0**	15.0

5. RESULTS

5.1 Digital data enclosure

A spread-sheet (Microsoft Excel 5.0) holding 2456 records for 36 chemical elements is enclosed in a sleeve at the back of this report (hard-copy available in Annex A). Each record comprises a sample number, locational data (latitude, longitude in UTM SAD69 format) and error-controlled analytical data. The format facilitates rapid perusal, sub-setting and graphic/statistical analysis. The file may be converted to tab-delineated text for importation into gridding and interpolation packages. In the following sections of this report, graphics generated using the software Interdex (Visidata Ltd.), Vertical Mapper (MapInfo) and NIH Image (Macintosh platform) are included for exemplification.

5.2 Summary statistics and geochemical imagery.

Geochemical images showing the distribution of 16 major and trace elements within the 2°-3°S area are presented in Figs. 7-22. The images were generated using an inverse-distance weighting algorithm within the software package NIH Image and are presented at a scale of approximately 1:1000000. An excellent correlation between lithology and sediment geochemical signatures is evident, suggesting a limited hydromorphic influence on geochemical dispersion. Summary statistics for the entire dataset are given in Table 7.

Cumulative frequency data indicate that populations for most elements are skewed and poorly amenable to non-parametric statistical analysis. A Pearson correlation matrix (Table 8) highlights the lithologically-controlled covariance of a suite of elements related to mafic rocks (Cu, Co, Ti, V, Cr, Mn). Coefficients of 0.513 for Pb vs. Zn and 0.609 for Cu vs. Mo are the product of coincident enrichment in zones of mineralisation, notably within the central (Chanlud Formation) sector of the study area and in the vicinity of Chaucha. A low Mn range is consistent with the limited control of labile mineral phases on the dispersion and precipitation of first row transition metals or metalloids.

Table 7. Summary statistics for all analysed samples from the GIMP 2°S-3°S area.

	Count	Mean	Std. Dev	Min	Max	Median
Au	2456	37.53	180.02	3.33	4989.00	3.33
Ag	2456	0.70	0.53	0.66	24.30	0.66
Cu	2456	57.13	121.26	3.00	2737.00	31.00
Pb	2456	13.30	22.54	2.66	634.50	8.00
Zn	2456	89.27	91.75	3.33	1519.00	71.00
Mo	2456	2.20	4.85	0.90	141.00	0.90
Ni	2456	22.26	38.66	2.20	560.00	13.00
Co	2456	14.80	8.60	1.73	72.00	13.00
Cd	2456	0.64	0.81	0.46	17.20	0.46
Bi	2456	4.42	1.70	4.00	45.00	4.00
Fe	2456	4.53	2.01	0.01	10.00	0.23
Mn	2456	809.55	907.30	22.66	18661.00	628.00
Te	2456	7.11	3.46	6.66	79.33	6.66
Ba	2456	112.48	77.87	3.60	1073.00	96.00
Cr	2456	70.70	35.75	2.46	430.50	33.00
V	2456	124.67	82.48	0.66	679.00	104.25
Sn	2456	13.53	1.64	13.33	43.00	13.33
W	2456	13.38	0.64	13.33	28.00	13.33
La	2456	8.77	6.93	0.66	129.00	7.50
Al	2456	2.34	1.07	0.01	7.94	2.12
Mg	2456	0.78	0.51	0.01	4.98	0.69
Ca	2456	0.67	0.52	0.01	9.11	0.52
Na	2456	0.04	0.03	0.01	0.19	0.03
K	2456	0.10	0.08	0.01	0.82	0.08
Sr	2456	38.39	31.55	-1.00	308.00	32.00
Y	2456	5.88	3.60	0.66	78.00	5.00
Ga	2456	4.52	3.45	1.33	34.00	4.00
Li	2456	12.38	8.72	0.80	66.00	10.00
Nb	2456	2.60	3.68	0.66	32.00	1.00
Sc	2456	5.94	4.91	3.33	39.00	3.33
Ta	2456	7.09	4.83	6.66	123.33	6.66
Ti	2456	0.11	0.08	0.01	0.63	0.10
Zr	2456	4.09	3.94	0.66	30.00	3.00
As	2456	19.09	47.56	2.66	1402.00	7.00
Sb	2456	1.99	10.94	1.26	532.25	1.26
Hg	2456	0.10	0.95	0.03	36.72	0.03

Table 8. Pearson correlation matrix for selected elements within the GIMP sheet two area

	Au	Cu	Pb	Zn	Mo	Ni	Co	Cd	Fe	Mn	Ba	Cr	V	La	W	Al	Mg	Ca	K	Sr	Hg	As	Ti
Au	***1.000***	0.097	0.188	0.111	0.001	-0.013	0.055	0.097	0.086	0.025	-0.006	0.028	0.066	-0.003	-0.004	-0.004	-0.013	-0.039	0.007	-0.038	0.005	0.196	-0.037
Cu	0.097	***1.000***	0.221	0.274	**0.609**	0.106	0.331	0.102	0.190	0.071	0.076	0.110	0.101	0.020	-0.016	0.250	0.210	0.091	0.120	-0.026	0.010	0.133	0.119
Pb	0.188	0.221	***1.000***	**0.513**	0.089	-0.057	0.078	0.347	0.018	0.152	0.029	-0.098	-0.134	0.090	-0.008	0.063	0.007	-0.078	-0.003	-0.101	0.010	0.259	-0.139
Zn	0.111	0.274	**0.513**	***1.000***	0.161	-0.014	0.293	**0.613**	0.087	**0.532**	0.170	-0.111	-0.110	0.119	0.006	0.144	0.050	0.004	-0.044	-0.039	0.001	0.226	-0.053
Mo	0.001	**0.609**	0.089	0.161	***1.000***	-0.029	0.115	0.090	0.035	0.093	-0.016	-0.045	-0.030	0.051	0.009	0.022	-0.003	-0.068	0.041	-0.120	-0.008	0.079	-0.066
Ni	-0.013	0.106	-0.057	-0.014	-0.029	***1.000***	**0.529**	-0.033	0.140	0.009	-0.161	**0.755**	0.080	0.009	-0.014	0.203	**0.778**	0.367	-0.145	0.015	0.007	-0.014	0.398
Co	0.055	0.331	0.078	0.293	0.115	**0.529**	***1.000***	0.111	**0.497**	0.330	-0.055	**0.506**	0.316	0.074	-0.001	**0.607**	**0.639**	**0.453**	-0.184	0.060	0.005	0.052	**0.510**
Cd	0.097	0.102	0.347	**0.613**	0.090	-0.033	0.111	***1.000***	-0.013	0.371	0.108	-0.090	-0.106	0.059	$3.293*10^{-4}$	-0.015	-0.039	-0.020	-0.033	-0.056	-0.004	0.218	-0.121
Fe	0.086	0.190	0.018	0.087	0.035	0.140	**0.497**	-0.013	***1.000***	0.105	-0.133	0.379	**0.831**	0.124	0.005	**0.431**	0.257	0.207	-0.008	-0.091	-0.009	-0.006	0.351
Mn	0.025	0.071	0.152	**0.532**	0.093	0.009	0.330	0.371	0.105	***1.000***	**0.531**	-0.089	-0.078	0.138	-0.006	0.210	0.048	0.117	-0.117	-0.005	0.003	0.157	-0.032
Ba	-0.006	0.076	0.029	0.170	-0.016	-0.161	-0.055	0.108	-0.133	**0.531**	***1.000***	-0.219	-0.165	0.105	0.016	0.105	-0.239	-0.090	0.206	0.165	0.012	0.077	-0.147
Cr	0.028	0.110	-0.098	-0.111	-0.045	**0.755**	**0.506**	-0.090	0.379	-0.089	-0.219	***1.000***	**0.415**	0.007	-0.017	0.244	**0.663**	0.288	-0.010	-0.010	-0.010	-0.068	**0.473**
V	0.066	0.101	-0.134	-0.110	-0.030	0.080	0.316	-0.106	**0.831**	-0.078	-0.165	**0.415**	***1.000***	0.027	0.011	0.279	0.136	0.192	0.010	0.031	-0.016	-0.144	**0.509**
La	-0.003	0.020	0.090	0.119	0.051	0.009	0.074	0.059	0.124	0.138	0.105	0.007	0.027	***1.000***	-0.013	0.115	-0.001	-0.006	0.033	-0.129	0.023	0.096	-0.044
W	-0.004	-0.016	-0.008	0.006	0.009	-0.014	-0.001	$3.293*10^{-4}$	0.005	-0.006	0.016	-0.017	0.011	-0.013	***1.000***	0.006	-0.017	-0.028	0.053	-0.021	-0.005	-0.013	-0.014
Al	-0.004	0.250	0.063	0.144	0.022	0.203	**0.607**	-0.015	**0.431**	0.210	0.105	0.244	0.279	0.115	0.006	***1.000***	**0.453**	**0.408**	0.057	0.109	0.025	0.031	**0.435**
Mg	-0.013	0.210	0.007	0.050	-0.003	**0.778**	**0.639**	-0.039	0.257	0.048	-0.239	**0.663**	0.136	-0.001	-0.017	**0.453**	***1.000***	**0.568**	-0.072	0.058	-0.019	-0.001	**0.462**
Ca	-0.039	0.091	-0.078	0.004	-0.068	0.367	**0.453**	-0.020	0.207	0.117	-0.090	0.288	0.192	-0.006	-0.028	**0.408**	**0.568**	***1.000***	-0.169	0.273	-0.012	-0.055	**0.454**
K	0.007	0.120	-0.003	-0.044	0.041	-0.145	-0.184	-0.033	-0.008	-0.117	0.206	-0.010	0.010	0.033	0.053	0.057	-0.072	-0.169	***1.000***	-0.053	-0.022	0.058	-0.137
Sr	-0.038	-0.026	-0.101	-0.039	-0.120	0.015	0.060	-0.056	-0.091	-0.005	0.165	-0.010	0.031	-0.129	-0.021	0.109	0.058	0.273	-0.053	***1.000***	-0.007	-0.073	0.268
Hg	0.005	0.010	0.010	0.001	-0.008	0.007	0.005	-0.004	-0.009	0.003	0.012	-0.010	-0.016	0.023	-0.005	0.025	-0.019	-0.012	-0.022	-0.007	***1.000***	0.026	-0.001
As	0.196	0.133	0.259	0.226	0.079	-0.014	0.052	0.218	-0.006	0.157	0.077	-0.068	-0.144	0.096	-0.013	0.031	-0.001	-0.055	0.058	-0.073	0.026	***1.000***	-0.160
Ti	-0.037	0.119	-0.139	-0.053	-0.066	0.398	**0.510**	-0.121	0.351	-0.032	-0.147	**0.473**	**0.509**	-0.044	-0.014	**0.435**	**0.462**	**0.454**	-0.137	0.268	-0.001	-0.160	***1.000***

2456 observations were used in this computation

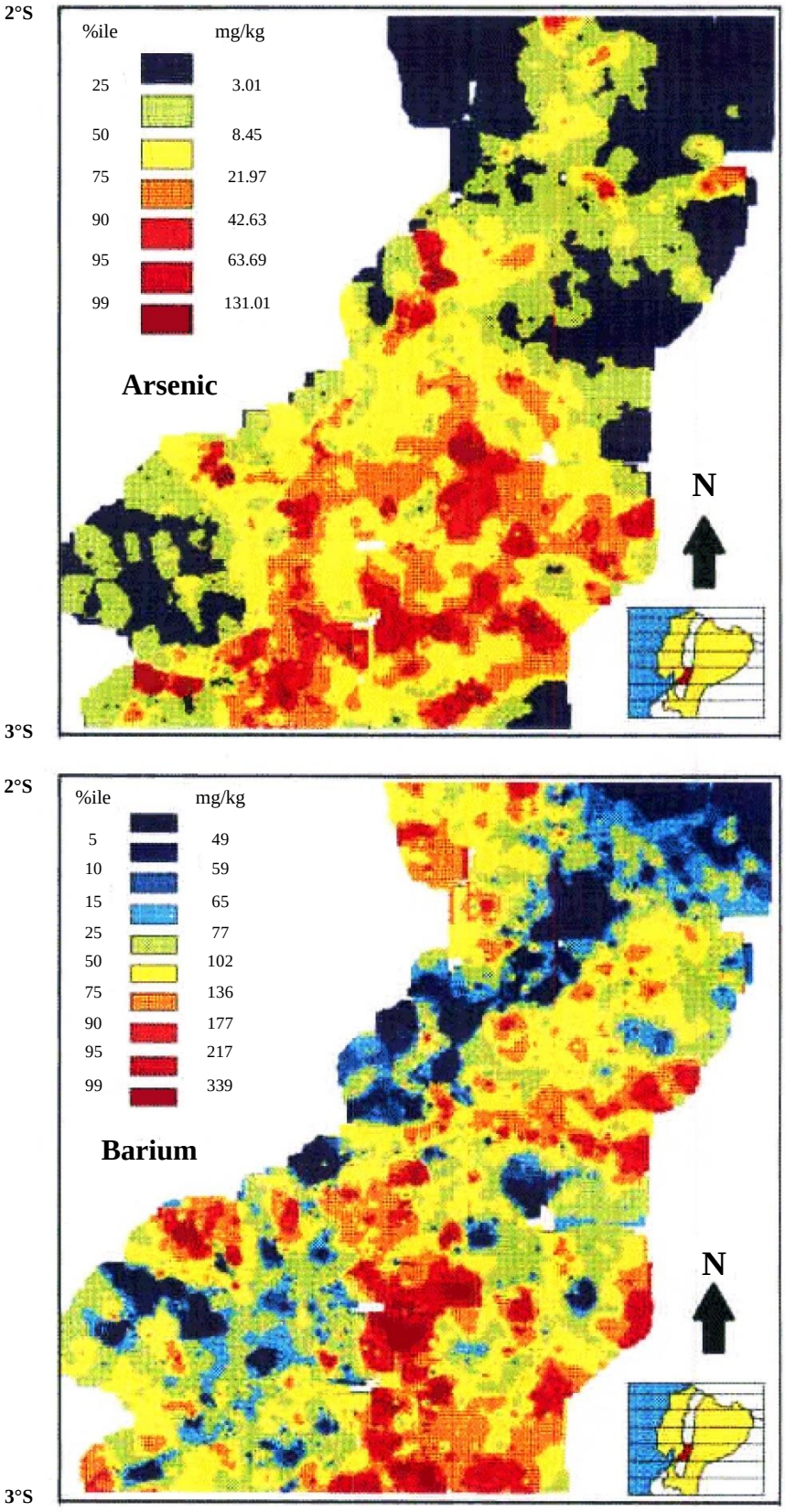

Figures 7-8. Regional distribution of As and Ba over the GIMP 2°S-3°S area.

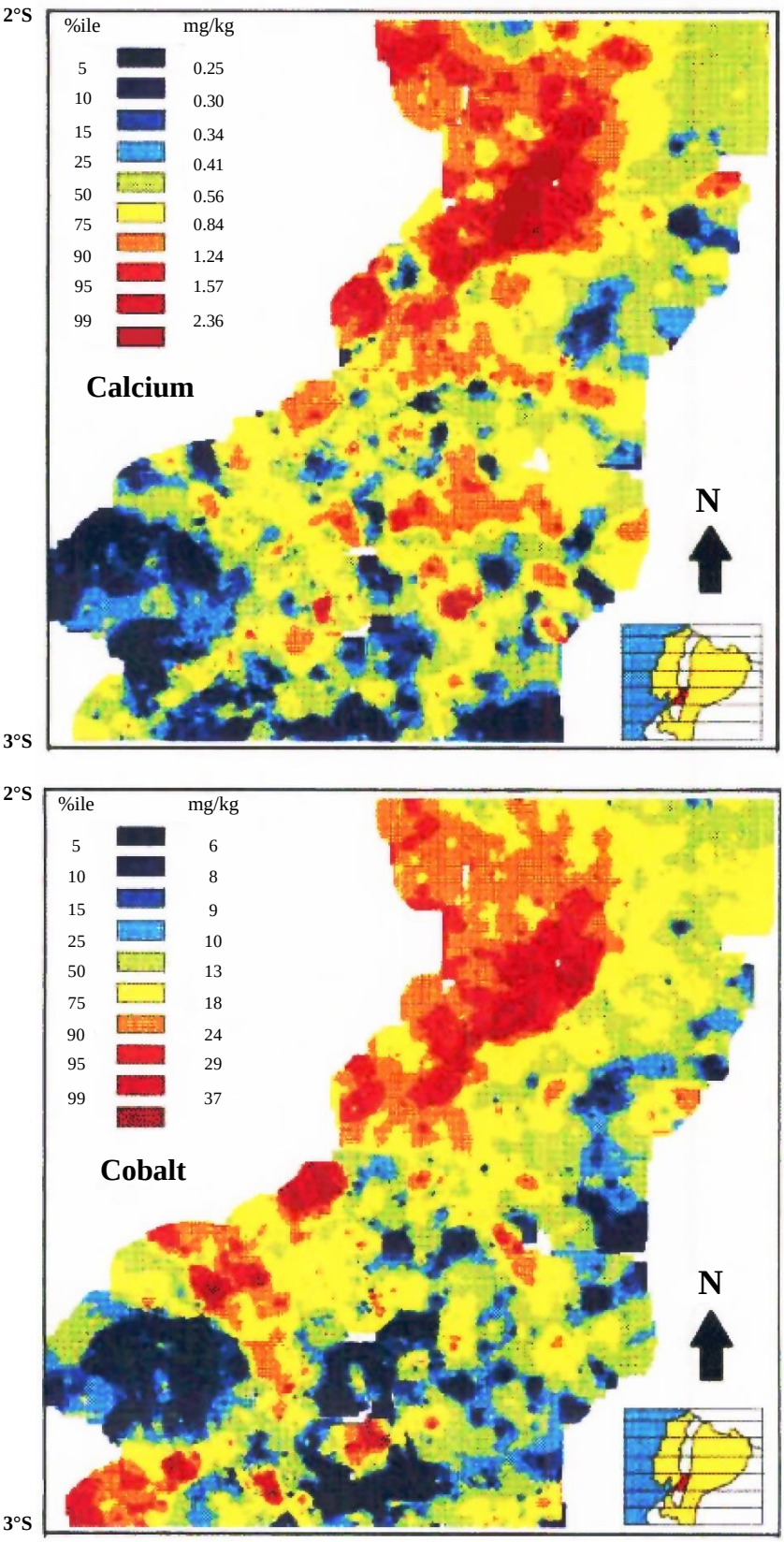

Figures 9-10. Regional distribution of Ca and Co over the GIMP 2°S-3°S area.

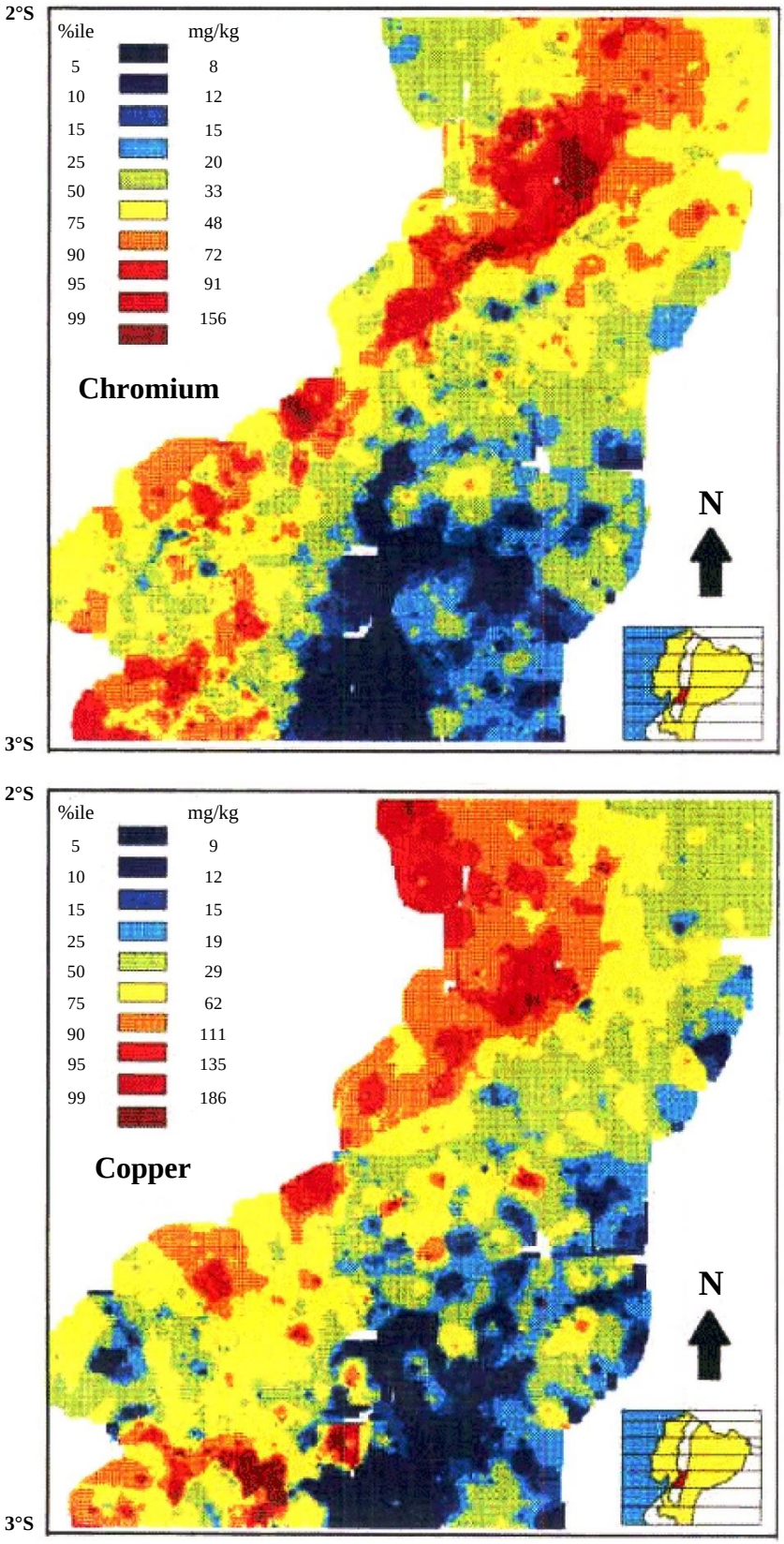

Figures 11-12. Regional distribution of Cr and Cu over the GIMP 2°S-3°S area.

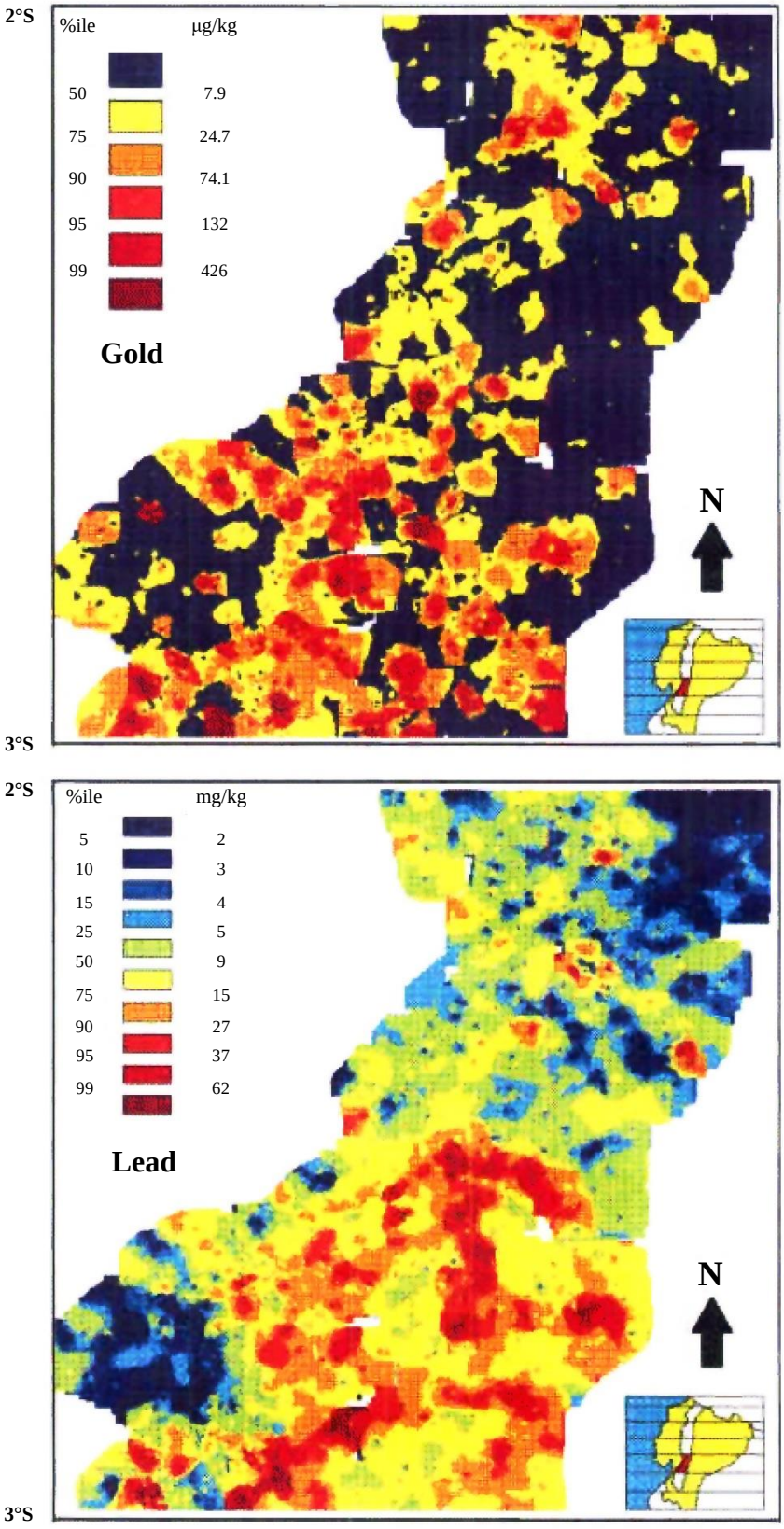

Figures 13-14. Regional distribution of Au and Pb over the GIMP 2°S-3°S area.

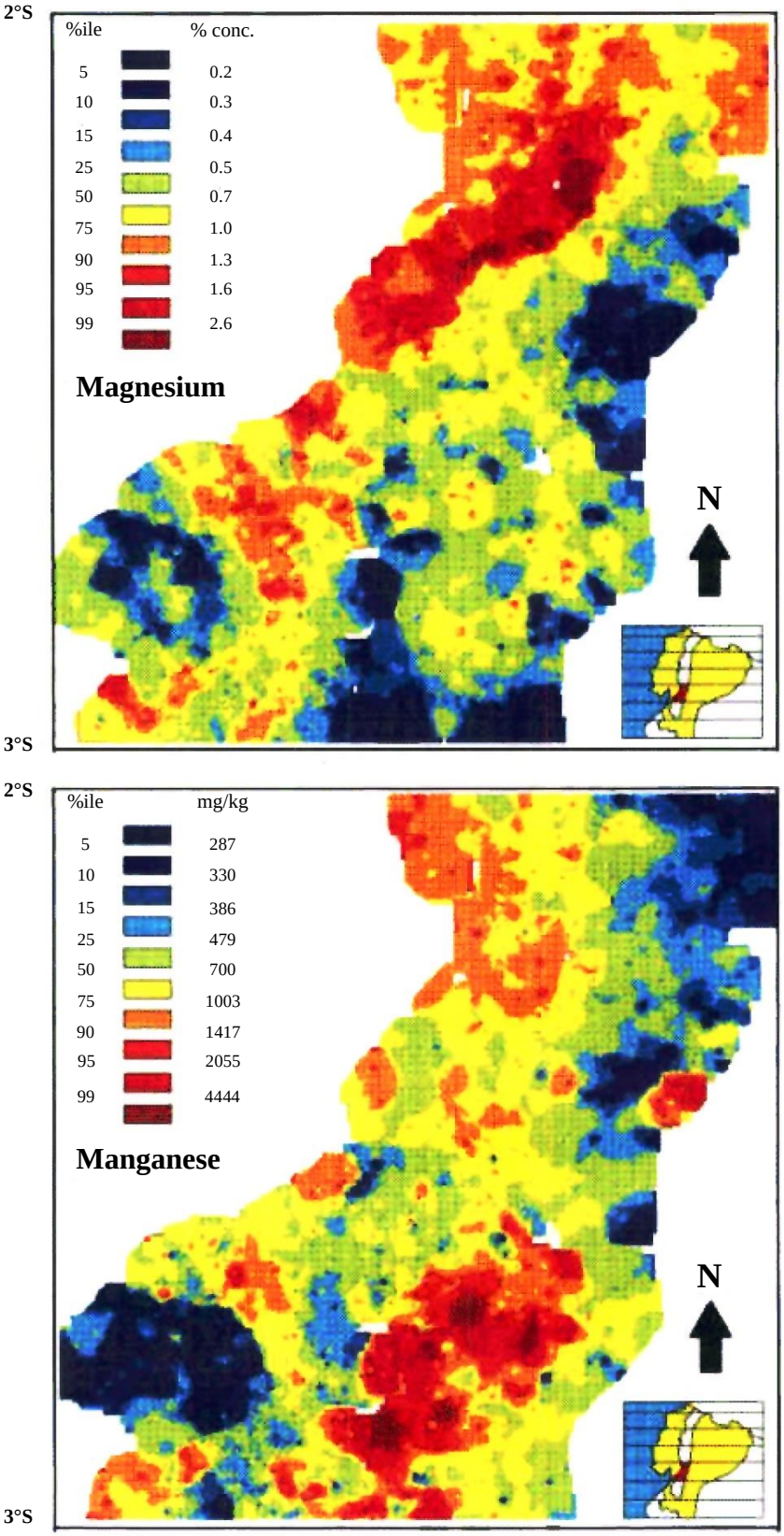

Figures 15-16. Regional distribution of Mg and Mn over the GIMP 2°S-3°S area.

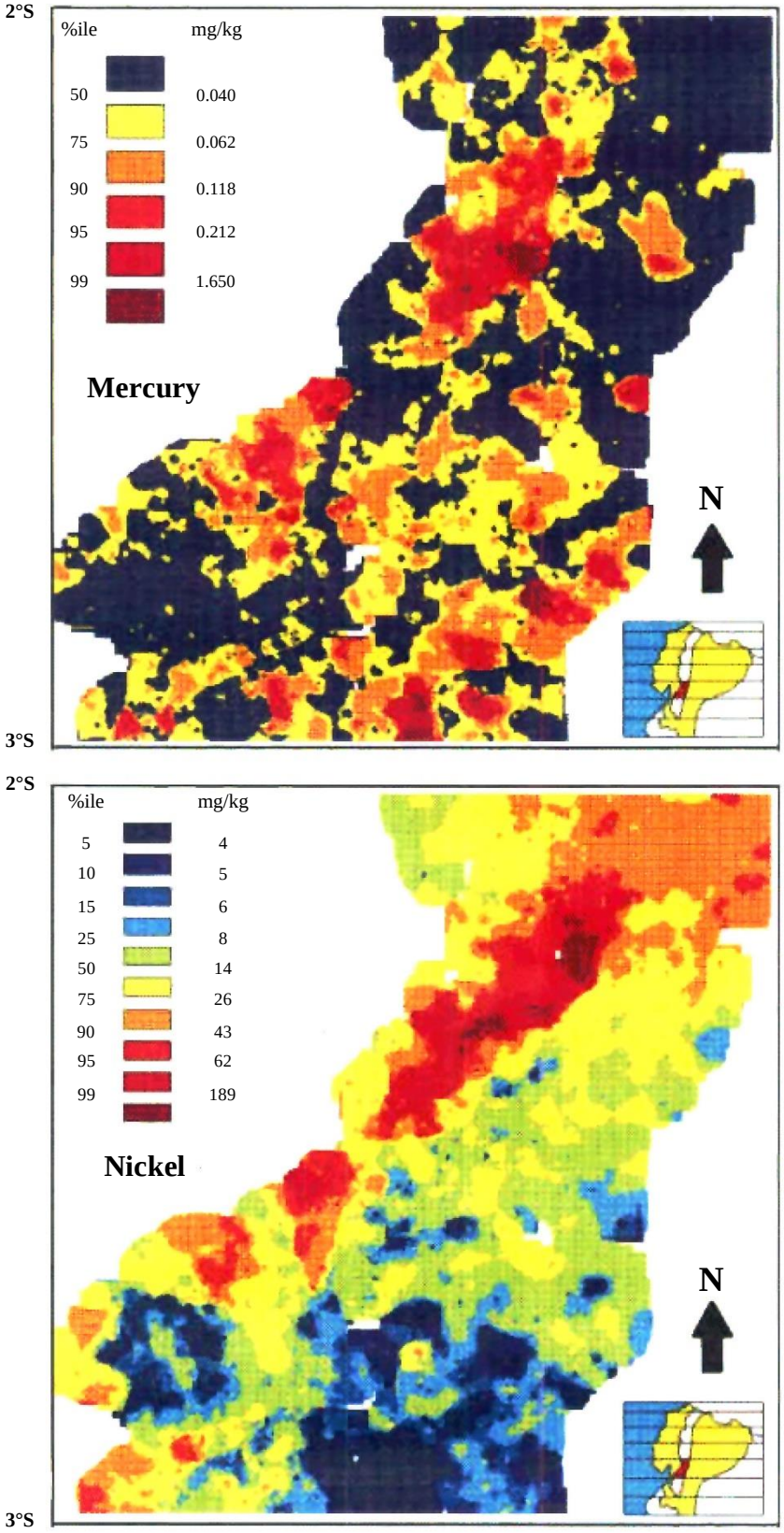

Figures 17-18. Regional distribution of Hg and Ni over the GIMP 2°S-3°S area.

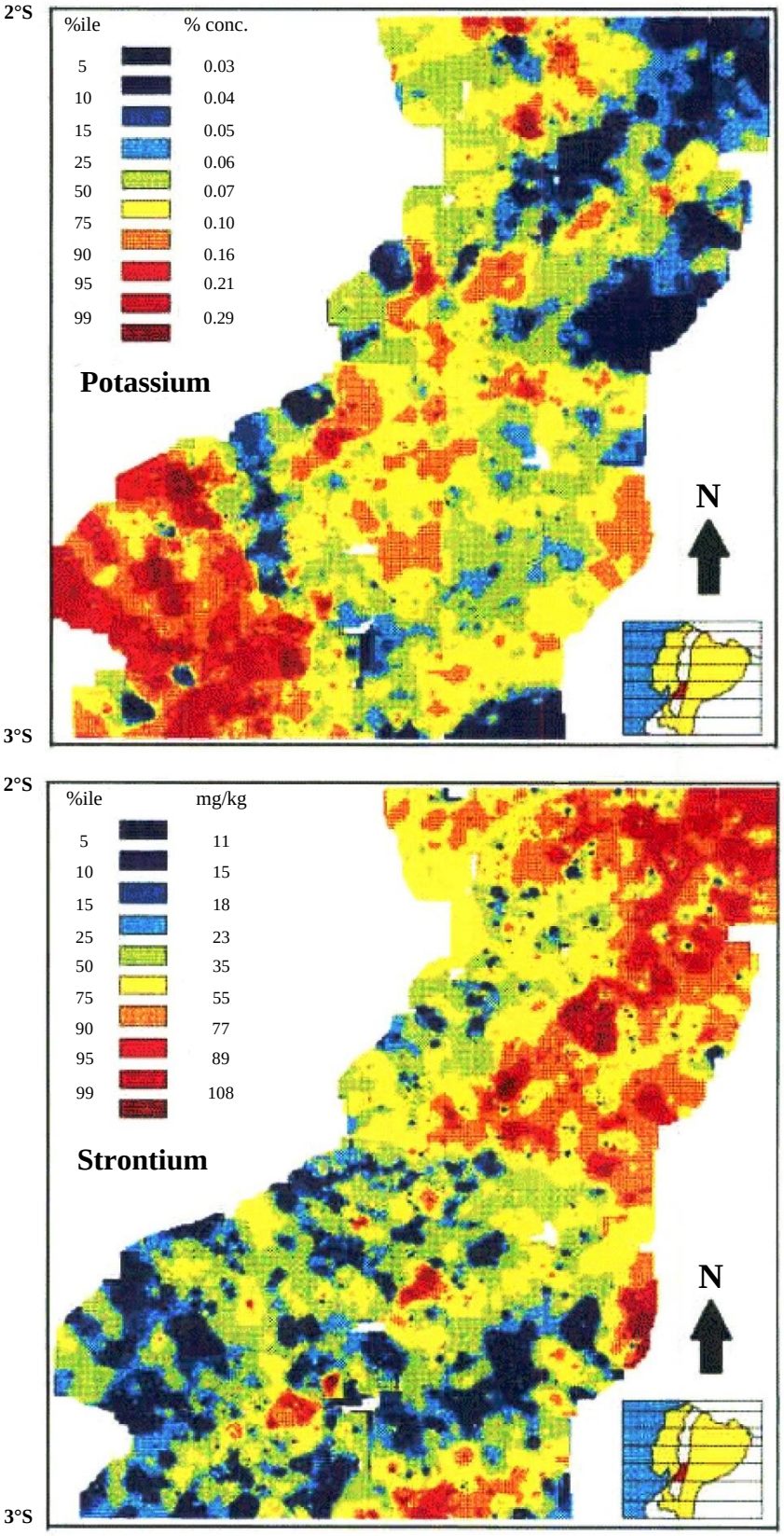

Figures 19-20. Regional distribution of K and Sr over the GIMP 2°S-3°S area.

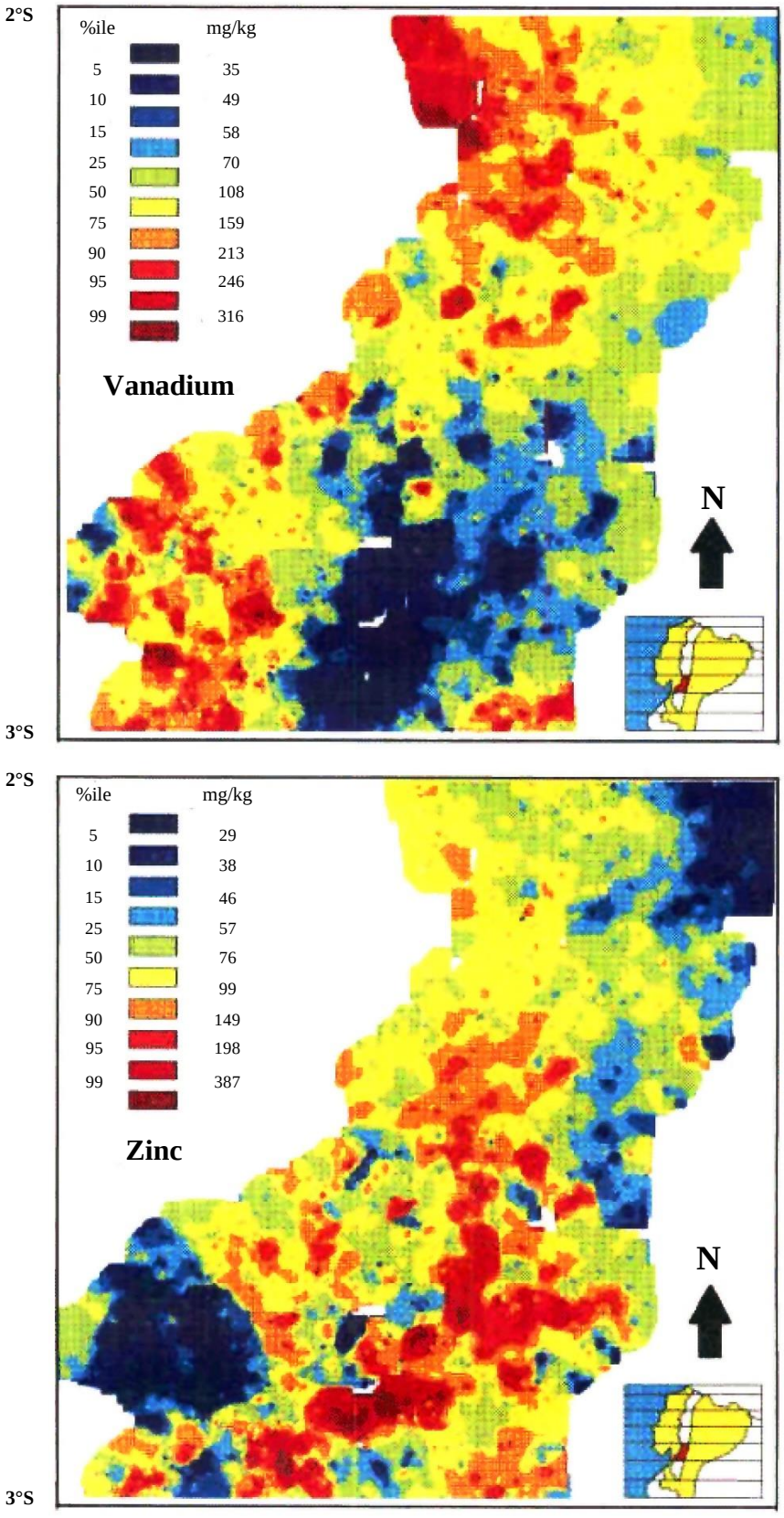

Figures 21-22. Regional distribution of V and Zn over the GIMP 2°S-3°S area.

5.3 Geochemical terranes

The principal lithotectonic units of the GIMP 2°-3°S area produce contrasting geochemical terranes.

(i) Tholeiitic basalts of the Pallatanga Unit display enrichment of Ca, Co, Cr, Cu, Mg and Ni to levels corresponding to the upper 10%ile of the dataset across >50% of the area of outcrop. Low concentrations of Ba (<60 mg/kg) and K (<0.1%) are systematically recorded.

(ii) The Macuchi Unit shows enrichment in an analogous suite to that of the Pallatanga Unit, but substantially higher ratios of Cu/Cr and Cu/Ni reflect a greater andesitic component.

(iii) Acidic components of the Saraguro Group, notably the Soldados Formation and the dacitic or rhyodacitic facies of the Chanlud Formation have a Co-Cu-Cr-Ni-V poor signature (most values within the lower 15%ile of the dataset). High background concentrations of Pb and Ba occur.

(iv) Intermediate lavas and derived volcanoclastic rocks of the Cisarán Formation are distinguished from other volcanic and intrusive lithologies by extremely high ratios of Sr/K. Backgrounds for Ca, Co, Cu, Cr and V are low relative to the more mafic lithologies of the Pallatanga Unit, but are high relative to much of the Saraguro Group (most values fall within the 40-60%ile range). The backgrounds for As, Pb, Mn, Hg and Zn are low relative to all non-intrusive lithologies.

(v) Granodioritic facies within the Chaucha Batholith are K-rich (upper 10%ile) with a low As-Co-Pb-Mn-Mg-Ni-Zn background (typically lower 15%ile).

On account of the above lithologically-controlled contrasts, the application of a single suite of background or threshold values to the entire mapped area is inappropriate as a basis for either exploration, or for the derivation of environmental baselines. Independent interpretation of data for individual lithological units is therefore advocated. This approach as exemplified in the succeeding sections, facilitates the resolution of subtle geochemical anomalies against backgrounds or thresholds appropriate to the local lithological setting.

5.4 Lithostratigraphic analysis

5.4.1 Procedure

Preliminary evaluation of stream sediment data by lithostratigraphic unit was undertaken using the exploration processing software Interdex (Visidata Ltd.). A geo-registered display of sample points was overlain by DXF file of polygonised lithologies (Fig. 23), which was then used to isolate sample points within selected units. Cumulative probability plots were generated for individual elements within each unit, and inflections were used to identify the thresholds defining anomalous values within the population. In instances where multiple inflections indicate the presence of more than two discrete components in the population, the median or upper inflection was generally utilised. All data values were subsequently normalised against the threshold, and anomaly maps were produced showing only those data points with threshold/concentration ratios >1.0. The process excluded analysis of the metamorphic basement, and other lithological units for which sample numbers were considered too small for the technique to retain statistical validity.

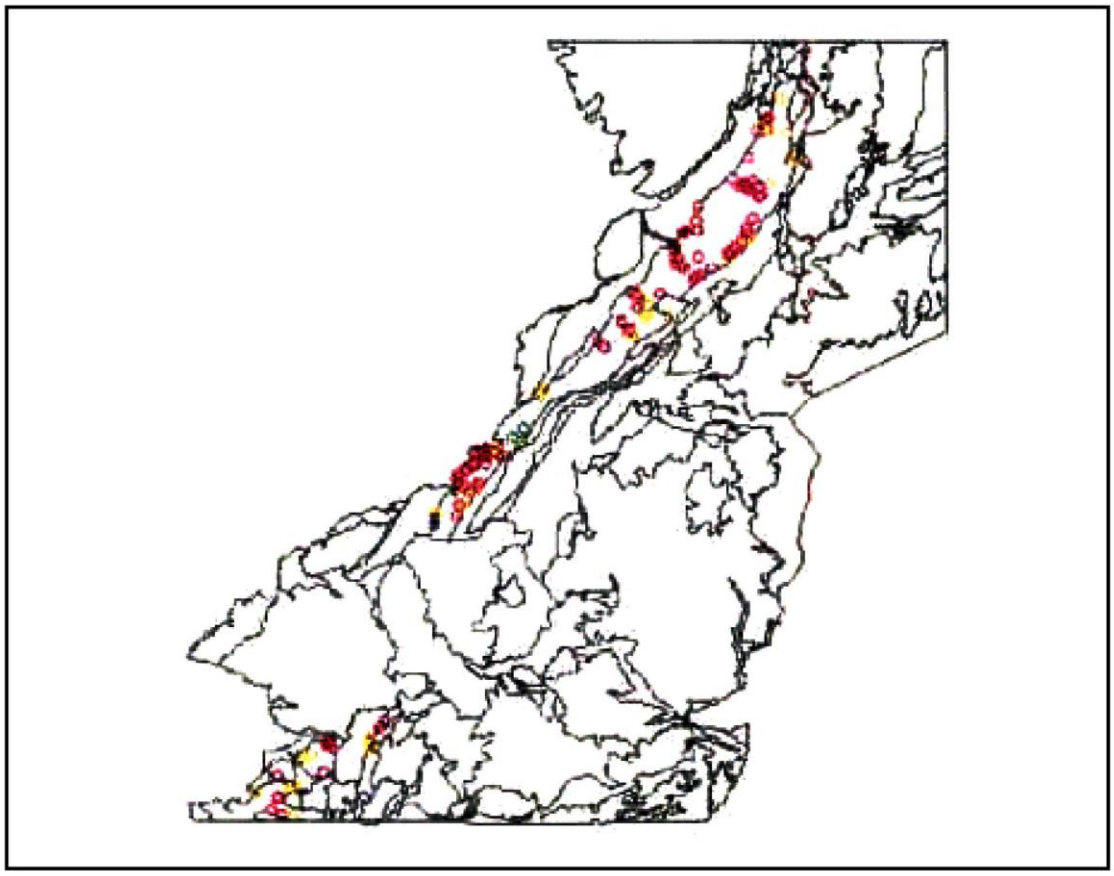

Figure 23. Interdex screen-dump showing sub-setting of data within Pallatanga Unit polygons.

(coloured by Cu concentration)

Sections 5.4.2-5.4.9 include summary statistics indicating the multi-element signatures of most major lithological units within the 2°-3°S area. Anomaly maps based on cumulative probability analysis for Au and a maximum of two additional elements are also provided. Environmental enrichment factors are given in brackets throughout the text. These depict the approximate ratio of the unit mean to the corresponding mean value for the mapped area as a whole. This approach is preferred to conventional normalization against mean upper crustal abundance values (Taylor and McLennan, 1985), because the partial extraction technique used during the analysis of GIMP samples renders such correction as invalid.

5.4.2 Pallatanga Unit

The characterisation of the Pallatanga Unit was undertaken using five polygons encompassing 170 sampling stations. Summary statistics (Table 9) indicate a relatively high background for Cu (2), Ni (1.2), V (1.3), Mg (2), Sc (2), Ti (2) and Hg (1.5). Backgrounds for Pb (0.7) and As (0.6) are low.

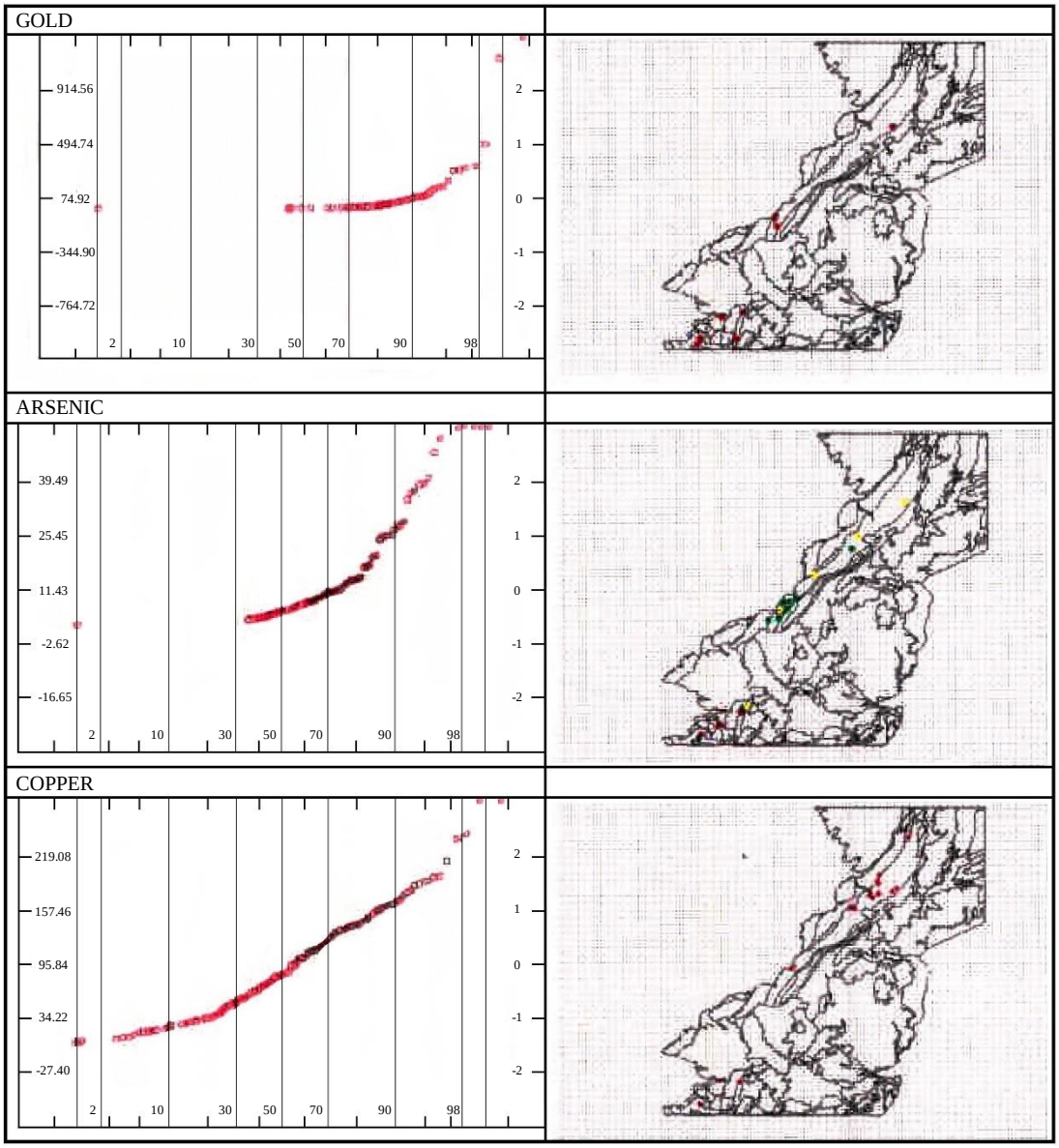

Figure 24. Cumulative probability plots and lithologically normalised anomaly maps for Au, As and Cu within the Pallatanga Unit. Axes indicate element concentration (left), standard deviation from mean concentration (right) and percentile class (base). Note: The presence of individual points on the anomaly maps reflects their exceedance of a threshold defined from cumulative probability plots for Pallatanga Unit samples. The colour coding of individual points reflects their percentile class within the population for the entire 2°-3°S area (see Figs 7-22).

Table 9. Pallatanga Unit. Summary Statistics.

	Count	Mean	Std. Dev	Min	Max	Median
Au	170	74.92	419.82	3.33	4989	1.995
Ag	170	0.66	NA	0.66	0.66	4.33
Cu	170	95.84	61.62	8	342	21.5
Pb	170	9.27	12.95	2.66	102	36
Zn	170	96.61	48.76	15.625	336	16.3125
Mo	170	1.88	1.90	0.9	17	6.5
Ni	170	86.10	106.35	2.2	560	34
Co	170	26.70	11.04	6	52	7
Cd	170	0.63	1.32	0.46	17.2	4
Bi	170	4.28	1.44	4	19	4
Fe	170	6.00	2.01	1.5	10	106
Mn	170	893.95	400.99	202	2566	108
Te	170	6.80	0.94	6.66	14	11.5
Ba	170	73.09	48.27	6	292.5	67
Cr	170	94.01	71.02	10	430.5	109
V	170	171.04	91.14	39	637	40.5
Sn	170	13.98	3.24	13.33	43	13.33
W	170	13.33	NA	13.33	13.33	13.33
La	170	9.90	9.14	0.66	66	4
Al	170	3.16	1.20	0.62	7.14	2.05
Mg	170	1.54	0.95	0.21	4.975	1.1975
Ca	170	1.23	0.84	0.13	4.59	0.14
Na	170	0.04	0.03	0.01	0.15	0.04
K	170	0.07	0.06	0.007	0.46	0.155
Sr	170	32.61	22.02	1	93	11
Y	170	7.62	3.61	3	23	7
Ga	170	6.67	3.98	1.33	17	7
Li	170	9.82	6.36	1.833	34	5
Nb	170	3.98	5.38	0.66	32	5
Sc	170	11.46	7.95	3.33	39	6.66
Ta	170	6.66	NA	6.66	6.66	3.645
Ti	170	0.21	0.12	0.007	0.63	0.645
Zr	170	7.49	5.47	0.66	29.5	6.45
As	170	11.43	14.08	2.66	77	2.66
Sb	170	1.66	1.46	1.26	15.917	1.26
Hg	170	0.17	0.44	0.026	3.953	0.064

The cumulative probability plot for Au (Fig. 24) highlights three sub-populations with a threshold at 195 μg/kg (95th %ile). Following normalization, the corresponding Au anomaly plot (Fig. 24) highlights seven prospective anomalies. The highest individual Au value (4989 μg/kg) is recorded in the headwaters of the Río Pijilí (ref. 668861-9671581) in a N-trending faulted inlier of Pallatanga Unit intruded by a granodiorite. There is no attendant enrichment of metalloids (As 2.66 mg/kg; Sb 1.26 mg/kg). Artisanal Au workings are evident several km downstream within the catchment. Approximately 10 km to the west (ref. 656882-9671188) a value of 1160 μg/kg Au occurs in an analogous setting at the faulted western contact of the same granodiorite intrusion with the Pallatanga Unit. Anomalous values of Cu (238 mg/kg), As (65 mg/kg), Sb (8.75 mg/kg) and Hg (0.7 mg/kg) are also recorded. The cumulative probability plot for As depicts a four component population from which a functional threshold of 21.5 mg/kg (86th %ile) can be derived. The colour-indices on the corresponding As anomaly map (Fig. 24) confirm that enrichment within the Pallatanga Unit does not exceed the 75th %ile of the (whole) 2°-3°S dataset. Spatial covariation with Au is strictly limited.

5.4.3 Macuchi Unit

The Macuchi Unit of the GIMP 2°-3°S area encompasses 152 sampling stations, the summary statistics for which are presented in Table 10. A typical calc-alkaline volcanic signature is recorded, with relatively high backgrounds for Ca (1.8), Cu (2), Co (1.5) and V (1.5), high Cu/Cr ratios and low Pb (0.5) and As (0.3). A lithogeochemical distinction is evident between the predominantly andesitic and basaltic pillow lavas of the eastern Macuchi Unit and the tuffs and volcanosedimentary facies to the west. The cumulative probability plot for Au (Fig. 25) shows three discrete components with an inflection at the base of the third limb corresponding to a threshold of 60 μg/kg (91st %ile). Values in excess of this occur exclusively in a sector of basaltic-andesitic pillow lavas in the eastern part of the Macuchi Unit. No identifiable anomalies occur in the tuffaceous and volcanosedimentary lithologies to the west. Two anomalous values to 414 μg/kg (with coincident Bi enrichment) occur in tributaries of the Río Chimbo (ref. 719502-9775689) at the faulted contact with a small granodiorite stock. Anomalies to 451 μg/kg occur in tributaries of the Río Loro. Free gold was not widely reported in heavy mineral concentrates from the eastern Macuchi Unit. Most anomalies are ascribed to refractory Au in disseminated pyrite within the basaltic facies. The As population displays two components with an inflection at ca. 10 mg/kg (93rd %ile). The coincidence of the higher As values with Au is poor, only one As-anomalous sample yielded >50 μg/kg Au. The threshold defined for Cu (160 mg/kg) is high relative to all other lithologies except the Pallatanga Unit. Anomalous values in excess of this level show no consistent trend within the Macuchi Unit.

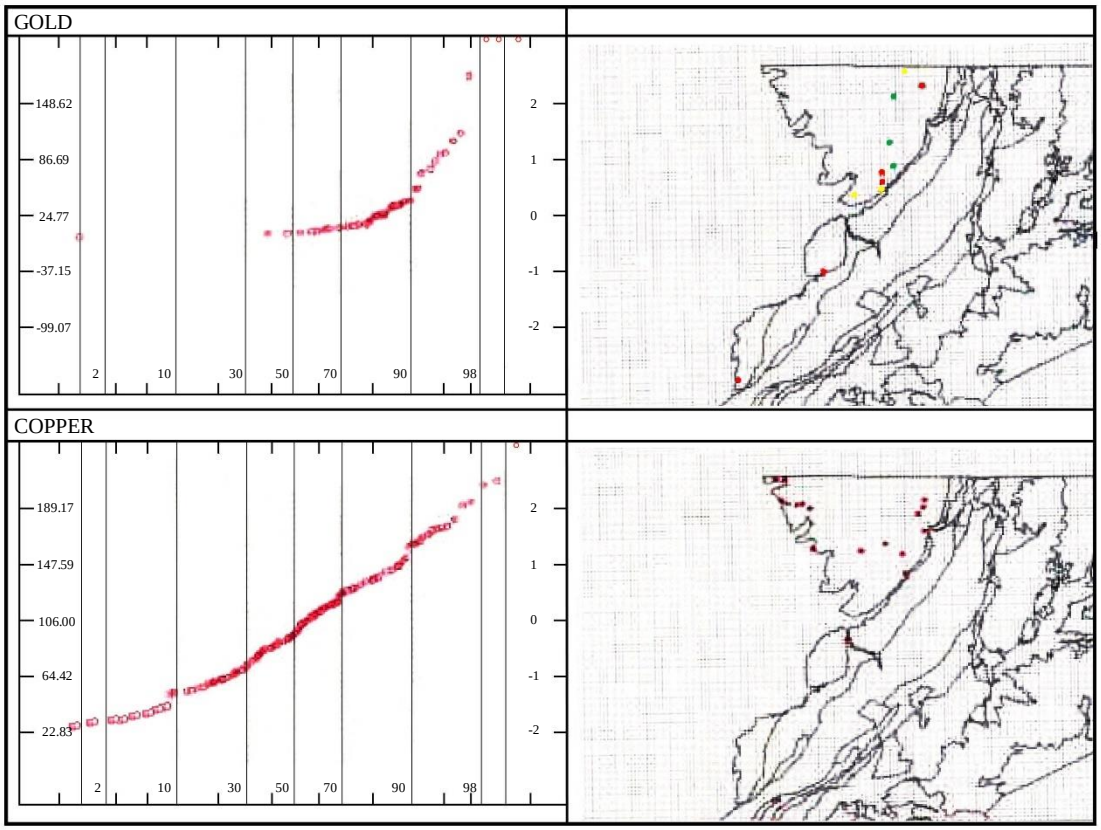

Figure 25. Cumulative probability plots and lithologically normalised anomaly maps for Au and Cu within the Macuchi Unit. Axes indicate element concentration (left), standard deviation from mean concentration (right) and percentile class (base). Note: The presence of individual points on the anomaly maps reflects their exceedance of a threshold defined from cumulative probability plots for Macuchi Unit samples. The colour coding of individual points reflects their percentile class within the population for the entire 2°-3°S area (see Figs 7-22).

Table 10. Macuchi Unit. Summary statistics.

	Count	Mean	Std. Dev	Min	Max	Median
Au	152	24.77	61.92252	3.33	451	7
Ag	152	0.66	NA	0.66	0.66	0.66
Cu	152	106.00	41.58437	34	264	101.5
Pb	152	6.38	4.738391	2.66	36	5
Zn	152	76.71	17.1975	30	129	76.5
Mo	152	1.94	1.87	0.9	13	0.9
Ni	152	20.38	8.26	7	58	19
Co	152	20.86	5.06	9	40.32	20
Cd	152	0.46	0.06	0.46	1.16	0.46
Bi	152	4.31	1.24	4	13	4
Fe	152	5.75	1.43	2.67	10	5.71
Mn	152	994.05	323.59	441	2338	979
Te	152	7.19	3.61	6.66	44	6.66
Ba	152	105.49	43.45	34	274	101
Cr	152	42.04	36.25	12	278	33
V	152	185.36	68.47	60	437	185
Sn	152	13.67	1.92	13.33	28	13.33
W	152	13.33	NA	13.33	13.33	13.33
La	152	7.47	6.19	0.66	36	6
Al	152	3.58	0.79	1.55	5.75	3.57
Mg	152	1.07	0.34	0.42	2.5	1.03
Ca	152	1.07	0.55	0.23	2.54	0.99
Na	152	0.03	0.02	0.007	0.12	0.03
K	152	0.09	0.08	0.02	0.82	0.07
Sr	152	48.42	27.51	0.66	133	53.5
Y	152	7.95	3.26	2	17	7.5
Ga	152	5.51	3.93	1.33	16	5
Li	152	7.44	4.16	0.8	32	7
Nb	152	3.93	5.47	0.66	24	1
Sc	152	12.90	6.32	3.33	35	12
Ta	152	7.10	3.50	6.66	44	6.66
Ti	152	0.16	0.04	0.01	0.31	0.17
Zr	152	6.84	2.93	0.66	15	6
As	152	5.20	8.17	2.66	83	2.66
Sb	152	1.31	0.38	1.26	5.3	1.26
Hg	152	0.04	0.02	0.02	0.18	0.026

5.4.4 Angamarca Group

The Angamarca Group tract encompasses 114 stations. Summary statistics (Table 11) show a calcareous composition with a significant mafic component. High relative backgrounds prevail for Ni (2.0), Co (1.5), Cr (1.5), Mg (1.5), Ca (1.5) and As (1.5). The Au cumulative probability plot (Fig. 26) shows an inflection at 37 µg/kg (93rd %ile). Higher values are concentrated in two areas, most notably close to Agua Caliente in the mid- and upper reaches of the Río Tixay catchment. The highest recorded values (1028 µg/kg at ref. 669293-9708144) on the NW-flank of Filo de Parva is coincident with the maximum As value for the 2°-3°S area (1402 mg/kg). Elevated Ag (2.3 mg/kg) and Hg (0.1 mg/kg) are also recorded. The locality lies 2-3 km north-west of a narrow highly silicified (and pyritic) outcrop of Pallatanga basalts. Anomalous As values exceed a threshold of 49 mg/kg (92nd %ile). With the exception of the Río Tixay locality, covariation between As and Au is limited. The principal zone of As enrichment occurs in the Estero Las Minas catchment, where sediments holding up to 596 mg/kg (ref. 700963-9738398) show no concomitant enrichment of other metals or metalloids.

5.4.5 Saraguro Group

5.4.5.1 Ocaña Formation

The Ocaña Formation is represented by 95 sampling stations (Table 12). An acid volcanic composition yields low backgrounds for Cu, Ni, V, Co and Cr (<1) and relatively high ambient concentrations of Pb (1.5) and Ba (2). Ratios of K/Ba are low. The cumulative probability distribution for Au within the Ocaña Formation (Fig. 27) shows an inflection at 56 µg /kg (92nd %ile). Strongly anomalous values of 1540 µg/kg and 1033 µg/kg respectively occur in the headwaters of the Quebrada de las Ánimas system 2 km west of San Antonio (ref. 699853-9720822) and in the upper Río Patul (ref. 691643-9707558). The former occurs in strongly silicified rhyolitic to rhyodacitic tuffs with abundant disseminated pyrite. The latter lies at a silicified dacite-diorite contact. Both catchments yield trailing values of 200-400 µg /kg Au with no coincident enrichment of pathfinder elements. An empirically defined As threshold of 48 mg/kg is significantly exceeded by a value of 423 mg/kg at the southern extremity of the Ocaña outcrop, with coincident enrichment of Bi to 28 mg/kg. Several anomalous Pb values to 159 mg/kg within the San Antonio area form the north-western limit of a major zone of Pb enrichment extending 30 km into the Chanlud Formation to the south and across the Tomebamba outcrop to the east.

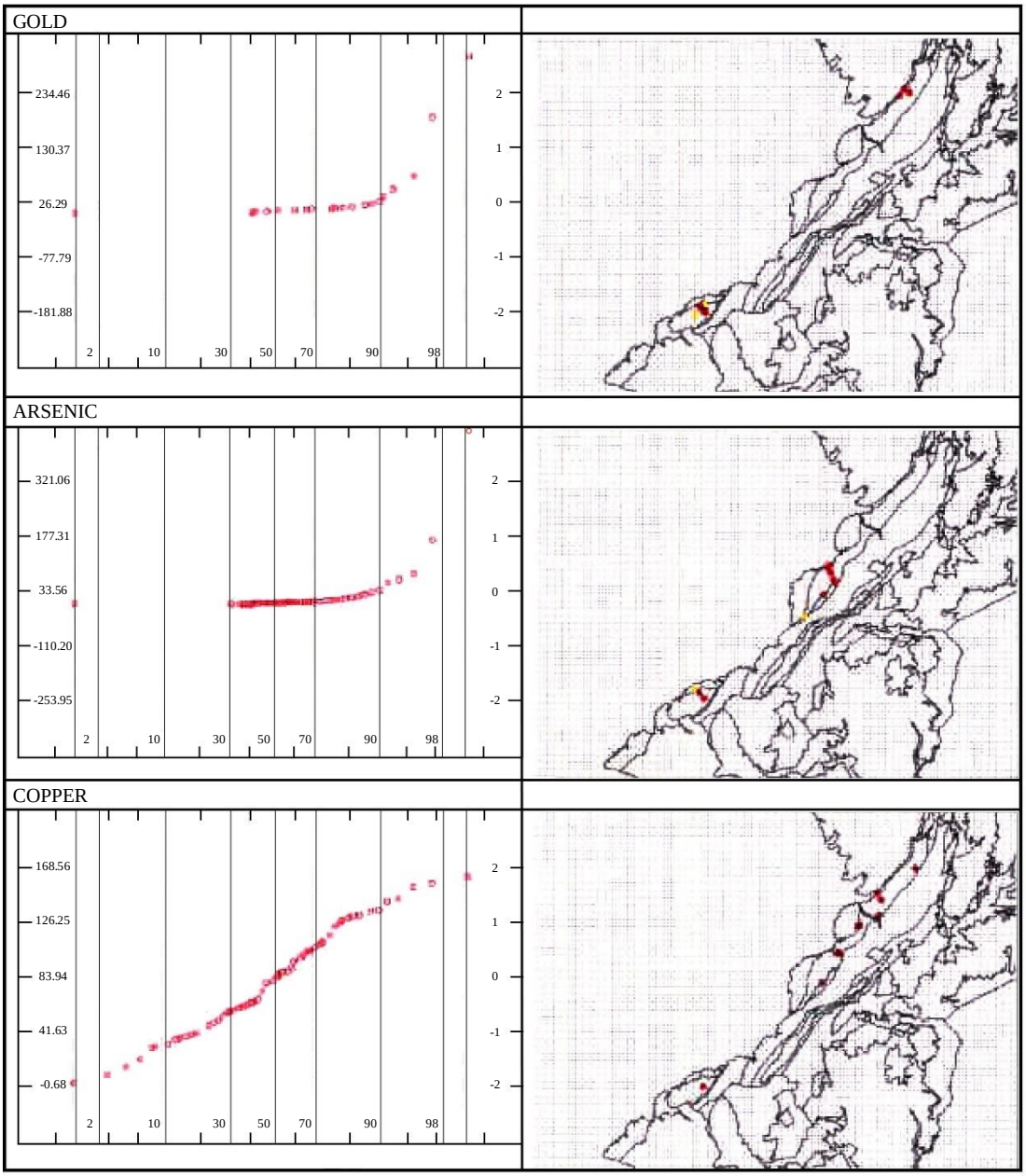

Figure 26. Cumulative probability plots and lithologically normalised anomaly maps for Au, As and Cu within the Angamarca Group. Axes indicate element concentration (left), standard deviation from mean concentration (right) and percentile class (base). Note: the presence of individual points on the anomaly maps reflects their exceedance of a threshold defined from cumulative probability plots for Angamarca Group samples. The colour coding of individual points reflects their percentile class within the population for the entire 2°-3°S area (see Figs 7-22).

Table 11. Angamarca Group. Summary Statistics

	Count	Mean	Std. Dev	Min	Max	Median
Au	114	26.29	104.08	3.33	1028.00	7.00
Ag	114	0.70	0.29	0.66	3.25	0.66
Cu	114	83.94	42.31	3.00	223.00	81.50
Pb	114	7.73	5.90	2.66	48.17	7.00
Zn	114	79.45	26.51	3.33	181.00	81.50
Mo	114	1.96	1.52	0.90	7.00	0.90
Ni	114	45.59	42.10	2.20	279.00	41.75
Co	114	21.23	9.07	1.73	46.50	21.00
Cd	114	0.55	0.45	0.46	3.70	0.46
Bi	114	4.34	1.27	4.00	12.00	4.00
Fe	114	5.35	1.62	0.01	10.00	5.32
Mn	114	759.87	317.30	22.66	1551.00	732.00
Te	114	7.43	5.06	6.66	56.00	6.66
Ba	114	98.46	68.52	3.60	457.00	84.25
Cr	114	64.66	35.88	4.00	236.00	58.50
V	114	149.70	72.28	0.66	436.00	132.00
Sn	114	13.74	1.94	13.33	24.00	13.33
W	114	13.40	0.72	13.33	21.00	13.33
La	114	8.22	6.24	0.66	31.00	7.00
Al	114	2.99	1.06	0.01	5.97	2.84
Mg	114	1.17	0.61	0.01	3.80	1.14
Ca	114	1.08	0.78	0.01	3.46	0.88
Na	114	0.03	0.02	0.01	0.13	0.03
K	114	0.11	0.09	0.01	0.47	0.08
Sr	114	31.51	19.90	-1.00	83.00	33.00
Y	114	6.73	3.10	0.66	17.00	6.00
Ga	114	5.42	3.44	1.33	16.00	5.00
Li	114	14.23	8.21	0.80	45.00	13.00
Nb	114	2.33	3.44	0.66	20.00	0.66
Sc	114	10.82	6.67	3.33	39.00	10.00
Ta	114	7.66	7.26	6.66	77.00	6.66
Ti	114	0.15	0.10	0.01	0.47	0.12
Zr	114	5.79	5.26	0.66	26.50	4.00
As	114	33.56	143.75	2.66	1402.00	6.65
Sb	114	1.34	0.43	1.26	4.20	1.26
Hg	114	0.10	0.23	0.03	2.38	0.05

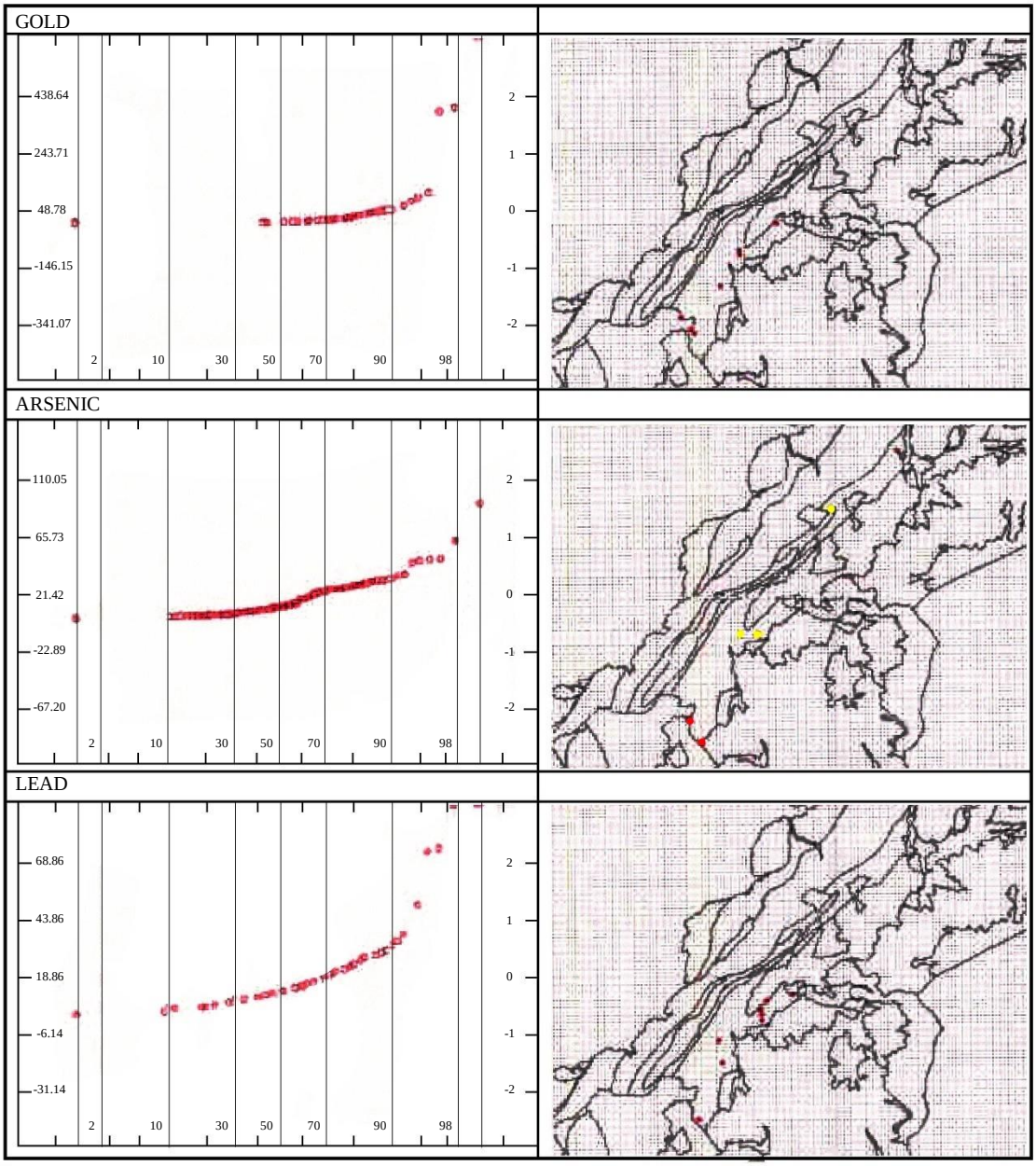

Figure 27. Cumulative probability plots and lithologically normalised anomaly maps for Au, As and Pb within the Ocaña Formation. Axes indicate element concentration (left), standard deviation from mean concentration (right) and percentile class (base). Note: the presence of individual points on the anomaly maps reflects their exceedance of a threshold defined from cumulative probability plots for Ocaña Formation samples. The colour coding of individual points reflects their percentile class within the population for the entire 2°-3°S area (see Figs 7-22).

Table 12. Ocaña Formation. Summary Statistics

	Count	Mean	Std. Dev	Min	Max	Median
Au	95	48.78	194.93	3.33	1540.00	6.00
Ag	95	0.66	NA	0.66	0.66	0.66
Cu	95	35.96	42.99	3.00	383.00	26.00
Pb	95	18.86	25.00	2.66	159.00	12.00
Zn	95	91.25	79.35	9.00	707.00	75.00
Mo	95	2.36	1.93	0.90	9.00	2.00
Ni	95	18.59	42.01	2.20	316.00	12.00
Co	95	13.64	6.57	1.73	35.00	13.00
Cd	95	0.65	0.89	0.46	8.75	0.46
Bi	95	4.86	3.02	4.00	28.00	4.00
Fe	95	4.55	1.69	0.81	10.00	4.52
Mn	95	697.47	313.20	39.00	2157.00	624.00
Te	95	7.19	3.70	6.66	36.00	6.66
Ba	95	145.41	87.34	9.00	703.00	131.00
Cr	95	31.00	27.40	2.46	173.00	24.00
V	95	108.72	62.95	8.00	340.00	106.00
Sn	95	14.12	3.99	13.33	40.00	13.33
W	95	13.40	0.68	13.33	20.00	13.33
La	95	10.97	13.27	0.66	129.00	9.00
Al	95	2.11	0.87	0.49	5.47	1.95
Mg	95	0.71	0.52	0.03	4.08	0.65
Ca	95	0.76	0.47	0.03	2.98	0.66
Na	95	0.04	0.03	0.01	0.15	0.03
K	95	0.09	0.03	0.01	0.16	0.09
Sr	95	41.37	33.96	0.66	174.00	35.00
Y	95	6.88	3.56	0.66	33.00	7.00
Ga	95	4.03	3.15	1.33	16.00	3.00
Li	95	11.10	5.25	0.80	28.00	11.00
Nb	95	2.82	3.68	0.66	20.00	1.00
Sc	95	4.72	2.26	3.33	13.00	3.33
Ta	95	6.97	3.01	6.66	36.00	6.66
Ti	95	0.10	0.08	0.01	0.39	0.08
Zr	95	4.52	4.40	0.66	22.00	3.00
As	95	21.42	44.31	2.66	423.40	11.80
Sb	95	1.71	1.08	1.26	7.60	1.26
Hg	95	0.23	1.79	0.03	17.47	0.04

5.4.5.2 Chulo Unit

The Chulo Unit outcrop incorporates 53 sampling stations, summary statistics for which (Table 13) confirm an acid composition with a high Ba background (2) and extremely low ambient levels of Co (0.5), Cu (0.3), Ni (0.25), Fe (0.5), Cr (0.2) and V (0.3). The threshold defined for Au (Fig. 28) is 80 μg/kg (90th %ile). An anomaly of 3127 μg/kg Au with 3.65 mg/kg Ag in the Quebrada Chocarhuaren system (ref. 698051-9700569) possibly signifies epithermal mineralisation in silicified andesitic volcanics of the overlying Chanlud Formation which outcrops in the catchment headwaters. Additional anomalies include values of 432 μg/kg Au in the Río de Curiquinga (ref. 699548-9699316) and 442 μg/kg (with modest As and Sb enrichment) in the Río Miguir catchment (ref. 687806-9690399). Covariation of As with Au over the Chulo Unit is otherwise limited. A threshold Ba value of 352 mg/kg (86th %ile) for the Chulo Unit lies in the uppermost 1 %ile of the 2°-3°S dataset as a whole. Values above this level (to 1073 mg/kg; ref. 694025-9693656) are influenced by altitude and soil type, notably the Río Cajas headwaters where organic overburden induces substantial mobilization and co-precipitation with hydrous Fe-Mn oxides. This is strongly suggested by the coincident enrichment of Ba with Mn to ca. 1%, Zn to >1000 mg/kg and As to ca. 60 mg/kg.

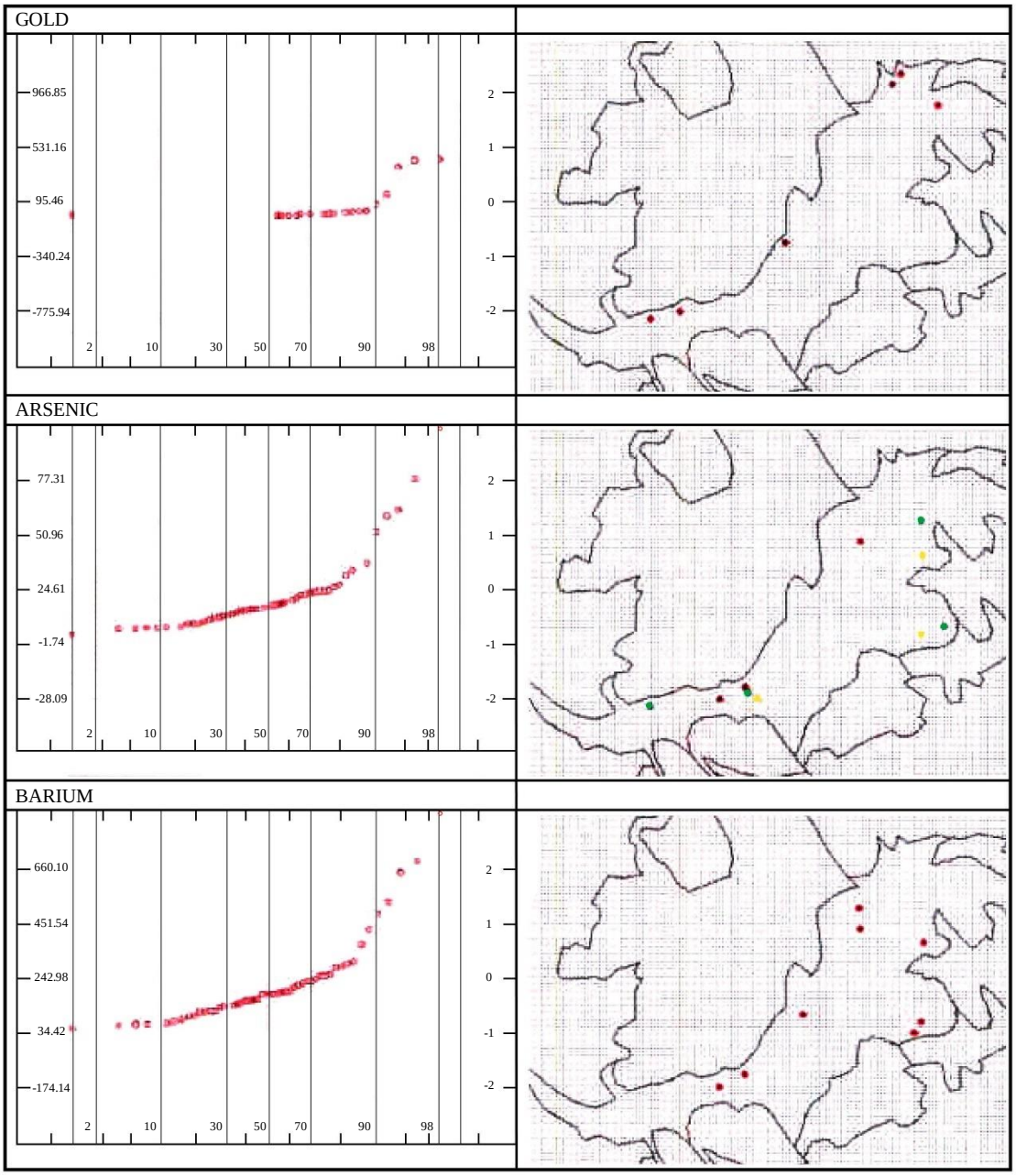

Figure 28. Cumulative probability plots and lithologically normalised anomaly maps for Au, As and Ba within the Chulo Unit. Axes indicate element concentration (left), standard deviation from mean concentration (right) and percentile class (base). Note: the presence of individual points on the anomaly maps reflects their exceedance of a threshold defined from cumulative probability plots for Chulo Unit samples. The colour coding of individual points reflects their percentile class within the population for the entire 2°-3°S area (see Figs 7-22).

Table 13: Chulo Unit. Summary Statistics

	Count	Mean	Std. Dev	Min	Max	Median
Au	53	95.46	435.70	3.33	3127.00	3.33
Ag	53	0.73	0.42	0.66	3.65	0.66
Cu	53	15.91	23.59	3.00	126.50	9.00
Pb	53	12.22	6.83	2.66	40.50	10.00
Zn	53	111.68	162.83	23.00	1052.50	60.00
Mo	53	2.55	2.67	0.90	13.00	2.00
Ni	53	5.91	6.63	2.20	50.00	5.00
Co	53	7.62	3.91	4.00	22.50	7.00
Cd	53	0.78	0.79	0.46	4.20	0.46
Bi	53	4.08	0.55	4.00	8.00	4.00
Fe	53	2.42	0.87	0.88	5.71	2.33
Mn	53	1946.17	2309.15	222.00	10319.00	1185.00
Te	53	6.66	NA	6.66	6.66	6.66
Ba	53	242.98	208.56	49.00	1073.00	189.00
Cr	53	7.74	3.25	2.46	16.00	7.00
V	53	31.92	14.69	10.00	93.50	30.00
Sn	53	13.33	NA	13.33	13.33	13.33
W	53	13.33	NA	13.33	13.33	13.33
La	53	10.97	5.18	0.66	27.00	11.00
Al	53	1.71	0.61	0.37	3.52	1.64
Mg	53	0.33	0.14	0.02	0.58	0.33
Ca	53	0.67	0.73	0.13	5.47	0.51
Na	53	0.02	0.01	0.01	0.07	0.02
K	53	0.10	0.05	0.03	0.38	0.10
Sr	53	36.07	38.92	-1.00	276.00	32.00
Y	53	7.50	3.30	3.00	19.00	6.00
Ga	53	4.57	5.61	1.33	34.00	3.00
Li	53	19.05	11.75	0.80	58.00	18.00
Nb	53	1.99	2.54	0.66	17.00	1.00
Sc	53	3.33	0.00	3.33	3.33	3.33
Ta	53	6.66	0.00	6.66	6.66	6.66
Ti	53	0.03	0.03	0.01	0.10	0.03
Zr	53	1.46	1.07	0.66	6.00	1.00
As	53	24.61	26.35	2.66	145.40	16.40
Sb	53	1.77	1.39	1.26	8.70	1.26
Hg	53	0.06	0.04	0.03	0.28	0.05

5.4.5.3 Filo Cajas Unit

Only 17 samples are incorporated in the Filo Cajas tract. The validity of summary statistics (Table 14) and cumulative probability plots is therefore limited. A high mean Au value of 136.98 µg/kg is, for example, strongly biased by outliers to 784 µg/kg (the median value is 11 µg/kg). An acid signature is indicated by low backgrounds for Cu (0.6), Ni (0.6), Cr (0.3) and V (0.3). High mean levels of Pb (1.7) and Ba (1.4) prevail relative to the regional background. A threshold Au value of 94 µg/kg (86th %ile) is exceeded in three localities (Fig. 29) each of which has values within the uppermost 1 %ile of the entire dataset. A value of 521 µg/kg in the headwaters of the Río Putucay (ref. 688855-9702706) lies 1 km downstream of silicified andesites assigned to a Chanlud Formation outlier. An anomaly of 717 µg/kg Au with modest enrichment of As (21 mg/kg) and Hg (0.108 mg/kg) occurs in Q. El Parco (ref. 686941-9691901), 1 km downstream of an intrusive contact on the south-western margin of the Filo Cajas Unit. Mineralisation along the NNW-trending Q. Suerococha Fault (ref. 690543-9691275) is indicated by a value of 784 µg/kg Au with coincident enrichment of As to 29 mg/kg (in excess of the empirical threshold derived from the As cumulative probability plot in Fig. 29).

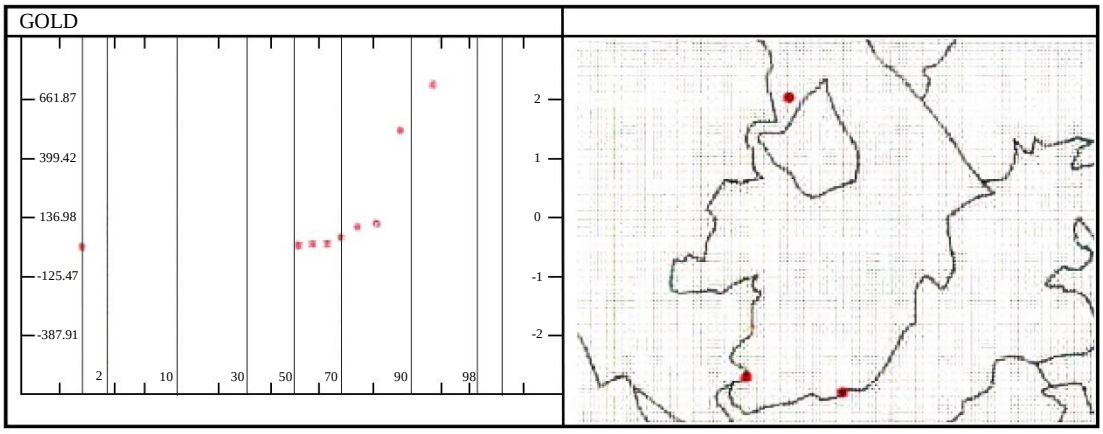

Figure 29. Cumulative probability plots and lithologically normalised anomaly maps for Au within the Filo Cajas Unit. Axes indicate element concentration (left), standard deviation from mean concentration (right) and percentile class (base). Note: the presence of individual points on the anomaly maps reflects their exceedance of a threshold defined from cumulative probability plots for Filo Cajas Unit samples. The colour coding of individual points reflects their percentile class within the population for the entire 2°-3°S area (see Figs 7-22).

Table 14. Filo Cajas Unit. Summary Statistics

	Count	Mean	Std. Dev	Min	Max	Median
Au	17	136.98	262.45	3.33	784.00	11.00
Ag	17	0.69	0.13	0.66	1.20	0.66
Cu	17	32.29	40.53	10.00	171.00	15.00
Pb	17	21.24	16.99	7.00	68.00	15.00
Zn	17	79.62	48.29	3.33	185.94	72.00
Mo	17	3.27	2.57	0.90	9.00	2.00
Ni	17	13.00	8.56	4.00	35.00	10.00
Co	17	16.76	11.89	6.00	47.00	13.00
Cd	17	0.79	0.55	0.46	2.10	0.46
Bi	17	4.18	0.73	4.00	7.00	4.00
Fe	17	3.24	1.13	1.56	5.45	3.13
Mn	17	706.12	364.75	267.00	1283.00	676.00
Te	17	6.66	0.00	6.66	6.66	6.66
Ba	17	165.82	83.18	61.00	330.00	165.00
Cr	17	11.76	6.38	4.00	28.00	10.00
V	17	42.71	19.52	20.00	92.00	36.00
Sn	17	13.33	0.00	13.33	13.33	13.33
W	17	13.33	0.00	13.33	13.33	13.33
La	17	9.61	4.86	0.66	17.00	9.00
Al	17	2.04	0.61	0.93	3.29	1.99
Mg	17	0.55	0.35	0.20	1.57	0.42
Ca	17	0.62	0.44	0.07	1.52	0.52
Na	17	0.02	0.01	0.01	0.04	0.02
K	17	0.10	0.03	0.06	0.16	0.09
Sr	17	28.65	17.39	0.66	73.00	27.00
Y	17	6.35	2.03	3.00	11.00	7.00
Ga	17	2.43	1.22	1.33	5.00	2.00
Li	17	18.35	5.48	12.00	32.00	17.00
Nb	17	1.72	1.35	0.66	4.00	1.00
Sc	17	3.49	0.65	3.33	6.00	3.33
Ta	17	6.66	0.00	6.66	6.66	6.66
Ti	17	0.02	0.03	0.01	0.12	0.01
Zr	17	1.15	0.82	0.66	3.00	0.66
As	17	21.15	9.27	4.00	33.50	22.10
Sb	17	1.46	0.57	1.26	3.20	1.26
Hg	17	0.06	0.05	0.03	0.23	0.05

5.4.5.4 Tomebamba Unit

Two areas of the Tomebamba Unit encompass 71 sampling stations within the mapped area (Table 15). Low backgrounds prevail with respect to Cu (0.5), Ni (0.5), Cr (0.5) and V (0.6), with relatively high concentrations of Pb (2) and As (1.8). The Au cumulative probability distribution (Fig. 30) shows an inflection at 80 μg/kg. Higher values occur in the Río Corazón at the western margin of the Cañar Valley outcrop (ref. 703952-9720295), where polymetallic mineralisation at the contact with a minor granodiorite intrusion yields 474 μg/kg Au, 2.3 mg/kg Ag, 170 mg/kg Pb, 441 mg/kg Zn, 10 mg/kg Bi and 44 mg/kg As. Numerous rhyolitic intrusive units outcrop 1-2 km upstream of this anomaly in a zone of intensely altered pyritic andesites. In the Quebrada Osoyacu catchment (ref. 709525-9723086) a value of 416 μg/kg Au is recorded in sediments 1 km downstream of minor artisanal workings.

A threshold As value of 52 mg/kg corresponds to the 86th %ile in the Tomebamba Unit population. Several higher values occur in the south-east flowing Río Tomebamba system (e.g. refs. 707398-9687921; 705975-9869591; 709559-9686519; 715765-968437; 714866-968362) to a maximum of 255 mg/kg As with coincident enrichment of Sb to 14 mg/kg. Much of the catchment is comprised of partially altered andesitic tuffs which in places contain disseminated pyrite The cumulative probability distribution for Pb indicates a threshold value of ca. 40 mg/kg for the Tomebamba Unit. In addition to the Río Corazón anomaly described above, a modest anomaly of 89 mg/kg Pb is coincident with 511 mg/kg Zn, 2.8 mg/kg Ag, 49 mg/kg As, 17 mg/kg Sb and 0.3 mg/kg Hg in a zone of silicified sulphidic tuffs at the eastern extremity of the Cañar Valley outcrop (Río de Raura; ref. 714822-9721513).

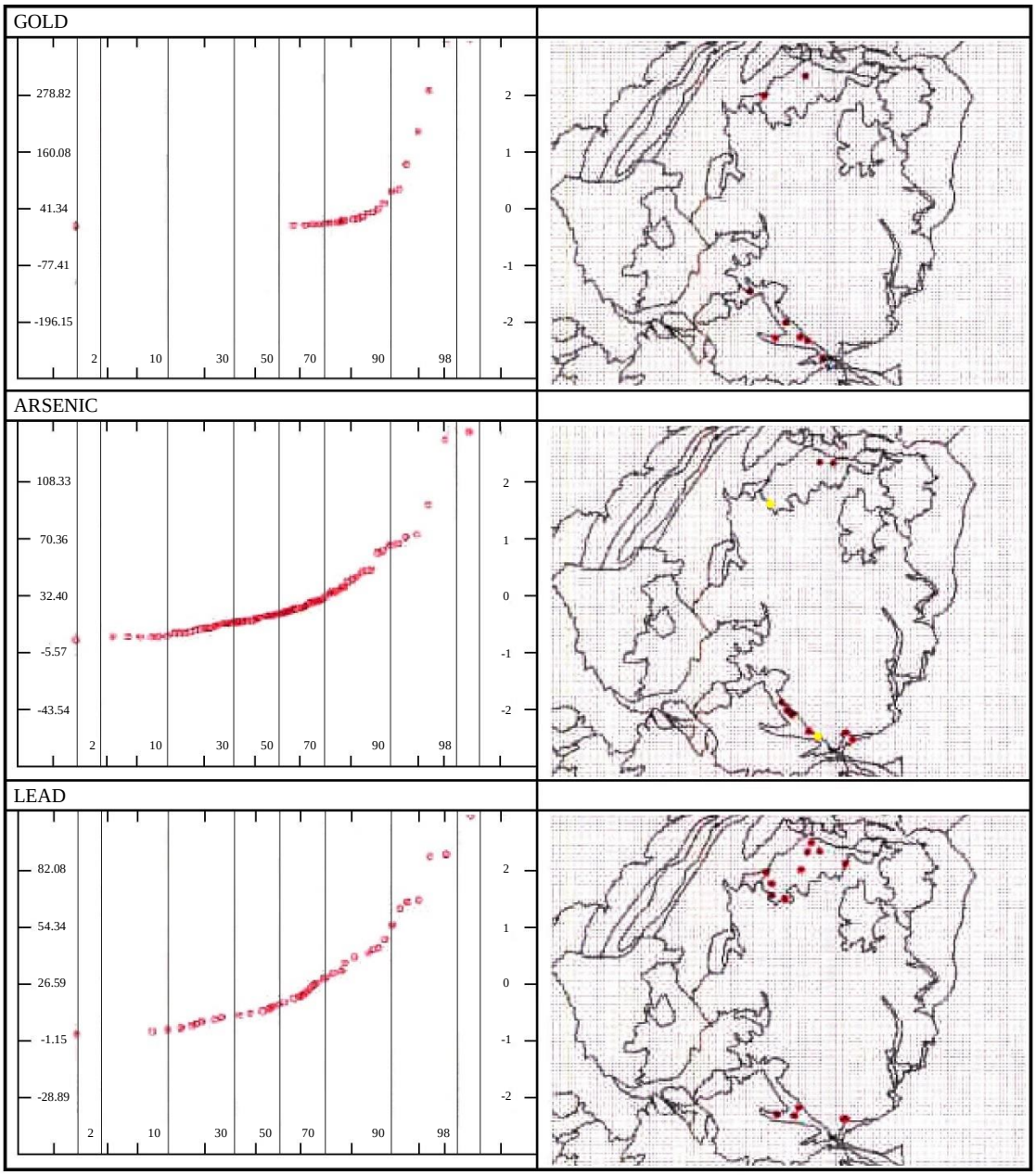

Figure 30. Cumulative probability plots and lithologically normalised anomaly maps for Au, As and Pb within the Tomebamba Tuffs. Axes indicate element concentration (left), standard deviation from mean concentration (right) and percentile class (base). Note: the presence of individual points on the anomaly maps reflects their exceedance of a threshold defined from cumulative probability plots for Tomebamba samples. The colour coding of individual points reflects their percentile class within the population for the entire 2°-3°S area (see Figs 7-22).

Table 15. Tomebamba Unit. Summary Statistics

	Count	Mean	Std. Dev	Min	Max	Median
Au	71	41.34	118.74	3.33	739.00	3.33
Ag	71	0.71	0.32	0.66	2.80	0.66
Cu	71	25.90	33.82	3.00	197.50	17.00
Pb	71	26.59	27.74	2.66	170.00	17.00
Zn	71	124.20	105.47	11.00	643.00	90.00
Mo	71	1.98	1.36	0.90	8.00	1.83
Ni	71	9.88	5.49	2.20	25.00	9.00
Co	71	11.80	5.17	1.73	32.00	11.50
Cd	71	0.78	1.12	0.46	7.40	0.46
Bi	71	4.18	0.85	4.00	10.00	4.00
Fe	71	3.77	1.42	0.61	8.85	3.62
Mn	71	877.30	452.21	129.00	2590.00	763.00
Te	71	6.66	NA	6.66	6.66	6.66
Ba	71	116.99	58.15	13.00	311.00	100.00
Cr	71	23.13	17.04	2.46	106.00	18.00
V	71	74.27	47.70	16.00	291.00	62.00
Sn	71	13.33	NA	13.33	13.33	13.33
W	71	13.33	NA	13.33	13.33	13.33
La	71	10.01	5.24	0.66	24.00	10.00
Al	71	2.00	0.63	0.19	3.91	2.03
Mg	71	0.67	0.22	0.06	1.22	0.66
Ca	71	0.79	1.10	0.06	9.11	0.56
Na	71	0.02	0.01	0.01	0.08	0.02
K	71	0.09	0.04	0.02	0.25	0.08
Sr	71	26.54	20.12	0.66	86.00	25.00
Y	71	6.39	2.09	0.66	11.00	6.00
Ga	71	4.62	2.94	1.33	14.00	4.00
Li	71	21.26	9.85	2.00	51.00	21.00
Nb	71	1.69	1.81	0.66	8.00	0.66
Sc	71	3.76	1.10	3.33	8.00	3.33
Ta	71	6.66	NA	6.66	6.66	6.66
Ti	71	0.07	0.04	0.01	0.24	0.07
Zr	71	2.85	2.57	0.66	13.00	2.00
As	71	32.40	37.97	2.66	255.70	20.40
Sb	71	2.28	2.51	1.26	17.00	1.26
Hg	71	0.05	0.05	0.03	0.30	0.03

5.4.5.5 Chanlud Formation

The Chanlud Formation suite is the largest of the Saraguro Group, encompassing 213 sampling stations. Although predominantly andesitic, summary statistics for the unit (Table 16) are influenced by a substantial zone of more acid (dacitic to rhyodacitic) lavas in the upper parts of the Formation south of the Río Tomebamba. This internal lithogeochemical contrast is highlighted by the IDW-grids for the GIMP 2°-3°S area (Figs. 7-22), the southern Chanlud showing relative enrichment in Ba and depletion in Cr and Cu. The Au cumulative probability distribution (Fig. 31) indicates a threshold at ca. 59 μg/kg (93rd %ile). Exceedance of this is evident along a 10 km section of the Río Chulco and headwater tributaries, with five Au values in the range 86-300 μg/kg. The Q. Chanludpungo tributary (ref. 714215-9698657) shows coincident enrichment of Ag (2.7 mg/kg), Zn (400 mg/kg) and Pb (93 mg/kg). An As threshold of 65 mg/kg is exceeded sporadically throughout the outcrop of the Chanlud Formation to a maximum of 527 mg/kg, but these anomalies are generally unrelated to independent evidence of mineralisation. Exceptions occur in the upper Río Corazón valley, where five anomalous As values show coincident enrichment of Pb and Zn. This Pb-Zn enrichment forms part of a larger feature also extending eastward along the Río Machángara. In the south of the Chanlud tract, a value of 136 mg/kg As is accompanied by anomalous Sb (9.9 mg/kg), Bi (8 mg/kg) and Hg (0.561 mg/kg) close to the contact with a minor outcrop of the Plancharumi Formation.

An intense Hg anomaly of 36.7 mg/kg in the headwaters of the Río Patamarca (ref. 716310-9690325) has been confirmed through the analysis of three independent sediment sub-samples. The feature occurs independently of enrichment in any other metal or metalloid, in a zone dominated by unaltered andesites.

The lack of geochemical response to mineralisation at Cerro Alumbre (ref. 712500-9797200) is a significant feature of the data for the Chanlud Formation. This consists of a large zone of intensely silicified andesite breccias with abundant sulphides and iron oxides, which is flanked in the low ground to the south of the mountain by an extensive area of bog rich in ferruginous colloidal precipitates. The mineralisation is drained by the Quebrada de Cebadas, Quebrada Luchicarrumi and Río Machángara. Five samples from these systems yield no Au values in excess of the analytical detection limit, and have sub-threshold metalloid and base-metal concentrations.

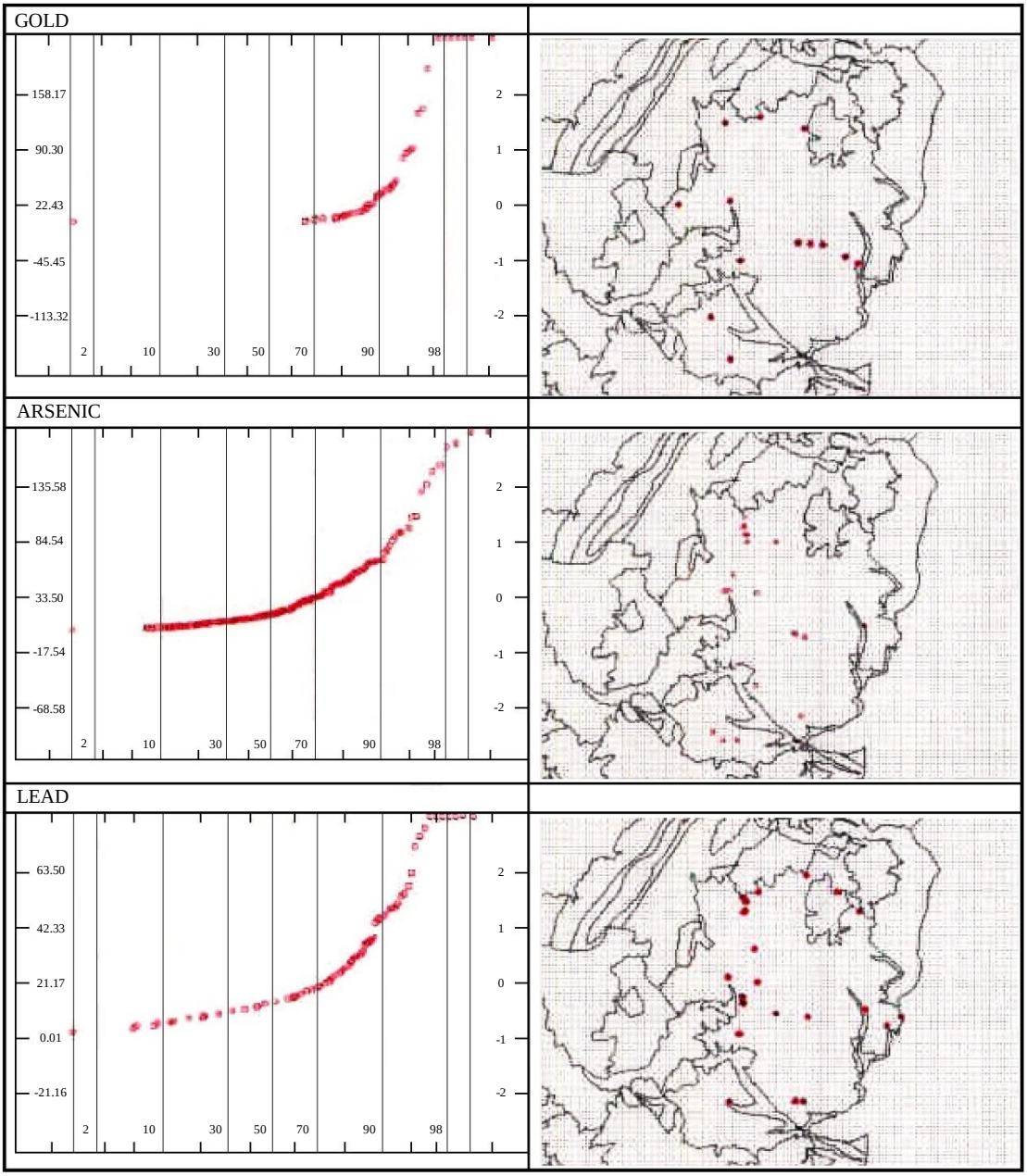

Figure 31. Cumulative probability plots and lithologically normalised anomaly maps for Au, As and Pb within the Chanlud Formation. Axes indicate element concentration (left), standard deviation from mean concentration (right) and percentile class (base). Note: the presence of individual points on the anomaly maps reflects their exceedance of a threshold defined from cumulative probability plots for Chanlud Formation samples. The colour coding of individual points reflects their percentile class within the population for the entire 2°-3°S area (see Figs 7-22).

Table 16. Chanlud Formation. Summary Statistics

	Count	Mean	Std. Dev	Min	Max	Median
Au	213	22.43	67.87	3.33	522.00	3.33
Ag	213	0.72	0.33	0.66	3.95	0.66
Cu	213	20.83	16.97	3.00	165.00	17.00
Pb	213	21.17	21.16	2.66	110.50	14.00
Zn	213	136.90	117.26	22.00	622.00	93.00
Mo	213	2.26	1.70	0.90	11.00	2.00
Ni	213	9.90	5.10	2.20	39.00	10.00
Co	213	12.40	5.30	3.00	45.00	12.00
Cd	213	0.94	1.11	0.46	9.60	0.46
Bi	213	4.49	1.44	4.00	11.00	4.00
Fe	213	3.91	1.25	1.19	10.00	3.86
Mn	213	1506.45	1885.69	80.00	18661.00	954.00
Te	213	6.83	2.49	6.66	43.00	6.66
Ba	213	132.57	107.35	11.00	1037.00	106.00
Cr	213	18.81	10.30	2.46	81.00	16.00
V	213	68.46	29.47	12.00	189.00	63.00
Sn	213	13.33	0.00	13.33	13.33	13.33
W	213	13.40	0.75	13.33	22.00	13.33
La	213	10.79	4.54	0.66	28.00	11.00
Al	213	2.21	0.68	0.92	4.13	2.16
Mg	213	0.66	0.28	0.03	1.67	0.64
Ca	213	0.70	0.38	0.01	2.20	0.61
Na	213	0.03	0.03	0.01	0.19	0.02
K	213	0.08	0.03	0.02	0.28	0.07
Sr	213	32.52	25.48	-1.00	156.00	29.00
Y	213	6.89	2.89	1.00	22.00	6.00
Ga	213	4.79	3.29	1.33	24.00	4.00
Li	213	20.18	10.25	0.80	66.00	19.00
Nb	213	1.93	2.05	0.66	10.00	1.00
Sc	213	4.23	1.54	3.33	10.00	3.33
Ta	213	6.92	3.79	6.66	62.00	6.66
Ti	213	0.07	0.05	0.01	0.29	0.07
Zr	213	3.04	2.49	0.66	16.00	2.00
As	213	33.50	51.04	2.66	527.30	17.80
Sb	213	1.83	1.14	1.26	9.90	1.26
Hg	213	0.24	2.51	0.03	36.72	0.05

5.4.5.6 Río Blanco Formation

The Río Blanco Formation is represented by 38 sampling stations. Summary statistics (Table 17) show concentrations of the most analysed elements to lie close to the regional mean for the area as a whole. Notable exceptions include Pb (1.8) and As (1.5), backgrounds for which are relatively high.

The cumulative frequency distribution for Au (Fig. 32) indicates a threshold of ca. 60 µg/kg for the Río Blanco Formation (90th %ile). Exceedance occurs in the Río Migsihuigsi catchment (ref. 680306-9685523) close to the Llano Largo prospect near Río Blanco, where a value of 940 µg/kg Au is coincident with 1.65 mg/kg Ag, 15.05 mg/kg Sb and 197 mg/kg As. This river follows one of two northeast-trending faults that confine the mineralisation which, in turn, is concentrated within zones of secondary Reidel shearing. Additional anomalies in the range 80-100 µg/kg Au occur in the Río Chorro and associated tributaries (e.g. ref. 681918-9688161) close to a highly silicified intrusive contact. The As threshold for the Río Blanco Formation is ca. 57 mg/kg (87th %ile). In addition to the Río Migsihuigsi Au-As anomaly, a further value of 142 mg/kg occurs in drainage to the southeast of the Llano Largo prospect.

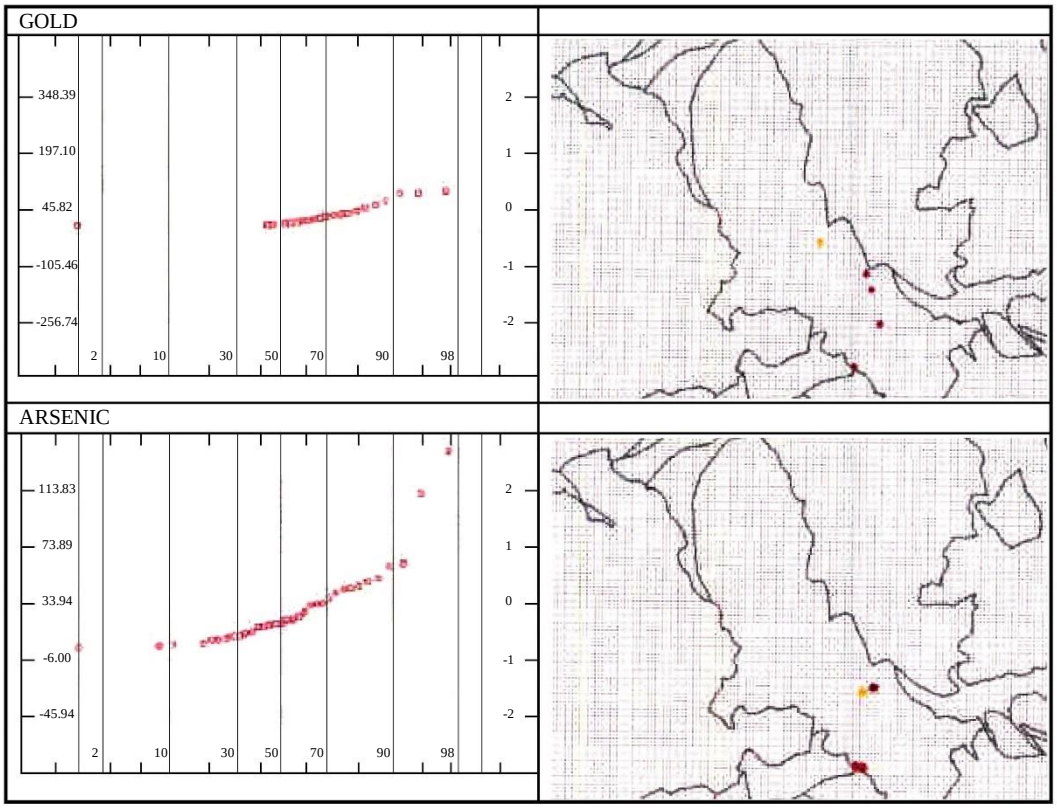

Figure 32. Cumulative probability plots and lithologically normalised anomaly maps for Au and As within the Río Blanco Formation. Axes indicate element concentration (left), standard deviation from mean concentration (right) and percentile class (base). Note: the presence of individual points on the anomaly maps reflects their exceedance of a threshold defined from cumulative probability plots for Río Blanco Formation samples. The colour coding of individual points reflects their percentile class within the population for the entire 2°-3°S area (see Figs 7-22).

Table 17. Río Blanco Formation. Summary Statistics

	Count	Mean	Std. Dev	Min	Max	Median
Au	38	45.82	151.28	3.33	940	8
Ag	38	0.68	0.160	0.66	1.65	0.66
Cu	38	37.65	19.65	8	102	36.5
Pb	38	23.07	21.83	7	132	17
Zn	38	97.76	44.04	24	245	87
Mo	38	1.95	1.57	0.9	7	0.9
Ni	38	13.72	6.19	4	33	13.5
Co	38	17.21	6.70	5	48	17
Cd	38	0.67	0.47	0.46	3.1	0.46
Bi	38	4.47	1.48	4	11	4
Fe	38	4.51	1.48	1.42	8.1	4.5425
Mn	38	844.97	366.29	250	2231	781.5
Te	38	6.66	2.60	6.66	6.66	6.66
Ba	38	91.25	33.31	42	212	84
Cr	38	34.97	16.16	6	66	36.5
V	38	94.51	37.71	38	174	91
Sn	38	13.76	1.85	13.33	22	13.33
W	38	13.33	4.15	13.33	13.33	13.33
La	38	8.13	6.13	0.66	36	6
Al	38	3.19	0.92	1.23	6.27	3.155
Mg	38	0.99	0.36	0.13	1.63	1.08
Ca	38	0.53	0.22	0.14	1.15	0.49
Na	38	0.02	0.01	0.007	0.05	0.02
K	38	0.07	0.06	0.007	0.32	0.06
Sr	38	33.92	23.85	-1	102	32
Y	38	6.18	2.32	2	12	6
Ga	38	5.71	3.72	1.33	20	5
Li	38	22.48	8.90	6	44	23
Nb	38	2.28	2.92	0.66	11	0.66
Sc	38	6.58	2.87	3.33	12	7
Ta	38	6.66	2.6	6.66	6.66	6.66
Ti	38	0.08	0.03	0.01	0.135	0.08
Zr	38	2.71	2.55	0.66	11	2
As	38	33.94	39.94	2.66	197.15	20.525
Sb	38	2.75	2.59	1.26	15.05	1.26
Hg	38	0.05	0.04	0.026	0.256	0.043

5.4.5.7 Soldados Formation

The Soldados Formation polygon encompasses 39 sampling stations (Table 18). The predominantly dacitic tuffs produce low backgrounds for elements of mafic affinity, with the exception of Zn (1.6) which is enriched in discrete zones of polymetallic mineralisation. High backgrounds prevail for As, Pb and Hg over substantial sectors of the outcrop. The cumulative probability distribution for Au (Fig. 33) is unusual, showing a series of increasingly anomalous outliers above the 72nd %ile (50 μg/kg). The most striking zone of enrichment occurs in the upper Río Angas system, notably the tributary Quebrada Chaupiurcu (ref. 687569-9681415). Here, auriferous polymetallic mineralisation is indicated by 100 μg/kg Au with 503 mg/kg Cu, 2.5 mg/kg Ag, 148 mg/kg Pb, 174 mg/kg Zn, 10.5 mg/kg Bi, 286 mg/kg As, 32.2 mg/kg Sb and 0.305 mg/kg Hg. At sample points approximately 200 m and 1.5 km downstream of the confluence of Q. Chaupiurcu with the Río Angas, Au values of 82 μg/kg and 334 μg/kg are recorded with coincident enrichment of Cd to 24.5 mg/kg, Pb to 74 mg/kg, Zn to 364 mg/kg, As to 74 mg/kg and Sb to 11.8 mg/kg. Additional Au anomalies of 192-379 μg/kg are recorded in the Río Soldados system (refs. 695934-9679678; 695720-9678340; 697714-9671701) and in the Río Yanuncay (706 μg/kg; ref. 697247-9674830) near the settlement of Soldados. The threshold As value determined for the Soldados Formation is 34 mg/kg (84th %ile). In addition to the Au-related As anomalies described above, a value of 119 mg/kg As in the northern sector of the Soldados Formation tract (ref. 694376-9682235) is ascribed to co-precipitation with hydrous Mn oxides (14.922 mg/kg Mn, 10.5 mg/kg Cd, 69 mg/kg Co, 1519 mg/kg Zn) in an area of predominantly poorly drained ground. Anomalous values of Cu occur exclusively in the Río Angas system, and are closely covariant with Au.

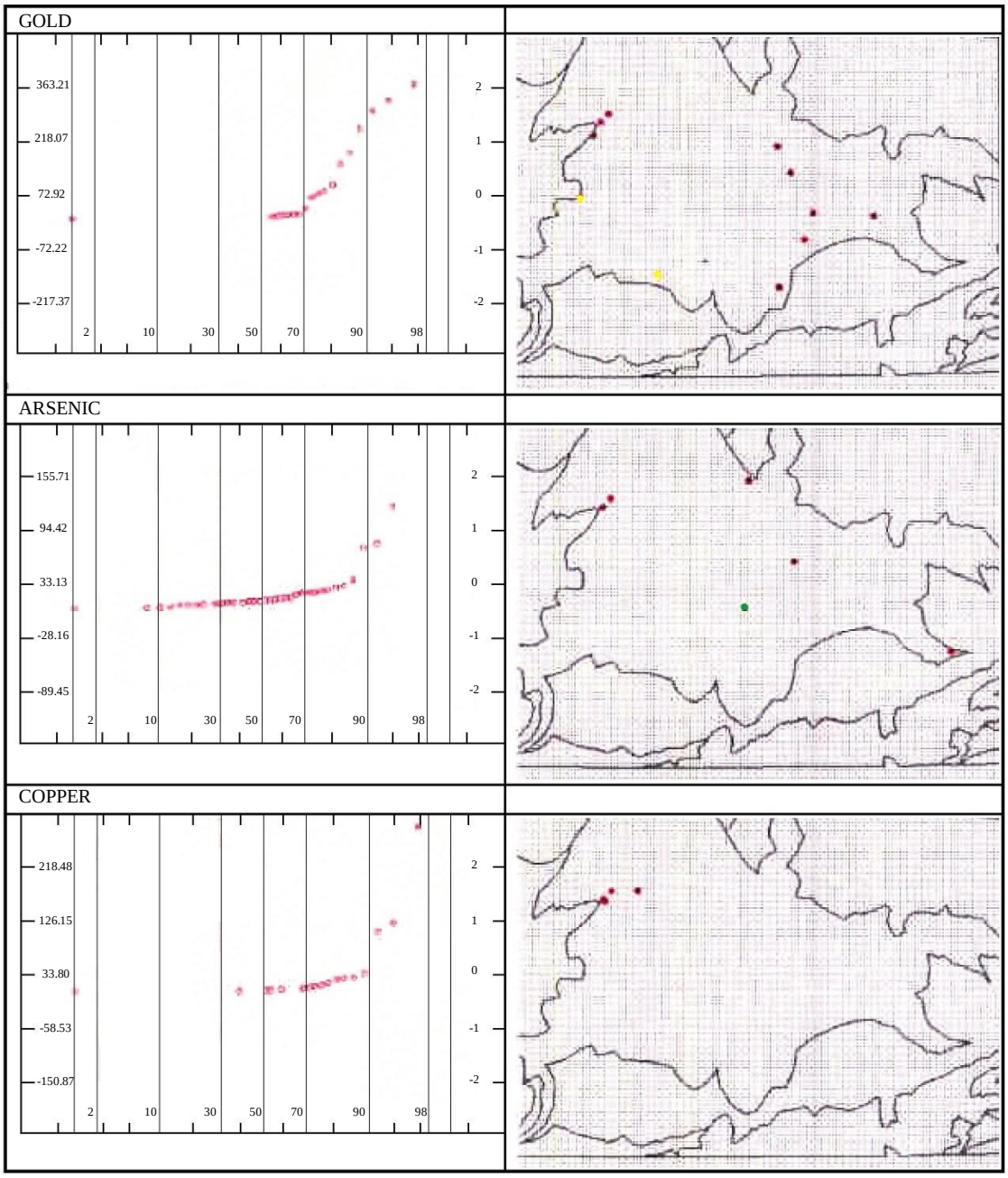

Figure 33. Cumulative probability plots and lithologically normalised anomaly maps for Au, As and Cu within the Soldados Formation. Axes indicate element concentration (left), standard deviation from mean concentration (right) and percentile class (base). Note: the presence of individual points on the anomaly maps reflects their exceedance of a threshold defined from cumulative probability plots for Soldados Formation samples. The colour coding of individual points reflects their percentile class within the population for the entire 2°-3°S area (see Figs 7-22).

Table 18. Soldados Formation. Summary Statistics

	Count	Mean	Std. Dev	Min	Max	Median
Au	39	72.92	145.14	3.33	706	3.33
Ag	39	0.70	0.29	0.66	2.5	0.66
Cu	39	33.80	92.33	3	503.5	6
Pb	39	19.31	27.70	2.66	148.5	12
Zn	39	158.72	285.80	3.33	1519	70
Mo	39	2.025	1.67	0.9	7.5	0.9
Ni	39	3.45	2.64	2.2	16	2.2
Co	39	9.46	13.33	1.73	69	5
Cd	39	1.23	2.20	0.46	10.5	0.46
Bi	39	4.46	1.69	4	11.665	4
Fe	39	2.54	1.61	0.29	9.11	2.12
Mn	39	1867.15	2819.00	159	14922	944
Te	39	6.66	2.68	6.66	6.66	6.66
Ba	39	168.141	114.42	10	588	135
Cr	39	6.99	4.33	2.46	18	6
V	39	39.42	22.6	9	109	34
Sn	39	13.33	4.09	13.33	13.33	13.33
W	39	13.33	4.09	13.33	13.33	13.33
La	39	9.64	4.38	0.66	19	10
Al	39	1.72	0.73	0.15	3.53	1.48
Mg	39	0.29	0.15	0.04	0.73	0.27
Ca	39	0.44	0.22	0.07	1.05	0.4
Na	39	0.02	0.01	0.007	0.05	0.02
K	39	0.073	0.03	0.007	0.13	0.07
Sr	39	33.08	32.40	-1	142	25
Y	39	5.61	2.53	0.66	12	5
Ga	39	3.97	4.25	1.33	24.665	2.665
Li	39	14.21	6.69	2	29	15
Nb	39	1.66	1.68	0.66	7	0.66
Sc	39	3.42	0.58	3.33	7	3.33
Ta	39	6.66	2.68	6.66	6.66	6.66
Ti	39	0.05	0.05	0.007	0.19	0.04
Zr	39	1.91	1.68	0.66	7	1
As	39	33.13	61.29	2.66	286.05	12.7
Sb	39	2.39	5.18	1.26	32.2	1.26
Hg	39	0.38	1.54	0.026	9.19	0.048

5.4.5.8 Plancharumi Formation

The outcrop of the Plancharumi Formation encompasses 41 sampling stations. This predominantly rhyolitic unit yields systematically low backgrounds with respect to Cu (0.2), Ni (0.2), Co (0.5), Cr (0.35), V (0.5) and Mg (0.4). A high ambient Ba concentration is recorded (1.8). The cumulative probability plot for Au (Fig. 34) indicates a high threshold of ca. 75 µg/kg (90th %ile). Values in excess of this occur primarily in the Río Yanuncay and tributary systems entering from the north and west. The most notable is Río Quingoyacu in which a maximum of 1582 µg/kg Au is recorded (ref. 691264-9669294). Several Au anomalies overlying Soldados Formation rocks to the north of Cerro Plancharumi may be sourced to the Plancharumi Formation, notably those in the Río Yanuncay at ref. 697247-9674893 (706 µg/kg) and ref. 700723-9676008 (161 µg/kg). Free (coarse) Au with a morphology characteristic of a local provenance has been observed in heavy mineral concentrates from Q. Chanchán (ref. 702700-9672200). Sub-detection 80 BSI fraction sediment Au concentrations are reported for the same drainage.

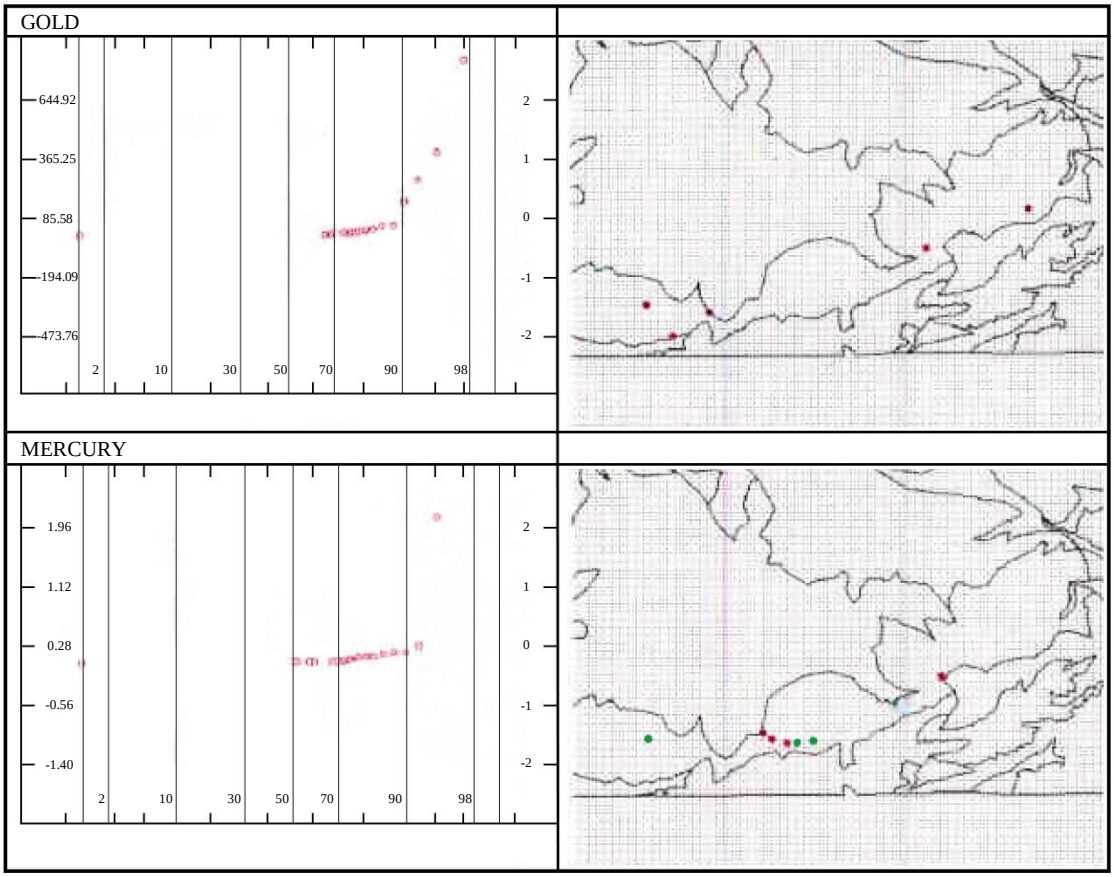

Figure 34. Cumulative probability plots and lithologically normalised anomaly maps for Au and Hg within the Plancharumi Formation. Axes indicate element concentration (left), standard deviation from mean concentration (right) and percentile class (base). Note: the presence of individual points on the anomaly maps reflects their exceedance of a threshold defined from cumulative probability plots for Plancharumi Formation samples. The colour coding of individual points reflects their percentile class within the population for the entire 2°-3°S area (see Figs 7-22).

Table 19. Plancharumi Formation. Summary Statistics

	Count	Mean	Std. Dev	Min	Max	Median
Au	41	85.58	279.67	3.33	1582.00	3.33
Ag	41	0.66	NA	0.66	0.66	0.66
Cu	41	10.60	8.48	3.00	38.00	8.00
Pb	41	16.94	13.06	5.00	72.00	13.00
Zn	41	83.82	35.75	36.00	207.00	74.00
Mo	41	1.32	0.87	0.90	4.00	0.90
Ni	41	4.14	2.23	2.20	9.00	4.00
Co	41	8.70	3.42	1.73	18.00	9.00
Cd	41	0.53	0.24	0.46	1.60	0.46
Bi	41	4.17	0.77	4.00	8.00	4.00
Fe	41	2.81	1.07	0.92	5.30	2.82
Mn	41	1134.96	894.62	401.00	4638.00	873.00
Te	41	6.66	NA	6.66	6.66	6.66
Ba	41	207.85	117.63	77.00	595.00	173.00
Cr	41	12.02	10.64	2.46	50.00	9.00
V	41	63.84	42.02	12.00	191.00	56.00
Sn	41	13.33	NA	13.33	13.33	13.33
W	41	13.33	NA	13.33	13.33	13.33
La	41	10.72	5.53	0.66	25.00	11.00
Al	41	2.08	0.82	0.80	5.33	1.97
Mg	41	0.30	0.20	0.05	0.79	0.24
Ca	41	0.38	0.18	0.12	1.14	0.35
Na	41	0.02	0.01	0.01	0.04	0.02
K	41	0.08	0.04	0.01	0.18	0.08
Sr	41	52.08	34.79	0.66	160.00	40.00
Y	41	5.38	2.09	1.00	12.00	5.00
Ga	41	4.75	4.27	1.33	25.00	4.00
Li	41	11.18	5.99	4.00	24.00	10.00
Nb	41	2.07	2.64	0.66	15.00	0.66
Sc	41	3.61	0.77	3.33	6.00	3.33
Ta	41	6.66	NA	6.66	6.66	6.66
Ti	41	0.08	0.06	0.01	0.24	0.06
Zr	41	3.10	2.01	0.66	9.00	3.00
As	41	33.34	71.79	2.66	458.10	16.30
Sb	41	2.49	4.71	1.26	31.40	1.26
Hg	41	0.28	0.84	0.03	4.02	0.04

A zone of pronounced Hg enrichment occurs in drainage surrounding the Cerro Plancharumi massif, including a sector of the Río Yanuncay to the north, Río Bermejos to the south-west and Q. Trigo Loma to the south (refs. 696848-9671207; 697752-9670943). Here several values of 0.18-19.0 mg/kg Hg occur, providing a further indication of prospectivity for epithermal mineralisation. The spatial correlation with Au is extremely poor. Samples anomalous in Hg (and Au) display a characteristic lack of enrichment in metalloids or other base/precious metals, possibly indicative of a low-sulphidation source, with the exception of a single Río Yanuncay sample yielding 4.023 mg/kg with 458 mg/kg As and 31 mg/kg Sb (ref. 706571-9674615 several km to the west of Cerro Plancharumi). Significant As anomalies occur over the Plancharumi Formation in Q. Chanchán (136 mg/kg with 4 mg/kg Sb at ref. 702930-9672366) and downstream close to the Plancharumi-Soldados Formation contact (262 mg/kg at ref. 704295-9673820). These values, coupled with the observation of particulate Au may define a priority for further reconnaissance.

5.4.5.9 Puñay Unit

The andesitic rocks of the Puñay Unit incorporate 68 stations (Table 20). Values for most major and trace elements within the tract are similar to the regional background, with the notable exception of Sr which is considerably enriched (1.9). The prospectivity of the sequence is limited. The cumulative probability plot for Au (Fig. 35) indicates a threshold at the 96th %ile of only 11.3 µg/kg. Higher values occur at three localities to a maximum of 95 µg/kg (with no coincident indication of mineralisation) at ref. 730553-9750084. An As threshold at the 88th %ile corresponds to a concentration of 8.3 mg/kg, with only one value recorded in excess of 20 mg/kg. No strongly anomalous base-metal values are recorded within the outcrop.

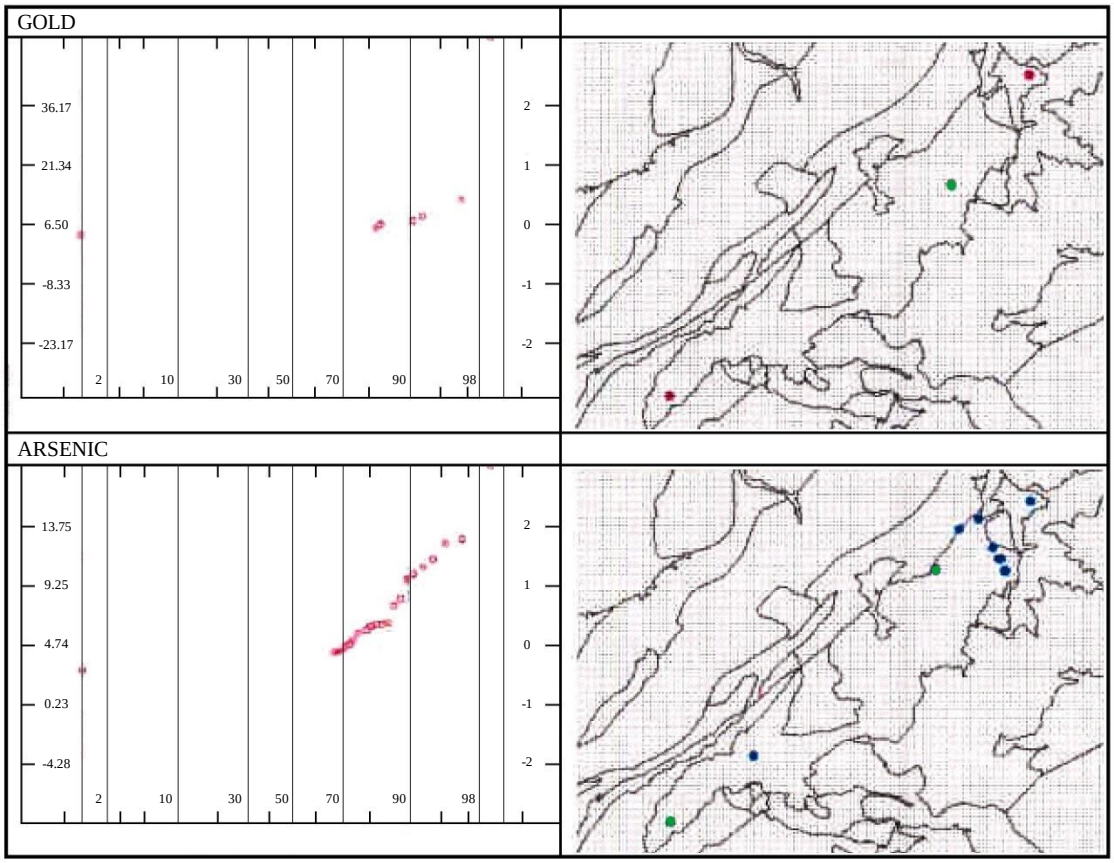

Figure 35. Cumulative probability plots and lithologically normalised anomaly maps for Au and As within the Puñay Unit. Axes indicate element concentration (left), standard deviation from mean concentration (right) and percentile class (base). Note: the presence of individual points on the anomaly maps reflects their exceedance of a threshold defined from cumulative probability plots for Puñay Unit samples. The colour coding of individual points reflects their percentile class within the population for the entire 2°-3°S area (see Figs 7-22).

Table 20. Puñay Unit. Summary Statistics

	Count	Mean	Std. Dev	Min	Max	Median
Au	68	6.50	14.84	3.33	95.00	3.33
Ag	68	0.66	NA	0.66	0.66	0.66
Cu	68	26.05	8.60	9.00	62.00	26.00
Pb	68	5.76	4.47	2.66	32.00	4.42
Zn	68	93.23	44.70	38.00	252.00	81.50
Mo	68	1.77	1.23	0.90	6.00	0.90
Ni	68	13.87	5.88	2.20	28.00	14.00
Co	68	13.71	3.96	6.00	28.00	13.00
Cd	68	0.48	0.17	0.46	1.80	0.46
Bi	68	4.36	1.50	4.00	15.00	4.00
Fe	68	4.91	2.04	2.08	10.00	4.61
Mn	68	738.26	373.11	214.00	2010.00	627.50
Te	68	7.38	3.31	6.66	31.00	6.66
Ba	68	119.79	38.46	63.00	266.00	111.00
Cr	68	35.35	17.70	4.00	93.00	33.50
V	68	166.89	76.96	51.00	437.00	165.00
Sn	68	13.54	1.22	13.33	21.00	13.33
W	68	13.33	0.00	13.33	13.33	13.33
La	68	8.51	5.59	0.66	41.00	7.00
Al	68	1.90	0.63	0.77	3.79	1.84
Mg	68	0.64	0.20	0.26	1.29	0.63
Ca	68	0.72	0.23	0.35	1.43	0.73
Na	68	0.08	0.03	0.02	0.17	0.08
K	68	0.07	0.03	0.02	0.20	0.06
Sr	68	75.23	43.75	-1.00	181.00	78.50
Y	68	4.13	1.55	2.00	9.00	4.00
Ga	68	4.27	3.11	1.33	12.00	3.00
Li	68	5.61	2.97	0.80	16.00	5.00
Nb	68	2.34	3.14	0.66	17.00	0.66
Sc	68	3.82	1.22	3.33	8.00	3.33
Ta	68	7.17	3.71	6.66	37.00	6.66
Ti	68	0.17	0.10	0.01	0.60	0.15
Zr	68	7.97	3.35	0.66	23.00	8.00
As	68	4.74	4.51	2.66	30.50	2.66
Sb	68	1.29	0.17	1.26	2.40	1.26
Hg	68	0.03	0.02	0.03	0.12	0.03

5.4.5.10 Undifferentiated Saraguro Group

Undifferentiated Saraguro Group rocks are represented by 65 stream sediment samples (Table 21). Geochemical affinities with rhyolitic or dacitic facies within the Group (and their reworked or sedimentary derivatives) are indicated by low backgrounds with respect to Ni, Cr, V and Co. A relatively high Au threshold of ca. 80 μg/kg (90th %ile) has been derived from cumulative probability data (Fig. 36). Anomalies occur primarily in a sector east of the Chaucha batholith. A value of 295 μg/kg is recorded close to the contact with this intrusion in the upper Río San Antonio, 1 km north of Chaucha settlement (ref. 677926-9681110). In the Río Jérez, possible mineralisation in dilational splays or related transverse structures associated with the Ñag Fault is indicated by Au values up to 108 μg/kg (ref. 683779-9682100). The Río Angas and tributaries yield anomalies of up to 153 μg/kg Au with attendant enrichment of Cu (up to 180 mg/kg), Pb (up to 140 mg/kg), Zn (up to 1241 mg/kg) and Sb (up to 9.3 mg/kg). These anomalies lie close to the contact with the Soldados Formation (e.g. 686109, 9680317; 684838-9679219) which hosts Au-Cu mineralisation within the same drainage (section 5.4.5.7 above). Coincident enrichment of As with Au is widely evident in the eastern sector of the undifferentiated Saraguro Group outcrop, notably in Río Jérez (eg. ref. 680022-9679023), Río Chaucha (e.g. refs. 668377-9679884; 669321-9676929) and immediately south of the Llano Largo prospect (e.g. 681028-9684597).

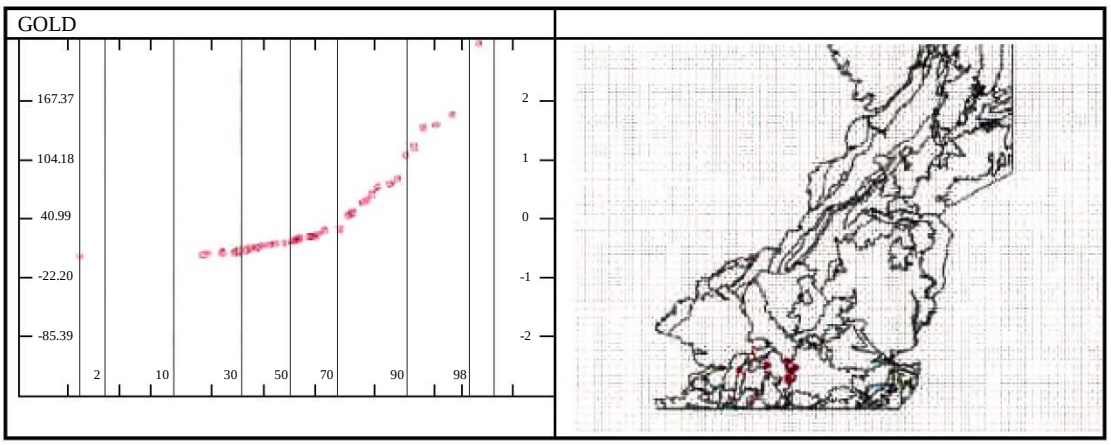

Figure 36. Cumulative probability plots and lithologically normalised anomaly maps for Au within the undifferentiated Saraguro Group. Axes indicate element concentration (left), standard deviation from mean concentration (right) and percentile class (base). Note: the presence of individual points on the anomaly maps reflects their exceedance of a threshold defined from cumulative probability plots for undifferentiated Saraguro Group samples. The colour coding of individual points reflects their percentile class within the population for the entire 2°-3°S area (see Figs 7-22).

Table 21. Undifferentiated Saraguro Group. Summary Statistics

	Count	Mean	Std. Dev	Min	Max	Median
Au	65	40.99	63.19	3.33	363.00	18.00
Ag	65	0.69	0.19	0.66	1.85	0.66
Cu	65	54.08	70.06	5.00	406.00	34.00
Pb	65	21.75	22.35	2.66	146.00	18.00
Zn	65	151.97	194.08	27.00	1241.00	80.00
Mo	65	2.28	1.99	0.90	11.00	1.50
Ni	65	13.63	30.33	2.20	240.00	6.00
Co	65	11.80	8.05	1.73	45.00	9.00
Cd	65	0.88	1.08	0.46	7.20	0.46
Bi	65	4.20	0.81	4.00	8.00	4.00
Fe	65	3.72	1.38	1.72	7.89	3.56
Mn	65	833.33	683.26	223.00	4323.50	628.00
Te	65	6.73	0.54	6.66	11.00	6.66
Ba	65	95.07	46.08	23.00	346.00	89.00
Cr	65	30.58	35.00	2.46	218.00	16.00
V	65	84.88	60.79	14.50	264.00	56.00
Sn	65	13.33	0.00	13.33	13.33	13.33
W	65	13.33	0.00	13.33	13.33	13.33
La	65	7.67	4.59	0.66	23.50	7.00
Al	65	2.14	0.91	0.89	4.47	1.96
Mg	65	0.67	0.37	0.17	2.67	0.60
Ca	65	0.57	0.28	0.05	1.27	0.53
Na	65	0.03	0.03	0.01	0.14	0.02
K	65	0.13	0.09	0.01	0.47	0.10
Sr	65	34.26	26.69	-1.00	116.00	30.00
Y	65	6.88	4.20	2.00	26.00	5.00
Ga	65	3.96	3.09	1.33	14.00	3.00
Li	65	13.88	7.19	3.00	33.00	13.00
Nb	65	2.49	2.93	0.66	19.00	1.33
Sc	65	4.30	3.04	3.33	25.00	3.33
Ta	65	6.77	0.91	6.66	14.00	6.66
Ti	65	0.09	0.06	0.01	0.27	0.07
Zr	65	1.90	2.16	0.66	10.00	0.66
As	65	27.63	22.79	2.66	93.35	23.50
Sb	65	2.13	2.06	1.26	13.60	1.26
Hg	65	0.04	0.02	0.03	0.13	0.04

5.4.6 Cisarán Formation

5.4.6.1 Andesites

Stream sediments derived from the andesitic lavas of the Cisarán Formation are characterised by low backgrounds for Li (0.35), Al (0.65) and K (0.6). A poorly evolved composition is indicated by conspicuous Sr enrichment (2.0), relatively low Ba/Sr and high Sr/Ca ratios (Table 22). Prospectivity is limited, with the possible exception of a south-west trending zone of kaolinized andesites in the Río Chanchán Valley. Here several Au values occur in excess of the lithological threshold (15 μg/kg, Fig. 37), generally in the range 26-28 μg/kg. Examples include stations in the north trending quebradas Lluguillay (ref. 734116-9751039) and Chiquicay (732532-9750116). An additional Au anomaly of 322 μg/kg is recorded over Cisarán andesites close to the northern limit of the mapped area (732667-9777365), with no attendant evidence of mineralisation. The threshold As value for the Cisarán andesite sub-unit is only 8 mg/kg (90th %ile). Higher values of up to 60 mg/kg occur primarily along the Río Chanchán (9 stations between longitudes 730000 and 734000). There is no evidence of base metal mineralisation within the sub-unit.

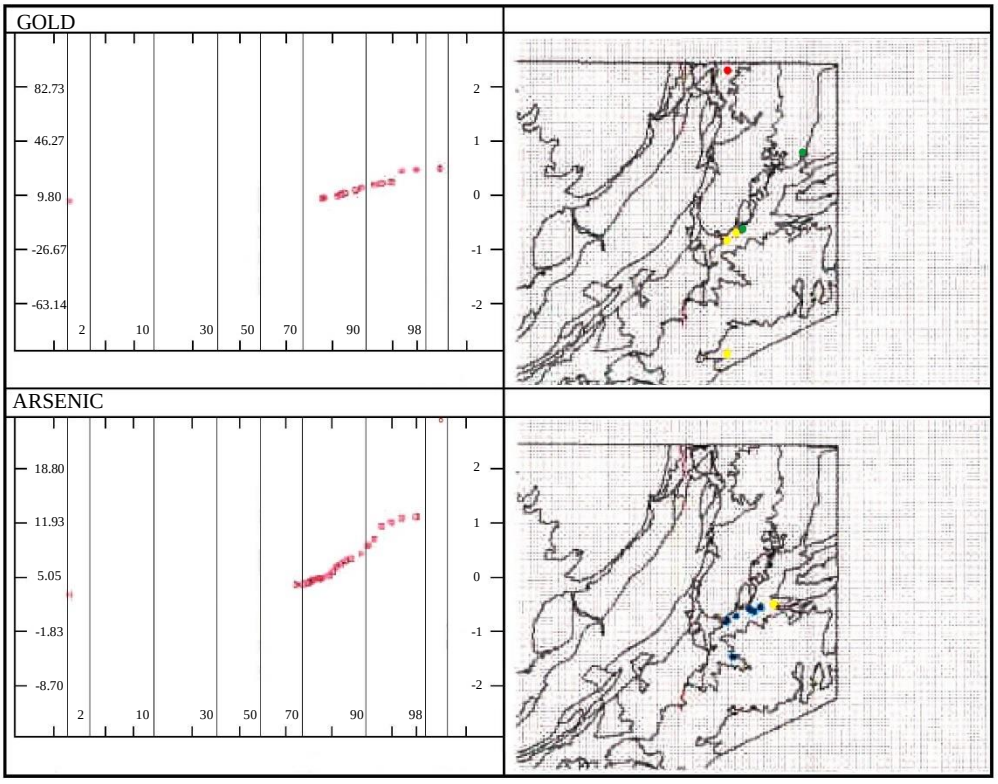

Figure 37. Cumulative probability plots and lithologically normalised anomaly maps for Au and As within the Cisarán Formation andesites. Axes indicate element concentration (left), standard deviation from mean concentration (right) and percentile class (base). Note: the presence of individual points on the anomaly maps reflects their exceedance of a threshold defined from cumulative probability plots for Cisarán andesite samples. The colour coding of individual points reflects their percentile class within the population for the entire 2°-3°S area (see Figs 7-22).

Table 22. Cisarán Andesites. Summary Statistics

	Count	Mean	Std. Dev	Min	Max	Median
Au	77	9.80	36.47	3.33	322.00	3.33
Ag	77	0.66	NA	0.66	0.66	0.66
Cu	77	28.88	7.77	13.00	51.00	28.00
Pb	77	5.33	3.79	2.66	26.00	4.00
Zn	77	60.84	21.47	27.00	118.00	59.00
Mo	77	1.44	0.97	0.90	5.00	0.90
Ni	77	24.71	10.44	2.20	61.00	24.00
Co	77	13.43	3.64	6.00	29.00	13.00
Cd	77	0.46	NA	0.46	0.46	0.46
Bi	77	4.16	0.80	4.00	9.00	4.00
Fe	77	3.17	0.96	1.58	7.52	3.09
Mn	77	563.66	602.09	247.00	5069.00	419.00
Te	77	6.66	NA	6.66	6.66	6.66
Ba	77	101.05	52.25	36.00	291.00	92.00
Cr	77	45.29	18.11	15.00	101.00	45.00
V	77	109.50	40.29	56.00	256.50	101.00
Sn	77	13.33	0.00	13.33	13.33	13.33
W	77	13.48	1.33	13.33	25.00	13.33
La	77	5.46	2.95	0.66	15.00	5.00
Al	77	1.44	0.44	0.70	3.34	1.35
Mg	77	0.66	0.31	0.11	1.52	0.64
Ca	77	0.55	0.18	0.30	1.56	0.54
Na	77	0.09	0.04	0.03	0.16	0.09
K	77	0.06	0.04	0.01	0.35	0.05
Sr	77	71.44	36.67	-1.00	163.00	80.00
Y	77	2.49	0.95	1.00	6.00	2.00
Ga	77	2.98	1.91	1.33	10.00	3.00
Li	77	4.15	2.42	0.80	13.00	3.00
Nb	77	1.87	2.68	0.66	15.00	0.66
Sc	77	3.33	NA	3.33	3.33	3.33
Ta	77	6.66	NA	6.66	6.66	6.66
Ti	77	0.15	0.04	0.03	0.25	0.15
Zr	77	6.32	2.83	0.66	13.00	6.00
As	77	5.05	6.88	2.66	50.90	2.66
Sb	77	1.33	0.54	1.26	5.90	1.26
Hg	77	0.039	0.030	0.026	0.196	0.026

5.4.6.2 Volcano-sedimentary facies

Reworked volcanoclastic rocks constitute >60% of the area of the Cisarán Formation outcrop. The predominance of andesitic detritus in these volcano-sedimentary units is apparent from their close geochemical affinity to the lavas described in section 5.4.6.1 (Table 23).

With respect to Cu, Pb, Zn, Ni, Co, Ba and Cr, mean concentrations vary between the lavas and the reworked volcanoclastic rocks by <10%. A strontium-rich signature is also evident in the sedimentary facies (mean 62 mg/kg). Very low backgrounds for Pb and As prevail. The prospectivity (for Au and base metals) of the Cisarán sedimentary tract is strictly limited. An Au threshold of 15 μg/kg has been defined at the 95th %ile (Fig. 38). Anomalous localities include Q. Caumal (ref. 738201-9761748) where a value of 467 μg/kg Au may be tentatively correlated with a poorly defined intrusive contact. In the south of the Cisarán volcano-sedimentary tract, values of up to 74 μg/kg Au are coincident with up to 3.1 mg/kg Ag and 12.55 mg/kg Sb in tributaries of Q. Chagra Castea (ref. 738009-9737972).

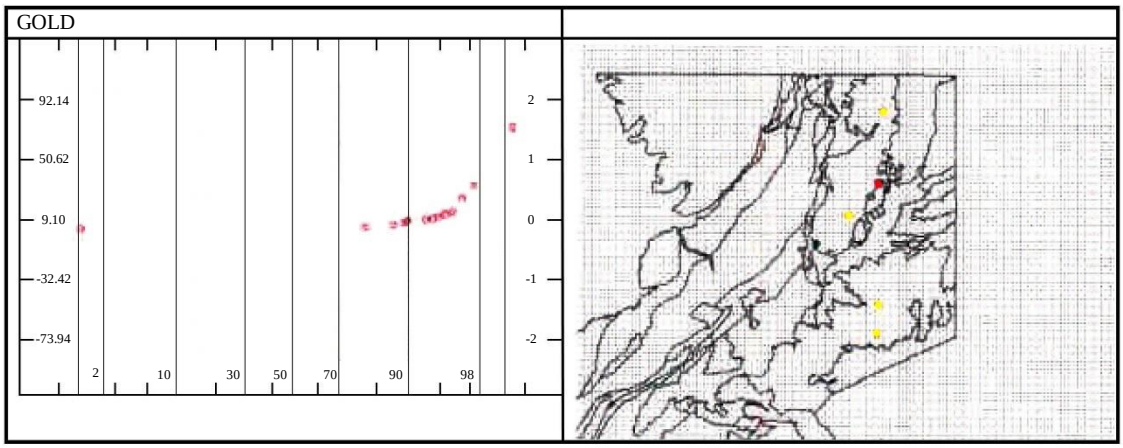

Figure 38. Cumulative probability plots and lithologically normalised anomaly maps for Au within the Cisarán Formation sediments. Axes indicate element concentration (left), standard deviation from mean concentration (right) and percentile class (base). Note: the presence of individual points on the anomaly maps reflects their exceedance of a threshold defined from cumulative probability plots for Cisarán Formation samples. The colour coding of individual points reflects their percentile class within the population for the entire 2°-3°S area (see Figs 7-22).

Table 23. Cisarán sediments. Summary Statistics

	Count	Mean	Std. Dev	Min	Max	Median
Au	128	9.10	41.52	3.33	457.00	3.33
Ag	128	0.68	0.22	0.66	3.10	0.66
Cu	128	26.59	10.91	6.00	76.00	25.00
Pb	128	5.76	7.48	2.66	61.00	4.00
Zn	128	55.47	21.99	14.06	151.00	54.50
Mo	128	1.33	0.91	0.90	6.00	0.90
Ni	128	20.61	8.87	5.00	46.00	19.25
Co	128	11.71	3.45	4.00	22.00	12.00
Cd	128	0.47	0.11	0.46	1.60	0.46
Bi	128	4.05	0.45	4.00	8.67	4.00
Fe	128	2.96	0.90	1.24	6.65	2.77
Mn	128	429.11	162.06	155.00	1209.00	400.50
Te	128	6.78	0.98	6.66	15.00	6.66
Ba	128	98.15	39.39	35.00	214.00	91.75
Cr	128	43.80	14.71	17.00	87.00	42.00
V	128	111.80	34.31	55.00	235.00	108.00
Sn	128	13.33	0.00	13.33	13.33	13.33
W	128	13.38	0.59	13.33	20.00	13.33
La	128	5.49	3.06	0.66	18.00	5.00
Al	128	1.64	0.75	0.67	4.48	1.38
Mg	128	0.54	0.28	0.10	1.29	0.47
Ca	128	0.46	0.14	0.17	0.87	0.44
Na	128	0.07	0.04	0.02	0.19	0.07
K	128	0.04	0.02	0.01	0.19	0.04
Sr	128	62.00	30.88	-1.00	114.00	65.50
Y	128	2.42	1.07	1	8.00	2.00
Ga	128	3.09	2.05	1.33	10.00	2.42
Li	128	3.84	1.55	1.33	10.00	3.50
Nb	128	2.07	2.48	0.66	12.00	0.66
Sc	128	3.40	0.49	3.33	8.00	3.33
Ta	128	6.72	0.65	6.66	14.00	6.66
Ti	128	0.16	0.05	0.05	0.31	0.16
Zr	128	6.01	2.75	0.66	14.00	5.00
As	128	2.96	1.46	2.66	13.60	2.66
Sb	128	1.42	0.91	1.26	7.80	1.26
Hg	128	0.03	0.03	0.03	0.32	0.03

5.4.7 Intrusive rocks

5.4.7.1 Granodioritic facies

Granodiorites or closely related intrusive facies form the largest lithological component of the Chaucha Batholith. This zone, in conjunction with a north-west trending granitoid outcrop within a broader zone of metamorphic basement in the central sector of the mapped area, incorporates 407 sampling stations. Summary statistics (Table 24) are strongly biased by ca. 20 samples derived from the zone of strong Cu-Mo porphyry mineralisation at Chaucha. Mean values thus provide an unreliable guide to lithogeochemistry. Within the large main outcrop of the Chaucha Batholith to the west of longitude 670000 and north of latitude 9680000, very low backgrounds prevail for Ca (<0.4%), Mg (<0.7%), Mn (<400 mg/kg), Ni (<10 mg/kg), Zn (<50 mg/kg), Pb (<5 mg/kg) and As (<10 mg/kg). High K/Ba ratios and significant V enrichment indicate limited magmatic evolution. The presence of increasingly mafic facies possibly enclaves of Piñón basalt, along a north-west trending axis in the central Chaucha Batholith is indicated by localised enrichment of Mg and Ni.

The Au cumulative probability distribution (Fig. 39) indicates the presence of three discrete populations (one relating to the northern-most granodiorite intrusion in the centre of the mapped area) with a threshold of 53 μg/kg at the 95th %ile. Over the sector of the Chaucha Batholith described above, the principal anomalous locality is Pan de Azúcar (e.g. refs. 668909-9692032; 667981-9691883; 669190-9692363) where values of 64-450 μg/kg Au occur. No coincident enrichment of other metals/metalloids of economic interest is recorded. Anomalies to 981 μg/kg in the Río Pijilí area occur in channel fill sequences currently worked by artisanal miners. In the area south and immediately west of Chaucha, multi-sample anomalies occur in the Q. Yubarpotrero (e.g. refs. 671409-9676913; 672007-9675401) and Río Pita systems. In the latter area modest anomalies (<100 μg/kg) occur in a zone constrained by north-east trending secondary faults orientated at 70-90° to the Ñag Fault. Slight silicification of both the intrusive facies and adjacent tuffs of the Saraguro Group has been recorded. At Agua Blanca (ref. 670950-9679004), a single value of 135 μg/kg is recorded in association with 1.2 mg/kg Ag, 450 mg/kg Cu, 10 mg/kg Mo, 92 mg/kg As, 3 mg/kg Sb and 0.101 mg/kg Hg at a faulted contact with basaltic rocks of the Pallatanga Unit. A zone extending between longitudes 673000-675000 and latitudes 9674000-9678000 hosts approximately 20 strongly anomalous Cu values (300-2000 mg/kg) with attendant Mo enrichment (7-141 mg/kg) within the drainage of the Río Chaucha, Río Malacatos, Río Pita and associated tributaries. Most are bounded by two north-east trending faults (the Ñag Fault and a parallel structure approximately 4 km to the west), the intersection of which with a series of secondary north-east trending structures constrains porphyry-style mineralisation in three discrete localities (e.g. UNDP, 1969). Zoned hydrothermal alteration assemblages range from weak propylitic to intense potassic, with porphyritic textures developed by phenocrysts of sericitized plagioclase, epidotized amphibole and sub-angular quartz. Sulphides occur both as disseminations and as fracture fillings. The metalliferous assemblage is dominated by pyrite with attendant chalcopyrite, covellite, molybdenite, secondary Cu phases (notably carbonates) and Fe oxides. Gold occurs only as a trace refractory component, as indicated by the prevalence of drainage sediment values in the range 5-50 μg/kg. The determination of an appropriate As threshold for the granodiorite suite is problematic and a slightly arbitrary value of 54 mg/kg (93rd %ile) has been applied. In the principal zone of porphyry mineralisation at Chaucha several values in the range 70-140 mg/kg occur in the Río Chaucha (e.g. northern margin of porphyry at 675560-9677013; 676595-9677678) Río Angas (e.g. 0.5 km from confluence with Río Chaucha at 676618-9677469) and Río Pita (e.g. west margin of porphyry zone at 674445-9677304).

Coincident enrichment of Sb (to 9.6 mg/kg), Zn (to 500 mg/kg), Ag (to 1.4 mg/kg), Cd (to 1.5 mg/kg), Cu (to 1551 mg/kg) and Mo (to 141 mg/kg) is evident. Several Hg values in excess of a threshold of 0.11 mg/kg (93rd %ile) occur within the Chaucha porphyry zone, in artisanal mining localities of the Río Pijilí area and, most prominently, over the Cerro Motilón intrusion in the Rïo Chilcales catchment north of Suscal (e.g. refs. 711283-9740860; 712197-9739759). Here values of 1-1.6 mg/kg Hg occur in association with low (<8 µg/kg) Au abundances. There is no pronounced enrichment of other metals or metalloids.

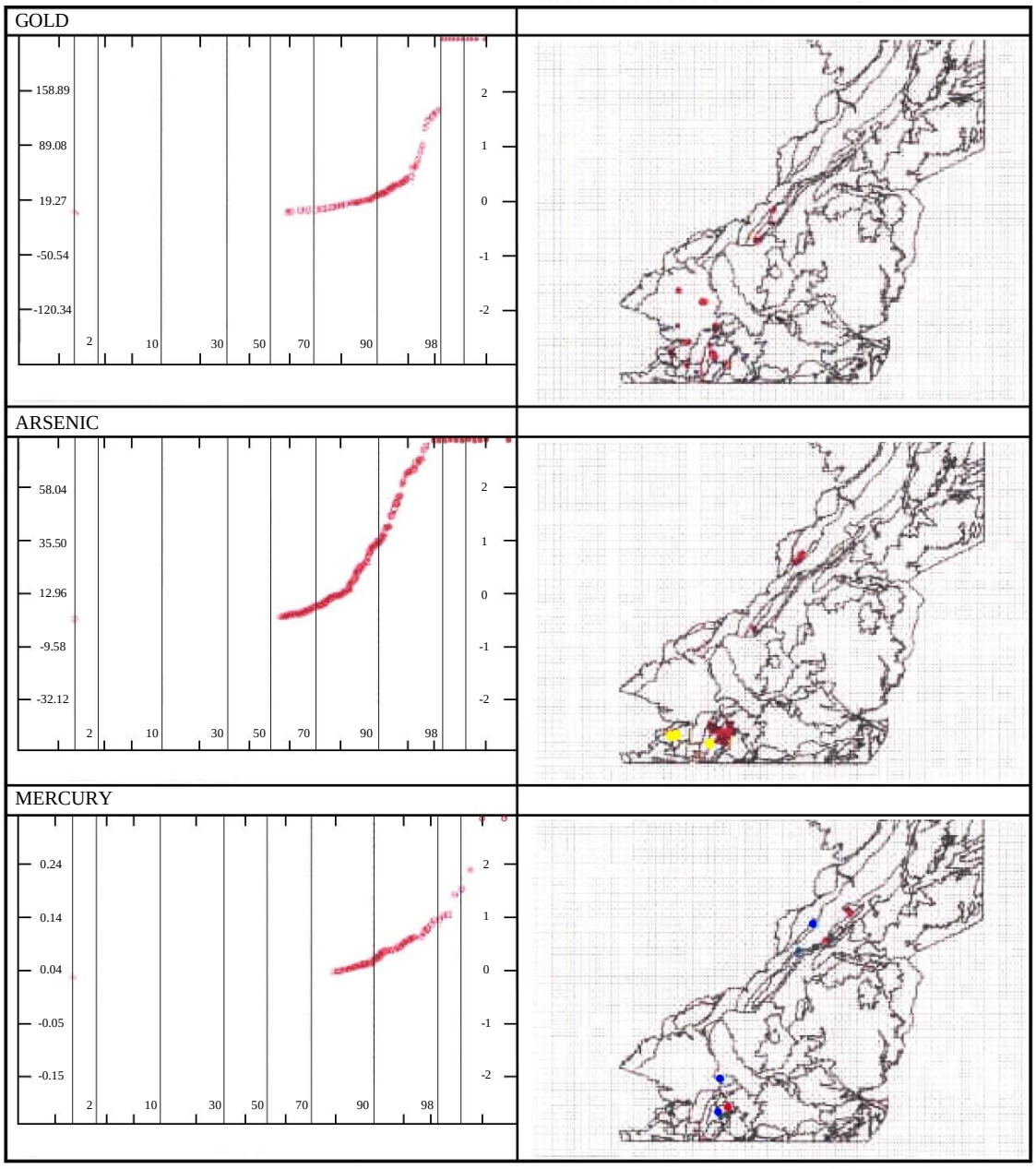

Figure 39. Cumulative probability plots and lithologically normalised anomaly maps for Au, As and Hg over granodiorites. Axes indicate element concentration (left), standard deviation from mean concentration (right) and percentile class (base). Note: the presence of individual points on the anomaly maps reflects their exceedance of a threshold defined from cumulative probability plots for granodiorite samples. The colour coding of individual points reflects their percentile class within the population for the entire 2°-3°S area (see Figs 7-22).

Table 24. Granodiorite intrusions. Summary Statistics

	Count	Mean	Std. Dev	Min	Max	Median
Au	407	19.27	69.80	3.33	981	3.33
Ag	407	0.69	0.31	0.66	6.35	0.66
Cu	407	80.05	207.66	3	2090	30
Pb	407	8.75	11.15	2.66	93	4
Zn	407	62.57	87.89	3.33	1221	37.41
Mo	407	3.18	10.85	0.9	141	0.9
Ni	407	13.11	19.77	2.2	173	8
Co	407	10.28	6.43	1.73	63	9
Cd	407	0.57	0.54	0.46	6.5	0.46
Bi	407	4.56	1.75	4	16	4
Fe	407	5.22	2.38	1.4	10	4.83
Mn	407	430.33	265.52	114	2756.5	344
Te	407	7.64	5.62	6.66	79.33	6.66
Ba	407	92.50	42.89	18	310	87
Cr	407	43.91	29.13	5	194	39
V	407	163.39	100.43	28	619	138
Sn	407	13.46	1.15	13.33	27	13.33
W	407	13.44	1.11	13.33	28	13.33
La	407	8.58	8.06	0.66	64	6
Al	407	1.99	0.86	0.43	7.5	1.83
Mg	407	0.59	0.36	0.075	2.86	0.52
Ca	407	0.40	0.23	0.04	1.81	0.34
Na	407	0.02	0.01	0.007	0.11	0.02
K	407	0.17	0.09	0.02	0.6	0.16
Sr	407	22.48	15.95	-1	93	23
Y	407	4.82	2.64	2	22	4
Ga	407	3.49	2.72	1.33	15	3
Li	407	11.62	6.68	0.8	48	10
Nb	407	3.01	4.46	0.66	24	1
Sc	407	4.17	2.27	3.33	22	3.33
Ta	407	7.43	8.18	6.66	123.333	6.66
Ti	407	0.09	0.04	0.01	0.33	0.09
Zr	407	1.49	1.79	0.66	14	0.66
As	407	12.96	22.54	2.66	142.5	2.66
Sb	407	1.56	1.07	1.26	9.6	1.26
Hg	407	0.04	0.09	0.026	1.617	0.026

5.4.7.2 Diorite facies

Diorites of the Chaucha, Molleturo and Cerro Hornillos intrusions encompass 209 stream sediment sampling stations (Table 25). High mean and median values for Au (median 16 µg/kg) and As (mean 32 mg/kg) are recorded. The Au cumulative probability plot (Fig. 40) indicates a high threshold value of 170 µg/kg at the 90th %ile. The most intense anomaly over the Chaucha Batholith lies in the upper reaches of Q. El Llanto (ref. 672294-9673548) at the contact with a minor outcrop of rhyolitic tuffs and/or lavas (of the Saraguro Group). Here, a value of 2524 µg/kg Au is coincident with 1705 mg/kg Cu, 404 mg/kg Pb, 1091 mg/kg Zn, 7.4 mg/kg Cd, 45 mg/kg Bi, 272 mg/kg As, 532 mg/kg Sb and 1.5 mg/kg Hg. Artisanal adit workings are reported to the south and east of this locality. Farther south in the Río Zambohuaycu system, values of 232-548 µg/kg Au are recorded with sporadic enrichment of Hg to 0.114 mg/kg in an area of highly silicified micro-diorites and intrusive rhyolitic facies. Over the Molleturo Diorite, some 17 sediment Au values in excess of 200 µg/kg are recorded, many along the eastern contact with tuffs of the Filo Cajas Unit. Values of 235-849 µg/kg Au, with As to 446 mg/kg, Sb to 7.6 mg/kg and Cd to 2.75 mg/kg occur in the Río Miguir and tributaries such as Q. Guegrahuaca (refs. 679626-9703438; 679132-9703175). In the upper Río Putucay, anomalies with concentrations up to 768 µg/kg Au occur downstream of intensely altered tuffs which extend eastward several km into the headwaters of the Río Patul (refs. 687078-9704459; 687039-9693454). Prospectivity over and/or at the margins of the minor diorites in the northern sector of the 2°-3°S area is, by comparison, low.

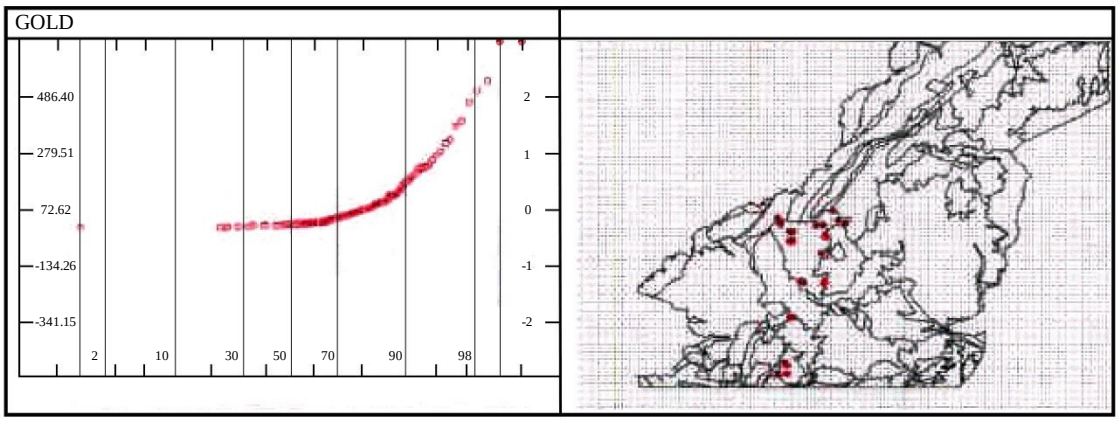

Figure 40. Cumulative probability plots and lithologically normalised anomaly maps for Au over diorites. Axes indicate element concentration (left), standard deviation from mean concentration (right) and percentile class (base). Note: the presence of individual points on the anomaly maps reflects their exceedance of a threshold defined from cumulative probability plots for diorite samples. The colour coding of individual points reflects their percentile class within the population for the entire 2°-3°S area (see Figs 7-22).

Table 25. Diorite intrusions. Summary Statistics

	Count	Mean	Std. Dev	Min	Max	Median
Au	209	72.62	206.88	3.33	2524	16
Ag	209	0.83	1.658	0.66	24.3	0.66
Cu	209	82.41	256.01	3	2737	36
Pb	209	23.61	33.97	2.66	404.5	15
Zn	209	115.20	107.88	3.33	1091	85
Mo	209	2.84	4.519	0.9	44	2
Ni	209	11.86	8.20	2.2	59	10.5
Co	209	15.05	8.77	1.73	72	14
Cd	209	0.77	0.87	0.46	7.4	0.46
Bi	209	4.83	3.25	4	45	4
Fe	209	4.56	1.69	0.63	10	4.25
Mn	209	716.59	405.49	161	3560.5	610
Te	209	6.84	1.10	6.66	15	6.66
Ba	209	99.32	43.55	12	245	94
Cr	209	31.43	22.07	2.46	186	26
V	209	102.84	76.76	5	679	82
Sn	209	13.40	1.08	13.33	29	13.33
W	209	13.36	0.46	13.33	20	13.33
La	209	8.61	5.96	0.66	42.5	8
Al	209	2.42	0.87	0.27	5.03	2.34
Mg	209	0.85	0.33	0.02	1.67	0.8
Ca	209	0.55	0.26	0.03	2.03	0.525
Na	209	0.02	0.02	0.007	0.13	0.02
K	209	0.09	0.05	0.007	0.335	0.08
Sr	209	28.29	23.92	-1	136	24.5
Y	209	7.04	5.61	1	78	6
Ga	209	4.54	2.91	1.33	16	4
Li	209	17.20	8.18	0.8	49	17
Nb	209	2.20	2.58	0.66	16	1
Sc	209	4.68	2.19	3.33	14.5	3.33
Ta	209	6.85	1.36	6.66	21	6.66
Ti	209	0.06	0.04	0.007	0.24	0.07
Zr	209	1.67	1.79	0.66	10	0.66
As	209	32.92	43.63	2.66	446.6	22.3
Sb	209	5.28	36.99	1.26	532.25	1.26
Hg	209	0.07	0.14	0.026	1.531	0.042

6. DISCUSSION AND CONCLUSIONS

6.1 Economic potential

6.1.1 Interpretive guidelines

The following guidelines warrant emphasis with regard to the utilisation of GIMP drainage reconnaissance data for the identification of follow-up targets within the 2°-3°S area.

6.1.1.1 Sampling density: At the resolution of GIMP sampling, potentially significant mineral occurrences (notably those related to non-porphyry style mineralisation) may be indicated by no more than a single anomalous value. This is exemplified at Río Blanco, where a broad zone of intense silicic/argillic alteration is highlighted by elevated Au/As values at only one station in the Río Migsihuigsi catchment.

6.1.1.2 Terrain influences: In the high páramo environment, sediment geochemical signatures are controlled by physical rather than hydromorphic processes. Hydrous oxides form only a very small component of the matrix. Peak to background ratios (notably for transition metals) in localities hosting mineralisation are thus low. This, coupled with the high energies characteristic of many watercourses sampled, may result in very subtle drainage geochemical responses to mineralisation. With respect to epithermal Au mineralisation, occurrences in the high páramo may be indicated by no more than ca. 30-50 μg/kg elevation of values above background. The background concentrations of many metals in stream sediments of the Western Cordillera are highly variable (e.g. mean Au range 6.5-85.0 μg/kg, median Au range 3.3-16.0 μg/kg). Consequently, the requirement for appropriate lithological normalization is fundamental.

6.1.2 Prospectivity

A synopsis of potentially prospective Au occurrences is provided in Table 26. The resolution of both geological mapping and drainage geochemistry reconnaissance undertaken by the GIMP precludes the unequivocal identification of host lithologies, structural controls on mineralisation and/or development of metallogenic models. Of the geochemical anomalies recorded, those of the Río Pijilí, Río Corazón, Río Migsihuigsi, Río Angas and Río Miguir localities are, however, coincident with independent observations of alteration or mineralisation made during GIMP geological mapping (Dunkley and Gaibor, 1997a). Most can tentatively be ascribed to one of two settings:

(a) Structurally controlled mesothermal assemblages at intrusive contacts.

(b) Epithermal mineralisation associated with silicic/andesitic volcanism.

Additional details relating to the setting of four identified prospects follow:

Table 26. Summary of anomalous localities with respect to Au within the GIMP 2°-3°S area

No.	Unit	Location	UTMX	UTMY	Au (ppb)	Element association	Setting
1	Pallatanga	Río Pijilí	668861	9671581	4989	-	Structural control at intrusive contact
2	Pallatanga	-	656882	9671188	1160	As, Cu, Hg	Intrusive contact
3	Macuchi	Río Chimbo	719502	9775689	414	Bi	Contact with minor diorite stock
4	Angamarca	Río Tixay	669293	7908144	1028	As, Hg, Ag	Probably sourced to silicified Pallatanga basalts
5	Ocaña	Q. Las Minas	699853	9720822	1546	-	Strongly silicified tuffs in catchment
6	Chulo	Q. Chorahuaren	698051	9700569	3127	Ag	Local silicification
7	Tomebamba	Río Corazón	703952	9720295	474	Ag, Pb, Bi, As	Granodiorite contact
8	Chanlud	Río Chulco	Numerous		300	Ag	-
9	Río Blanco	R. Migsihuigsi	680306	9685523	940	As, Sb, Ag	Silicic and argillic alteration. Hydrothermal breccias
10	Soldados	Upper R. Angas	687569	9681415	100	Cu, Ag, Pb, Bi, As, Sb, Hg	Tourmaline breccias and higher temperature assemblages
11	Soldados	Río Soldados	Numerous		379	-	-
12	Plancharumi	Río Bermejos and Yanuncay	Numerous		1582	Hg??	Silicic volcanics with possible alteration textures
13	Saraguro (und.)	R. San Antonio	677926	9681110	295	-	Contact with Chaucha Batholith
14	Saraguro (und.)	Río Jérez	683779	9682100	108	-	-
15	Chaucha (GD)	Pan de Azúcar	668909	9692032	450	-	-
16	Chaucha (D)	Q. El Llanto	672294	9673548	2524	Cu, Pb, Zn, Cd, Bi, As, Sb, Hg	Contact with former cover of rhyolitic tuffs/lavas
17	Molleturo (D)	Río Miguir	Numerous		849	As, Sb, Cd	Contact with Filo de Cajas Unit

6.1.2.1 Río Migsihuigsi: Mineralisation at Río Blanco (principally the Llano Largo concession), highlighted in the GIMP survey by a strong Au-As anomaly in Q. Migsihuigsi, has been subject to recent commercial investigation including a diamond-drilling programme by Río Tinto Ltd. and venture partners. Details regarding structural controls, alteration signatures and paragenesis remain, however, to be fully ascertained. Investigations such as those incorporated into PRODEMINCA sub-component 3.5 (Evaluation of Ore Districts) are thus warranted both as an aid to economic appraisal, and for the development of a regional metallogenic framework. In November 1997, a brief visit to Río Blanco (Llano Largo prospect) was undertaken as a component of the GIMP regional geochemistry programme to validate interpretations placed on preliminary reconnaissance data.

The Río Blanco-Llano Largo prospect is subdivided into several named concessions delimited (approximately) to the north by the (4000 m) interfluve of the Canoas and El Choro/Miguir basins, to the east by the Río Migsihuigsi and to the west by a parallel (unnamed) fault-controlled quebrada draining into Quebrada Canoas. The primary lithologies are andesitic ash-flow tuffs, with varying degrees of recrystallisation, with interbedded andesitic lavas and volcanic sandstones. Intermediate intrusive rocks outcrop at an altitude of ca. 3400 m in the south-west corner of the concession.

Aerial photographs of the Río Blanco area indicate the presence of a sub-circular competent block (possibly a concealed intrusion) to the south-east of the prospect. This appears to have controlled the orientation of numerous secondary lineations (sigmoidal shears) within the zone of mineralisation. Intense argillic alteration and silicification along these conduits has produced several topographically proud elongate structures up to 20 m wide, trending mainly ESE in the central and northern sectors of the prospect (Penelope, Alejandra and Minerva).

Alteration within the concession is clearly zoned. At the eastern margin, propylitically altered andesite tuffs are evident. In the principal area of Río Tinto exploration, lower elevations (Dorada zone) are characterised by broad areas of relatively homogeneous argillic alteration and a greater presence of base metal sulphides. In Penelope, Alejandra and Minerva, narrow zones of intense argillic alteration and silicification (described above) are separated by relatively fresh rocks, with original lithologies identifiable. Zones of brecciation (mainly angular tectonic fabrics with possible hydrothermal overprints) are evident at these higher levels. Multiple phases of quartz veining form a characteristic feature of Alejandra and Penelope. There is evidence that some phases are barren while others carry a high sulphide content. Further characterization of this multiple phase veining (with respect to distribution and mineralogy) may contribute significantly to the identification of priority target areas within the Río Blanco prospect. Such work is, however, now embodied within the schedule for PRODEMINCA sub-component 3.5, and is thus considered beyond the GIMP remit.

6.1.2.2 Upper Río Angas: Mineralisation in the upper Río Angas has been known for three decades. Anomalous Zn values were highlighted during phase one of a UNDP exploration programme in the Chaucha area in 1969 (UNDP, 1969). During the second phase of the same project strongly silicified brecciated structures were reported (UN, 1972), with two such occurrences to the north of the Río Angas showing evidence of polymetallic mineralisation (Au, Cu, Pb, Zn, Bi, Sb). A subsequent INEMIN-funded programme coordinated by the Misión Belga established the presence of 19 discrete brecciated structures within an arcuate zone of fragmentation and argillic-propylitic alteration around the Atugpamba sub-volcanic complex (west of Laguna de Pallacocha). This high-level intrusive unit is interpreted by van Thournout and Guzmán (1988) to relate to one of two (or more) non-contemporaneous eruptive centres of the Tarqui Formation (as defined under the UNDP and INEMIN programmes) within which all mineralisation was reported to be hosted. More recent mapping by Dunkley and Gaibor (1997b) indicates that the Tarqui Formation does not occur in the region. Instead, the mineralisation is hosted in much older Oligocene volcanic rocks of the Saraguro Group, principally within the dacitic ash-flow tuffs of the Soldados Formation. Van Thournout and Guzmán (1988) have classified the occurrences as acid-sulphate epithermal deposits on the basis of their geochemical signature. The presence of tourmaline breccias in the Lagunas de Pallacocha area (Dunkley and Gaibor, 1997b), plus the high Bi/Sb and Bi/As ratios recorded in Q. Chaupiurcu during GIMP geochemical reconnaissance may, however, signify higher temperature assemblages.

Data generated under the GIMP geological mapping (Dunkley and Gaibor, 1997b) and geochemical reconnaissance surveys indicate that the prospective zone may extend south and west of the above-described area, possibly in relation to independent high-level intrusive units and/or former eruptive centres. Five kilometres south-west of Laguna de Pallacocha, breccia pipe occurrences are reported by Dunkley and Gaibor (1997b) in the vicinity of Loma Chilchiloma. These show rounded polymict clasts (tuffites) with disseminations of pyrite, chalcopyrite and covellite, as well as secondary Cu phases (malachite). The pipes cross-cut undifferentiated rhyolitic tuffs of the Saraguro Group, over which anomalies described in section 5.4.5.10 of this report occur close to the contact with the Soldados Formation. The As-Sb-Hg rich signature of stream sediments in the vicinity of all the above described breccias is in contrast to that in drainage entering the Río Angas from the south (Laguna de Patos), in which an independent phase of pyrite-chalcopyrite mineralisation may be indicated.

6.1.2.3 Upper Río Bermejos and Yanuncay: Anomalous values of Au (to 706 μg/kg) and Hg (to 19 mg/kg) in drainage to the south (Trigo Loma), west (Bermejos) and north (Yanuncay and Soldados) of Cerro Plancharumi delineate a substantial zone with economic potential. The Plancharumi Formation, from which several anomalous values can be sourced, has been interpreted by Dunkley and Gaibor (1997b) as a favourable setting for epithermal mineralisation. The sequence is characterised predominantly by rhyolitic air-fall tuffs, pyroclastic flows and lavas, erupted into a lacustrine environment. Coarse epiclastic mass-flow breccias indicate possible proximity to intrusive lava domes (though not observed at surface), while fine air-fall tuffs with accretionary lapilli, vesicular ash-flow tuffs and abundant pumice (together with independent evidence of high syn-eruptive water contents) are consistent with phreatomagmatic activity. Base-surge activity is indicated by the cross-bedding of coarse pumice lapillistones. Subject to the existence of flow-domes or related feeders, the setting may bear analogy to the Yanacocha high-sulphidation system of northern Perú (although the Yanacocha lithologies are essentially andesitic).

Considerable uncertainty remains with respect to the interpretation of Au and Hg data for the Cerro Plancharumi-Lower Río Soldados tract, in part due to the poor local covariation of these elements (Fig. 41). Given the substantial number of Au- and/or Hg anomalous samples recorded, explanations relating to Au nugget effects or differential dispersion mechanisms cannot plausibly be invoked. From available evidence, it is probable that at least two genetically unrelated zones of mineralisation exist, the first in the headwater reaches of the Río Bermejos and the second in the Río Soldados catchment. In addition, it is possible that multiple (possibly non-contemporaneous) zones of mineralisation exist *within* the upper Río Bermejos sector.

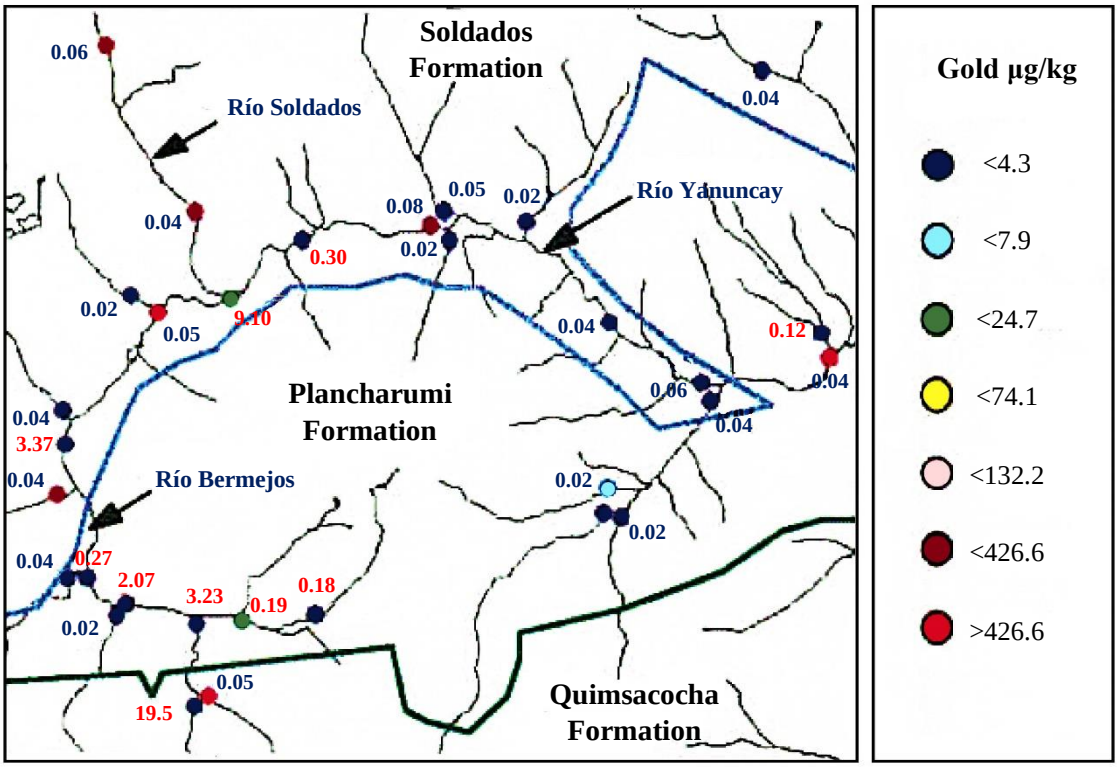

Figure 41. Geochemical data for Au (colour coded) and Hg (values posted in mg/kg) for drainage surrounding the Cerro Plancharumi massif. Approximate contacts of the Quimsacocha, Plancharumi and Soldados Formations are indicated.

- ***Upper Río Bermejos*:** A discrete epithermal target within the Río Bermejos headwaters is indicated by an intense Hg anomaly of 19.57 mg/kg with a north-trending dispersion train yielding Hg values in the range 0.277-3.3 mg/kg in the channel section to the Q. Ishcayrrumi-Río Bermejos-Río Yanuncay confluence. Values of Au in this sector are consistently below the detection limit (although an Au value of 713 µg/kg is recorded in a headwater tributary of the Río Bermejos to the east of the perceived Hg source).

From the position of the presumed source, mercurious mineralisation in the upper Río Bermejos is likely to be hosted, in part, by andesitic lavas of the Quimsacocha Formation (which overlies the Plancharumi Formation close to the southern watershed). Disseminated cinnabar has been reported in the Quimsacocha Formation close to the southern limit of the mapped area, and Hg-rich epithermal mineralisation in the vicinity of the Quimsacocha caldera is well known. Other Hg values in the range 0.17-0.18 mg/kg occur, however, in west-trending Río Bermejos tributaries (e.g. Río Trigo Loma) which are exclusively confined to the Plancharumi tract. This, coupled with the occurrence of modest (non-coincident) gold enrichment and particulate Au in north-east trending drainage emanating from the same source area is indicative of epithermal mineralisation within the Cerro Plancharumi massif. Relations between occurrences tentatively sourced to the Quimsacocha and Plancharumi Formations are unclear. Possible scenarios include:

(a) a zoned epithermal system, principally hosted within the Plancharumi with a distinct Hg-rich halo transgressing the contact.

(b) weak syn-eruptive (Upper Oligocene) epithermal mineralisation within the Cerro Plancharumi massif, with later (Mio/Pliocene) Hg-rich deposits associated with precipitation from hot springs at the margin of the Quimsacocha pile (Fig. 42).

The latter scenario is consistent with the northward asymmetrical outflow and palaeohydrogeology of the Quimsacocha system. The absence of metalloid enrichment in these marginal settings remains, however, problematic.

- ***Río Soldados and Yanuncay:*** Downstream of the Río Bermejos-Río Yanuncay confluence, sporadic Hg and Au enrichment is evident along ca. 6 km channel length. High Au values, (systematically without Hg enrichment) occur near the confluence with an unnamed south-east flowing tributary draining from Lagunas de Chushalongo (706 μg/kg), and at the confluence with Q. Coles (161 μg/kg) 5 km further downstream. Anomalous Hg values to 9.19 mg/kg occur at independent stations in the intervening channel sector. The observed distribution of elevated Au values within the Río Yanuncay as a whole may reflect inputs from two genetically unrelated sources:

  (a) the south flowing Río Soldados, in which mineralisation hosted within the Soldados Formation is indicated by several Au values in the range 190-380 μg/kg in a 4 km channel sector above the confluence with Río Yanuncay.

  (b) inputs from weak epithermal mineralisation within the Cerro Plancharumi massif (described above).

  The poor correlation between high Au and Hg values in the Río Yanuncay is partially attributable to the influx of Río Soldados detritus, in which Hg enrichment has nowhere been recorded. An additional complexity may be introduced by hot spring emanations into the Río Yanuncay (>70°C at surface, with high dissolved sulphide content) between 699000E-702000E. Such emanations are considered to constitute the surface expression of a major structural conduit for deep circulating fluids which may remobilise Hg from epithermal sources within the Plancharumi (or possibly the Quimsacocha) tract.

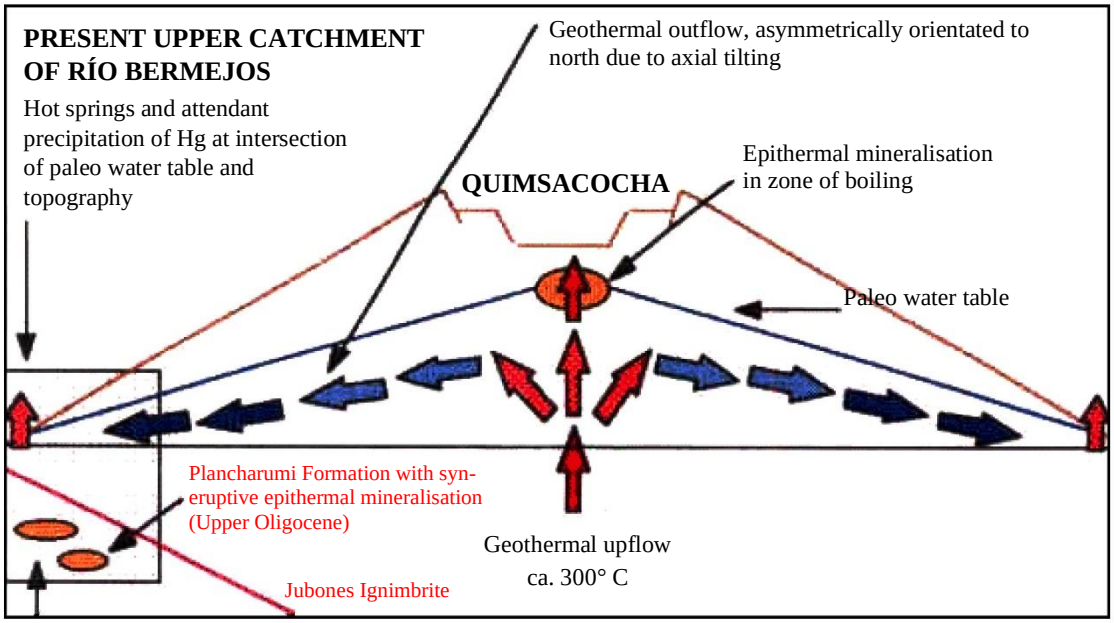

Figure 42. Possible Mio-Pliocene metallogenetic setting for the Upper Río Bermejos catchment, indicating epithermal mineralisation at Quimsacocha and mercurious mineralisation related to hot spring emanations at the northern margin of the lava pile. Earlier low-sulphidation mineralisation hosted by the Plancharumi Formation is related to late Oligocene silicic volcanism within a lacustrine environment.

6.1.2.4 Quebrada El Llanto

Strong enrichment of Au (2524 µg/kg), metalloids (As 272 mg/kg, Sb 532 mg/kg) and base metals (Cu 1705 mg/kg, Zn 1091 mg/kg) in the mid-reaches of Q. El Llanto occurs in an area of known, yet poorly evaluated mineral potential. A small adit on the eastern side of the quebrada at ca. 6788-96730 has been driven to exploit a high-grade vein, debris from which has entered the river and has enhanced the drainage anomaly recorded downstream. Both the geochemical signature and the geological setting remain, however, of interest, with possible analogies to mineralisation in the Río Angas system. In the Q. El Llanto vicinity, fine grained diorite with intermittent silicification and disseminated pyrite is reported to the north and south of the settlement of Cascajo. Close to the polymetallic anomaly the interfluve west of Q. El Llanto shows intense silicification and the presence of a well-developed gossan (similar to that capping porphyry mineralisation of the Chaucha system at Naranjos). Although intensely altered, the parent lithology along the interfluve is recognisable as volcanoclastic, with relatively fresh diorite exposed downslope. The gossanous cap and underlying zone of sulphide mineralisation must thus be hosted within a volcanic roof pendant of the Chaucha Batholith. Modest Au anomalies in the Río Pita, some 3 km to the west, may relate to mineralisation hosted in the same silicified, oxidized pendant. In both cases, the signatures are conspicuously As-Sb rich, with high base-metal concentrations.

6.2 Lithogeochemical signatures

The utility of regional stream sediment geochemical data as a tool for elucidating and/or delineating lithological boundaries, depositional regimes and paleoenvironments has been demonstrated previously (e.g. Williams et al., 1995a; Stone et al., in press). With respect to the GIMP 2°-3° S area, such data reflect the basic lithotectonic model of:

(i) accretion of an ocean-floor basalt suite (Cr, Co, Cu, Mg, Ni) faulted against a metamorphic basement,

(ii) accretion of an Early Tertiary ensimatic arc (high Cu/Cr) onto the continental margin,

(iii) silicic subduction-related volcanism (Pb, Ba rich with low Cu-Cr-Ni-V) with later intermediate facies,

(iv) emplacement of a suite of granodiorite (Ca, Co, Mg, Ni, Sr-poor, K-rich) and diorite intrusions.

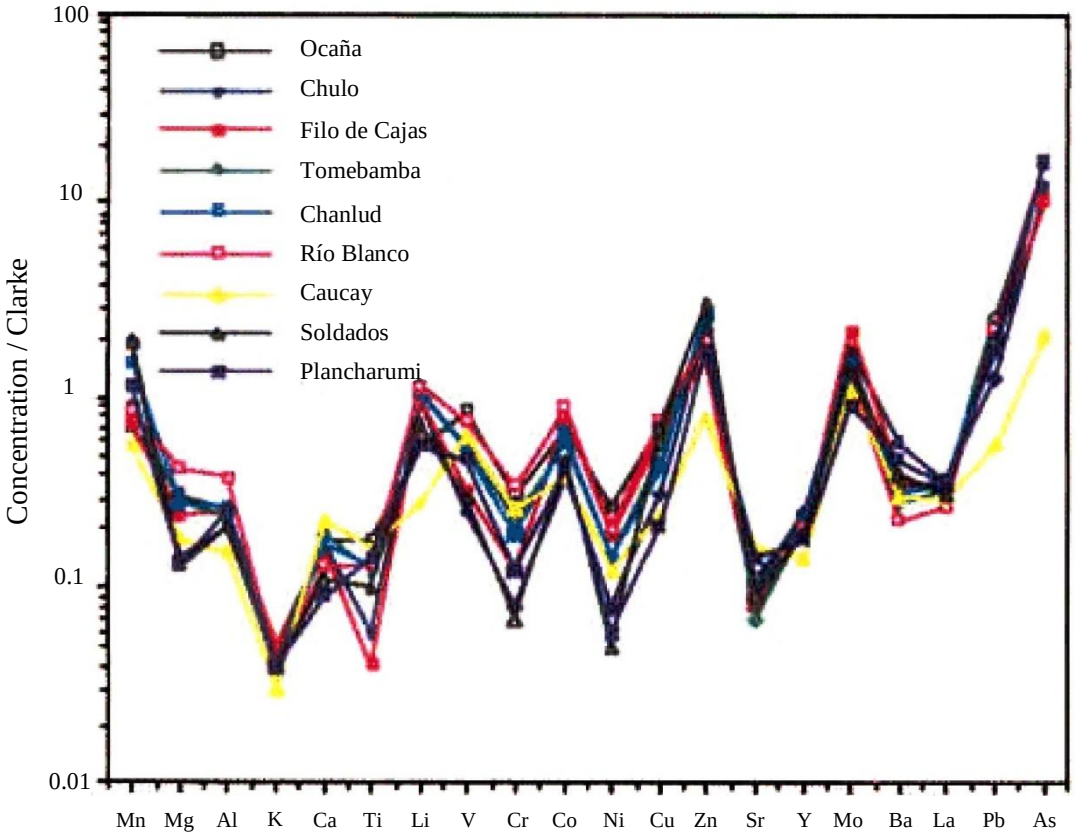

Figure 43. Geochemical signatures of nine component units of the Saraguro Group based on crust-normalised sediment data for the GIMP 2°-3°S area

Through more detailed interrogation, it is possible to highlight more subtle contrasts within the regional lithostratigraphy. Figure 43 exemplifies a simple approach to geochemical data manipulation, applied to the newly defined lithostratigraphic units of the Saraguro Group. Spidergrams were produced by isolating multi-element data for individual Formations of Dunkley and Gaibor (1997b) using the Interdex polygonal sub-setting routine, from which mean 'within-unit' element values were calculated. Each mean was subsequently normalised against the average upper-crustal concentration (Clarke value) for the corresponding element, facilitating the projection of values for some 20 elements of widely varying abundance on a single axis. It requires emphasis that these normalised sediment values, while internally comparable, cannot be used as direct whole-rock surrogates due to complexities arising from (i) weathering, (ii) concentration or dilution of minerals in the fluvial environment, and (iii) partial dissolution effects during chemical analysis.

The spidergrams for the Saraguro Group units presented show particular discordance of signature between units in the V-Cu sector of the spectrum. Low normalised values of Cr and Ni, for example, clearly define the silicic facies of the Chulo and Soldados Formations while the andesitic lavas and tuffs of the Río Blanco Formation yield high normalised levels of Mg, Al, V, Co, Cu, with low Ba and La. Differentiation between units is, however, masked in some instances by within-group heterogeneity, for example in the Chanlud Formation which comprises both intermediate and acid sub-components. Further refinement of the sub-setting approach for the more complex geological units is therefore required in order to maximise the utility of the data.

6.3 Environmental baselines

6.3.1 Rationale

Drainage geochemistry data, although generated almost exclusively for metalliferous mineral exploration prior to the 1980's, are now recognised as a valuable resource for environmental auditing, risk assessment and land-use planning at scales ranging from site-specific to global. The requirement for internally consistent, national and international multi-element datasets for environmental purposes has provided the impetus for the development of a global geochemical database under IGCP 259 (Darnley et al., 1995) to which the GIMP will ultimately contribute. Within the specific context of the Ecuadorian Western Cordillera, the contribution of GIMP geochemistry datasets to long-term environmental monitoring and protection may be particularly pronounced, as collation has in many cases preceded any major human perturbation. The data thus provide an environmental baseline against which the impacts of future industrial, extractive or related activities can be quantitatively appraised.

6.3.2 Development of sediment quality criteria

The availability of sediment quality criteria remains limited relative to the established water quality standards (mostly derived from US-EPA and WHO potable water limits) routinely deployed by environmental regulatory authorities worldwide. In recent studies of mining and urbanization impacts on sediment quality in Ecuador, the Philippines, Indonesia and East Africa (e.g. Williams et al., 1996a, 1996b, 1997; Appleton et al., 1996) guidelines from the EC Draft Criteria Document (Van Veen and Strotelder, 1988) presented to the International Sediment Quality Forum (1992), and/or the Canadian Sediment Quality Criteria for the Protection of Aquatic Life (Environment Canada, 1992; reviewed in MacDonald, 1994) have been applied. The former are, however, based solely on statistical analysis of sediment data from the Netherlands and thus have no specific human or ecotoxicological significance. The latter (Table 27), although based on modelled and experimental dose-response data, assumes 100% bioavailability for sediment-bound contaminants (although the effect of pH is accommodated, thus accounting for the relatively high Pb toxic effect threshold at pH 7.0) with the result that action thresholds are unrealistically low (see section 6.3.3 below).

Table 27. Sediment Quality Criteria for the Protection of Aquatic Life. Source: Environment Canada (1992), reviewed by MacDonald (1994).

Element	No effect threshold	Minimal effect threshold	Toxic effect threshold
As	3	7	17
Cd	0.2	0.9	3
Cu	28	28	86
Pb	23	53	170
Hg	0.05	0.2	1
Zn	100	150	540

The application of universal trace element standards for soil or sediment quality assessment at the regional, national or international scale is now recognised as a weakness in this field of environmental regulation in Europe and North America. Such standards fail to account for the natural (lithologically controlled) variability of ambient environmental concentrations of both micro-nutrients and potentially toxic trace elements. The resultant problems can be exemplified by applying the Sediment Quality Criteria for the Protection of Aquatic Life (Environment Canada, 1992) toxic effect threshold for As (Table 27) to the GIMP 2°-3°S area, in which median As values range from <4 mg/kg over the Macuchi, Puñay and Cisarán Formations to >20 mg/kg over the Filo de Cajas Unit, Tomebamba, Chanlud and Río Blanco Formations. A threshold of 17 mg/kg thus corresponds to >4 × the background (as defined by the median) within the former units, yet falls below the background of the latter. Through the application of a (cautionary) bioavailability quotient of 20% (see section 6.3.3 below) a more realistic toxic effect threshold may be ca. 85 mg/kg. However, the adoption of such a high threshold for regulatory purposes is, in turn, unsatisfactory, facilitating, for example, the indiscriminate use of (high bioavailability) arsenical pesticides without exceedance of statuary action limits in areas with the lowest natural backgrounds.

A more pragmatic approach to the development of quality criteria for environmental monitoring and protection, now gaining international acceptance, involves the derivation of lithologically normalised background, threshold and action levels for sediment (or soil) contaminants (e.g. Darnley et al., 1995). These provide a basis for assessing the environmental impact of agricultural, industrial and residential developments within their specific local or regional context. The establishment of such normalised thresholds is, however, dependent on the existence of regional or national-scale geological and multi-element geochemical data which depict the natural lithological spectrum. In this respect, the geological mapping and regional reconnaissance programmes conducted under the GIMP may directly underpin the development under PRODEMINCA sub-component 2.3 (Policy Development) of national environmental legislation.

6.3.3 Significance of contaminant speciation

The influence of solid-phase speciation on the mobility and toxicity of sediment (or soil) contaminants is an important consideration in threshold derivation. With respect to Pb, for example, the bioavailability of oxides at pH 7 may exceed that of detrital sulphide, secondary carbonates (cerussite) or phosphates (pyromorphite) at the same pH by a factor of 100 (Fergusson, 1994). With respect to As, the toxicity of arsenite compounds may exceed that of arsenates by a factor of 10, and that of mono or dimethyl species by 100 (Williams et al., 1995b).

Existing environmental risk thresholds for many inorganic toxins have, in part, been derived from experimental dose-response data for high solubility compounds, which have then been applied unadjusted in environmental impact assessment (e.g. Environment Canada, 1992) and/or human risk assessment (e.g. within the US-EPA package Risk Assistant; Hampshire Research Inst., 1996). With respect to soils and sediments in which contaminant bioavailabilities are much lower, the perceived risk associated with 'threshold' heavy metal or metalloid loads is thus characteristically exaggerated. Studies of areas of As, Pb and Hg contaminated soil in the US (Davis et al., 1993), the Philippines (Williams et al., 1996a) and Thailand (Williams et al., in press) have demonstrated that such inaccurate risk evaluation can result in the implementation of unwarranted, often costly remediation schemes.

Characterisation of sediment micro-mineralogy, metal speciation and mobility across the diverse physiographic and climatic regimes of Ecuador would be both time-consuming and expensive, and lies beyond the current project remit. Speciation influences may, however, be accounted for in the establishment of national sediment quality criteria by reference to the large body of published data for sediments worldwide. Studies by BGS of heavy metal and metalloid mobility in compositionally diverse contaminated sediments from the UK, Greece, Malaysia, Thailand, the Philippines, Zimbabwe, and Kenya (e.g. Williams, 1992; 1997; Williams et al., 1994; Breward et al., 1995) indicate a probable bioavailability spectrum of 1-20% for As, Sb, Cu, Zn, Pb, Hg and Cd under naturally occurring pH-Eh conditions. The application of a 20% factor may in many respects prove practical. Adjustment in this manner of the toxic effect thresholds for Pb and Zn quoted in Table 27 yields values of 430 mg/kg and 2700 mg/kg respectively. These are closely analogous to the EC Draft Criteria Document 'limit' values of 400 mg/kg for Pb and 2500 mg/kg for Zn (Van Veen and Strotelder, 1988).

The value of determining a series of toxic threshold concentrations for individual elements which can be selectively applied in accordance with local environmental conditions has been recognised in the development of the UK-DOE CLEA risk assessment model (Ferguson and Denner, 1995). This utilises independent ‘soft-water’ and ‘hard-water’ toxicity quotients for Pb and other heavy metals. An analogous approach to sediment quality appraisal is strongly advocated, with differing thresholds applied on the basis of (i) sediment pH, (ii) hydrous oxide, (iii) carbonate and (iv) organic content.

6.3.4 Data application in the prediction and control of mining impacts

Studies of the hydrochemistry of drainage waters from over fifty Au and complex sulphide operations in Africa and SE Asia (Williams and Breward, 1995) have shown the composition of leachates to be a predictable function of deposit type, ore mineralogy and geological setting (Fig. 44). In addition to defining exploration targets, drainage sediment geochemistry data also elucidate the sulphide composition of the assemblage. Such data therefore provide an early insight into potential geochemical hazards associated with deposit exploitation, of value at the project planning and preliminary impact assessment stages.

Williams et al. (1994) have summarised the principal determinants of mine drainage quality as:

(i) abundance of pyrite, other acid-generating and/or heavy-metal bearing sulphides,

(ii) susceptibility of sulphides to dissolution (controlled by grain size, structure and exposure),

(iii) gangue and host rock buffering capacity (carbonates, hydrous oxides, aluminosilicates),

(iv) water-rock interaction with respect to sulphide bearing material (permeability),

(v) interaction of permeating fluids with atmosphere (O_2 content),

(vi) microbial activity (notably Thiobacilli),

(vii) mining and beneficiation technology,

(viii) climate.

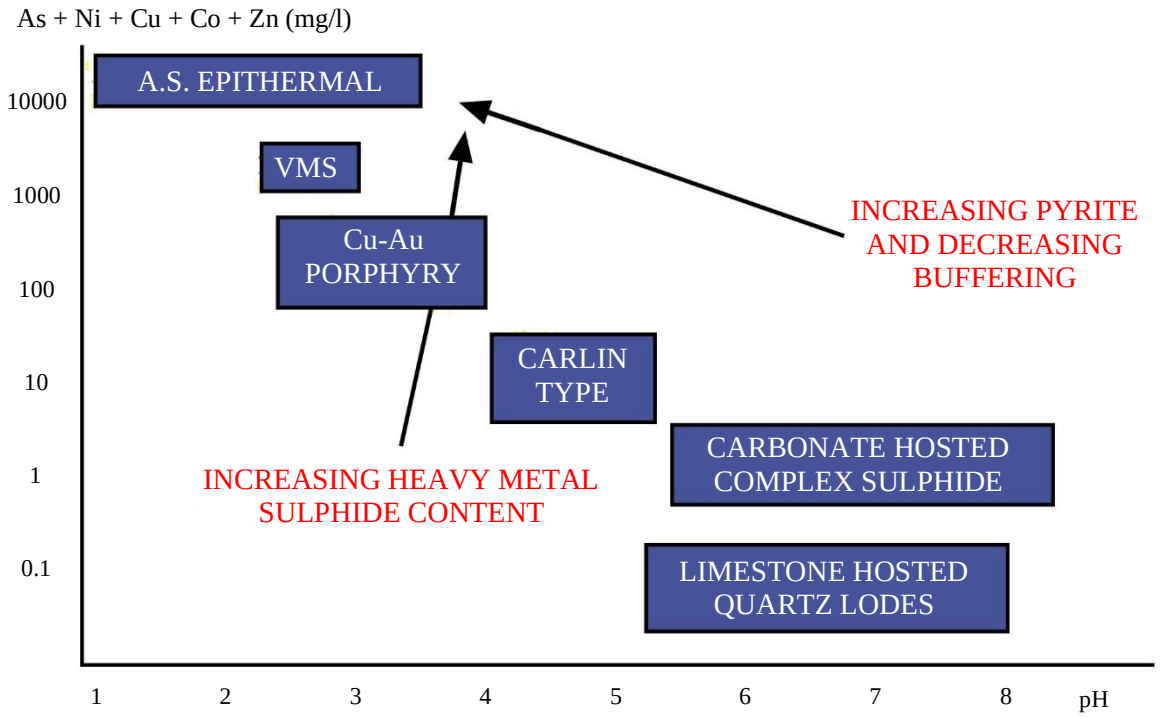

Figure 44. Characteristic pH and dissolved contaminant characteristics of mine-water associated with contrasting metallogenic settings, based on empirical data from Thailand, Malaysia, Zimbabwe, the Philippines and the USA

In most settings the fundamental process driving contaminant dispersal is acid rock drainage (ARD) generation.

Spontaneous oxidation of pyrite and other sulphides can occur in all oxygen-containing environments in accordance with the thermodynamics of the Fe-S-H_2O system:

$O_2 + 4H^+ + 4e^- \rightarrow 2H_2O$ driving reactions such as:

$FeS_2 + 8H_2O \rightarrow Fe^{2+} + 2SO_4 + 16H^+ + 14e^-$

At higher electrode potentials (and pH > 2) the reaction may be:

$FeS_2 + 11H_2O \rightarrow Fe(OH)_3 + 2SO_4 + 19H^+ + 15e^-$

or:

$FeS_2 + 19H_2O \rightarrow Fe_2O_3 + 4SO_4 + 38H^+ + 30e^-$

Oxidation of sulphides by ferric iron (significantly soluble at low pH) may also occur in accordance with the reaction:

$FeS_2 + 14Fe^{3+} + 8H_2O \rightarrow 15Fe^{2+} + 2SO_4 + 16H^+$

The number of free H^+ ions liberated during sulphide oxidation is non-uniform, being strongly dependent on the metal/sulphur ratio, the oxidant (O_2 or Fe^{3+}) and the precipitates formed. Oxidation processes involving pyrite are most prolific with respect to proton generation, roughly followed by pyrrhotite, chalcopyrite, arsenopyrite, enargite and tennantite. Acid generation associated with the oxidation of pure sphalerite is theoretically zero. From a knowledge of the oxidation chemistry of the respective sulphides. GIMP sediment data (ideally coupled with information collected throughout the survey for heavy mineral concentrates) can be applied to provide a qualitative indication of the magnitude of ARD and attendant heavy metal mobilization problems which may follow the exploitation of any given prospect. It requires emphasis that net acid generation is a function of H^+ production through sulphide oxidation and hydrolysis, countered by buffering effects derived from the weathering of carbonates, aluminosilicates and hydrous oxides in the gangue assemblage and host lithology. Accordingly, there is a requirement to incorporate lithological information of the nature collected under the GIMP geological mapping programme into any preliminary predictive model.

Within the GIMP 2°-3°S area a fundamental contrast should be drawn between low-sulphidation prospects (Río Blanco and Cerro Plancharumi) and acid-sulphate epithermal or polymetallic mesothermal targets (Q. El Llanto, upper Río Angas) with respect to their environmental geochemistry. In the latter, problems of high ARD generation capacity are compounded by high levels of As and Sb, which form stable oxyanions with mobility across a wide pH range. While such factors do not inevitably result in adverse post-exploitation impacts, they should be an essential consideration in any operational and post-closure plan.

6.3.5 Natural geochemical hazards

The importance of environmental geochemistry in the aetiology of numerous trace element-related diseases has been emphasised by Mills (1996). Lithologically-controlled variations in the concentrations of P, I, Se, Cu, Co and other trace elements exert a first-order control on the distribution of numerous animal and/or human diseases related to micro-nutrient deficiency, of which goitre and cretinism related to I-deficiency (e.g. Fuge, 1996) and Se-responsive cardiomyopathic diseases (e.g. Mills, 1996) are best documented. Darnley et al. (1995) have shown extensive regions of the world to have natural levels of essential trace elements well below those recommended for agricultural soils and pasture. Chronic toxicity problems (in humans and/or livestock) associated with natural exposure to F (notably East Africa), As (India, Bangladesh, Thailand, Argentina, Mexico, Chile, Uruguay) and Se (China, USA) are also widely known (e.g. Plant et al., 1996).

Within the context of human and animal health, potentially significant natural geochemical features of the GIMP 2°-3°S area include a zone of intense Mo enrichment (to 100×mean upper crustal abundance) over Chaucha and localised Hg enrichment (to 400×mean upper crustal abundance) near Soldados and in the Río Patamarca (ref. 716310-9690325). High environmental Mo levels (typically restricted to Cu-Mo porphyry systems and black shales) are a potential cause of secondary Cu deficiency through the inhibition of Cu assimilation in ruminants (Mills, 1996). The influence is strongly pH-dependent, and further characterisation of local physico-chemical conditions would be necessary to fully evaluate the risk. With respect to Hg, peak values recorded in the upper Río Bermejos and Río Patamarca systems (both of which show no significant anthropogenic disturbance) are analogous to maxima reported for the Nambija artisanal mining field (34 mg/kg; Williams and Orbea, 1997), and a factor of 5 higher than at Ponce Enríquez (Appleton, 1996). These natural anomalies also lie within the upper range of sediment values documented for major gold-rush localities in Brazilian Rondonia and Venezuela (Pfeiffer et al., 1989; 1991; Martinelli et al., 1988). It requires emphasis that Hg toxicity is strongly influenced by chemical speciation. Marked contrasts usually exist between zones of natural and anthropogenic Hg enrichment in this respect. In the former, stable (detrital sulphide and/or secondary oxyhydroxide) phases predominate while the latter are typically dominated by metallic Hg with relatively rapid rates of volatisation and biologically-mediated methylation. The presence of labile Hg sulphide or chloro-complexes is, however, possible in the hot springs of the Río Yanuncay system (indicated by sediment Hg anomalies close to major emanations). These waters warrant hydrochemical characterization as part of a broader toxicological evaluation.

6.4 Concluding statement

All data incorporated within this document were compiled in accordance with the specific objectives of PRODEMINCA sub-component 3.4 (Thematic Mapping), and the broader PRODEMINCA goals outlined in the Project Memorandum of the World Bank (1993). To achieve the latter, the integration of geochemical data with geoscientific, social and economic outputs of other project sub-components is a central requirement. Probable areas of application for geochemical reconnaissance data (excluding exploration) within the context of PRODEMINCA include Policy Development (2.3). Monitoring of Pollution and Health Related to Mining Activities (3.1), Containment and Neutralization of Hazardous Mining Wastes (3.2), Geological Mapping (3.3) and Assessment of Ore Districts (3.5). Utilisation of geochemical information within these sub-components has been facilitated to the greatest possible extent under the GIMP by the adoption of an Oracle database and Intergraph GIS, compatible with IT systems used under all other technical PRODEMINCA sub-components.

The function of this document as a methodological/data overview is outlined in section 1.2. Following the 1998 release of digital geochemical data for the GIMP 3°-4°S and 2°-3°S areas, the strategic and economic return will be determined largely by private sector interest. The demand for the involvement of CODIGEM, DINAPA, DINAMI and other government departments in data management, the provision of multi-thematic datasets and interpretive guidance will, however, remain. This longer-term public-sector contribution may ultimately be no less important than private investment in achieving the central PRODEMINCA goal of sustainable development of Ecuador’s metalliferous minerals sector.

7. BIBLIOGRAPHY

APPLETON J. D. (1996) Assessment of mercury contamination in the Ponce Enríquez artisanal gold mining area, Ecuador. British Geological Survey, Overseas Geology Series Technical Report WC/96/55.

BOLVIKEN B. and SINDING-LARSEN B. (1973) Total error and other criteria in the interpretation of stream sediment data. In: Geochemical Exploration 1972 (London: Institution of Mining and Metallurgy).

BREWARD N., WILLIAMS T. M. and BRADLEY D. (1995) Comparison of alternative extraction methods for determining particulate metal speciation. Applied Geochemistry, vol. 11, 101-104.

BRISTOW C. R. and PARODIZ J. J. (1982) The stratigraphical palaeontology of the Tertiary non-marine sediments of Ecuador. Bulletin of Carnegie Museum of Natural History, No. 19, 1-53. (Pittsburgh, Pennsylvania).

BRITISH GEOLOGICAL SURVEY (1993) Regional geochemistry of southern Scotland and part of northern England. NERC, Keyworth, Nottingham, UK.

DARNLEY A. G., BJÖRKLUND A., BØLVIKEN B., GUSTAVSSON N., KOVAL P. V., PLANT J. A., STEENFELT A., TAUCHID M., XIE XUEJING, GARRETT R. G. and HALL G. E. M. (1995) A global geochemical database for environmental and resource management: Recommendations for international Geochemical Mapping. Final Report of IGCP Project 259. UNESCO, Paris, 122 p.

DAVIS A., DREXLER J. W., RUBY M. V. and NICHOLSON A. (1993) Micromineralogy of mine wastes in relation to lead bioavailability, Butte, Montana. Environmental Science and Technology, 27, 1415-1424.

DUNKLEY P. N., GAIBOR A. and BOLAÑOS J. E. (1997) Geochemical orientation survey, Río Junín. Geological Information Mapping Programme (GIMP) Report No. 5. World Bank Mining Development and Environmental Control Project (PRODEMINCA), Misión Geológica Británica, CODIGEM, Quito, Ecuador.

DUNKLEY P. N. and GAIBOR A. (1997a) Control of quality of geochemical data. Geological Information Mapping Programme (GIMP) Report No. 6. World Bank Mining Development and Environmental Control Project (PRODEMINCA), Misión Geológica Británica, CODIGEM, Quito, Ecuador.

DUNKLEY P. N. and GAIBOR A. (1997b) Geology of the area between 2 and 3 degrees south. Western Cordillera, Ecuador. Report No. 2. World Bank Mining Development and Environmental Control Project (PRODEMINCA), Misión Geológica Británica, CODIGEM, Quito, Ecuador.

EGÜEZ A. (1986) Evolution Cénozoïque de la Cordillère Occidentale Septentrional d’Equateur (0°15’S o 1°10’S). Les mineralisation associées. Unpublished Ph.D. Thésis; Université Pierre et Marie Curie, Paris, 116p.

EGÜEZ A., DUGAS F. and BONHOMME M. (1992) Las Unidades Huigra y Alausí en la Evolución Geodinámica del Valle Interandino del Ecuador. Boletín Geológico Ecuatoriano, 3, 47-56.

FERGUSON C. C. and DENNER J. M. (1995) UK Action (or intervention) values for contaminants in soil for protection of human health. Proceedings of the Fifth International FZK/TNO Conference on Contaminated Soil 1995. Maastricht, Netherlands, 2. 1199-1200.

FERGUSSON J. E. (1994) The heavy elements: Chemistry, Environmental impact and health effects. Oxford, Pergamon Press.

FUGE R. (1996) Geochemistry of iodine in relation to iodine deficiency diseases. In: Environmental geochemistry and health with special reference to developing countries. Geological Society Special Publication No. 113, 201-213. Geological Society of London.

GARRETT R. G. (1983) Sampling methodology. In: Howarth R. J. Ed. Handbook of exploration geochemistry volume 2: Statistics and data analysis in geochemical prospecting. Chapter 4, 83-111. Elsevier, London.

HAMPSHIRE RESEARCH INSTITUTE (1996) RISK ASSISTANT for Windows. 9426 Forest Haven Drive. Alexandria. Virginia 22309-3151. USA.

HUNGERBÜHLER D. and STEINMANN M. (1996) Curso internacional geología de cuencas sedimentarias (Mioceno, Sur del Ecuador). Guía del campo. Escuela Politécnica Federal de Zürich, 27.

MACDONALD D. D. (1994) A review of environmental quality criteria and guidelines for priority substances in the Fraser River basin. DOE-FRAP. 1994-30.

MARTINELLI L. A., FERREIRA J. R., FORSBERG B. R. and VICTORIA R. L. (1988) Mercury contamination in the Amazon: a gold rush consequence. Ambio, 17 No. 4, 252-254.

MCCOURT W., DUQUE P. and PILATASIG L. (1997) Geology of the Cordillera Occidental of Ecuador between 1° and 2° S. Geological Information Mapping Programme (GIMP) Report No. 3. World Bank Mining Development and Environmental Control Project (PRODEMINCA). Misión Geológica Británica, CODIGEM, Quito, Ecuador.

MILLS C. F. (1996) Geochemical aspects of the aetiology of trace element related diseases. In: Environmetal geochemistry and health with special reference to developing countries. Geological Society Special Publication No. 113, 1-7. Geological Society of London.

MÜLLER-KAHLE E. and DAMON P. E. (1969) K-Ar age of a biotite granodiorite associated with primary Cu-Mo mineralization at Chaucha, Ecuador. In Damon P. E. (Editor). Correlation and chronology of ore deposits and volcanic rocks. United States Atomic Energy Commission Annual Progress Report CCO-689-130. University of Arizona Tucson, 46-48.

NAKASHIMA S. (1979) Selective determination of arsenic (iii) and arsenic (v) by atomic absorption spectrophotometry following arsine generation. Analyst. Vol. 104, pp. 172-173.

PÉREZ H. O. (1990) Sansahuin y Quimsacocha: centros de emisión de la Formación Tarqui. *Boletín Geológico Ecuatoriano,* Vol. 1, 69-73.

PFEIFFER W. C., LACERDA D. L., MALM O., SOUZA C. M. M., DE SILVA E. G. and BASTOS W. R. (1989) Mercury concentrations in inland waters of gold mining areas in Rondonia, Brazil. Science of the Total Environment. 78, 233-240.

PFEIFFER W. C., MALM O., SOUZA C. M. M., LACERDA D. L., DE SILVA E. G. and BASTOS W. R. (1991) Mercury in the Madeira River ecosystem. Rondonia, Brazil. Forest Ecology and Management, 38, 239-245.

PLANT W. C. (1973) A random numbering system for geochemical samples. Transactions of the Institution of Mining and Metallurgy, section B. 83.

PLANT J. A. and MOORE P. J. (1979) Regional geochemical mapping and interpretation in Britain. Philosophical Transactions of the Royal Society of London, Vol. 288, B95-112.

PLANT J. A., JEFFREY J. K., GRILL E. and FAGE C. (1975) The systematic determination of error, accuracy and precision in geochemical exploration data. Journal of Geochemical Exploration, Vol. 4, 467-486.

PLANT J. A., BALDOCK J. W. and SMITH B. (1996) The role of geochemistry in environmental and epidemiological studies in developing countries: a review, In: Environmental geochemistry and health with special reference to developing countries. Geological Society Special Publication No. 113, 7-23. Geological Society of London.

PRATT W. T., FIGUEROA J. F. and FLORES B. G. (1997) Geology of the Cordillera Occidental of Ecuador between 3° and 4° S. Geological Information Mapping Programme (GIMP) Report No. 1. World Bank Mining Development and Environmental Control Project (PRODEMINCA), Misión Geológica Británica, CODIGEM, Quito, Ecuador.

RIVERA M., EGÜEZ A. and BEATE B. C. (1992) El volcanismo Neógeno de Los Andes Australes: Sus manifestaciones en la zona entre Cuenca y Soldados. Ecuador. Memorias de la Segunda Jornada en Ciencias de la Tierra, 56-57.

SNELLING N. J. (1969) Personal communication in Bristow C. R. and Hoffstetter R. (1977) (Compilers). Lexique Stratigraphique International, Ecuador. Second edition. Paris: Centre National de la Recherche Scientifique.

STONE P., GREEN P. M. and WILLIAMS T. M. (1997) Relationship of source and drainage geochemistry in the British paratectonic Caledonides: and exploratory assessment. Transactions of the Institution of Mining and Metallurgy, section B. Vol. 106, B79-B84.

TAYLOR S. R. and MCLENNAN S. M. (1985) The Continental Crust: its Composition and Evolution. Blackwell, Oxford.

THOMPSON M. and HOWARTH R. J. (1976) Duplicate analysis in geochemical practice. Analyst, 101, 690-709.

THOMPSON M. and HOWARTH R. J. (1978) A new approach to the estimation of analytical precision. Journal of Geochemical Exploration, 9, 23-30.

THOURNOUT V. F. and GUZMÁN J. (1988) Brechas hidrotermales relacionadas con posibles centros eruptivos en los volcánicos Tarqui cerca de Angas, Azuay. Significado metalogénico para la formación, Politécnica, Monografía de Geología 6, Vol. 13, No. 3, 7-31.

UNITED NATIONS DEVELOPMENT PROGRAMME (1969) Survey of metallic and non-metallic minerals. Coal Investigations (Operation No. 1, Cuenca-Biblián and Loja). *Technical Report, United Nations Development Programme, Quito-New York.*

UNITED NATIONS DEVELOPMENT PROGRAMME (1972) Survey of metallic and non-metallic minerals. Technical Report No. 16, Quito-New York.

VAN VEEN R. J. and STROTELDER P. B. M. (1988) Research on contaminated sediments in the Netherlands. In Wolf K., Van de Brink W. J. and Colon F. J. (Eds). Contaminated soil. 1263-1275. Academic Publ.

WILLIAMS T. M. (1992) Trace metal speciation in surficial sediments from Loch Dee, southwest Scotland, U.K. Environmental Geology 21, 62-70.

WILLIAMS T. M., ROBOTHAM H. and SIMPSON P. R. (1992) Soil geochemistry of the Central, Above Rocks and Blue Mountains inliers and intervening Cenozoic sequences. Jamaica. British Geological Survey Geochemistry Series Technical Report WP/92/13/R.

WILLIAMS T. M. and BREWARD N. (1995) Environmental impacts of gold and complex sulphide mining (with particular reference to arsenic contamination). British Geological Survey Overseas Geology Series Technical Report WC/95/2.

WILLIAMS T. M., HENNEY P. J., LINTERN B. C. and STONE P. (1995a) Rare earth element geochemistry of Lower Palaeozoic turbidites in the Trans-Iapetus Zone: Provenance patterns and basin evolution. Scottish Journal of Geology, 32, part 1.

WILLIAMS T. M., FORDYCE F. M., PAIJITPRAPAPON A. and CHAROENCHAISRI P. (1995b) Arsenic contamination in surface drainage and groundwater in part of the Southeast Asia tin belt. Nakhon si Thammarat Province, Southern Thailand, Environmental Geology, 27, 16-33.

WILLIAMS T. M., WEEKS J. M., APOSTOL A. and MIRANDA C. (1996a) Assessment of mercury toxicity hazard associated with cinnabar mining and tailings disposal in Honda Bay, Palawan, Philippines. British Geological Survey. Overseas Geology Series Technical Report WC/96/31/R.

WILLIAMS T. M., REES J. G., KAIRU K. K. and YOBE A. C. (1996b) Assessment of contamination by metals and selected organic compounds in coastal sediments and waters of Mombasa, Kenya. British Geological Survey. Overseas Geology Series Technical Report WC/96/37.

WILLIAMS T. M. (1997) Environmental Arsenic Exposure: Health Risks and Geochemical Solutions (DFID Contract R6491). Mining sub-project, Thailand case-study summary report. British Geological Survey. Overseas Geology Series Technical Report WC/97/49.

WILLIAMS T. M. and ORBEA H. (1997) Dispersal of mercury and ore-derived metals in surface drainage of the Nambija artisanal mining field, Ecuador. British Geological Survey. Overseas Geology Series Technical Report WC/97/37.

WILLIAMS T. M., REES J. and SETIAPERMANA D. (1997) Land-derived contaminant influx to Jakarta Bay, Indonesia, Volume 1: Geochemistry of marine water and sediment. British Geological Survey. Overseas Geology Series Technical Report WC/97/19.

WILLIAMS T. M., RAWLINS B. G., SMITH B. and BREWARD N. (in press) In-vitro determination of arsenic bioavailability in contaminated soil and beneficiation waste from Ron Phibun, Southern Thailand. Environmental Geochemistry and Health.

APPENDIX 1 OF REPORT:

GEOCHEMICAL RECONNAISSANCE SURVEY OF THE WESTERN CORDILLERA OF ECUADOR BETWEEN 2°00' AND 3°00' S

PRECISION CONTROL CHARTS

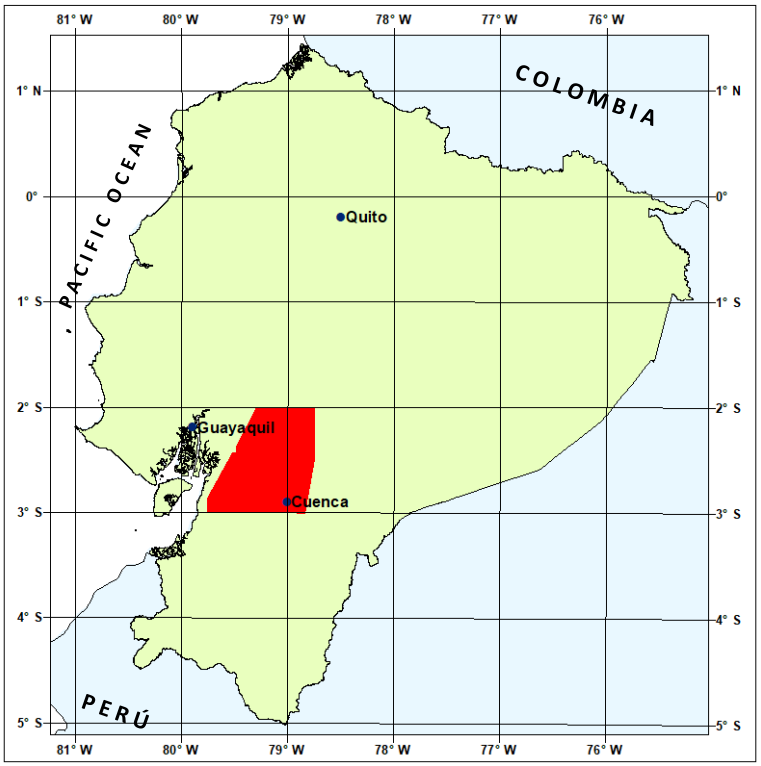

GEOLOGICAL INFORMATION MAPPING PROGRAMME (LOCATION OF MAP 2 AREA)

QUITO, 1997

Precision-control charts for selected elements determined under the GIMP regional geochemical survey programme, showing 90th and 99th percentile concordance lines in each case.

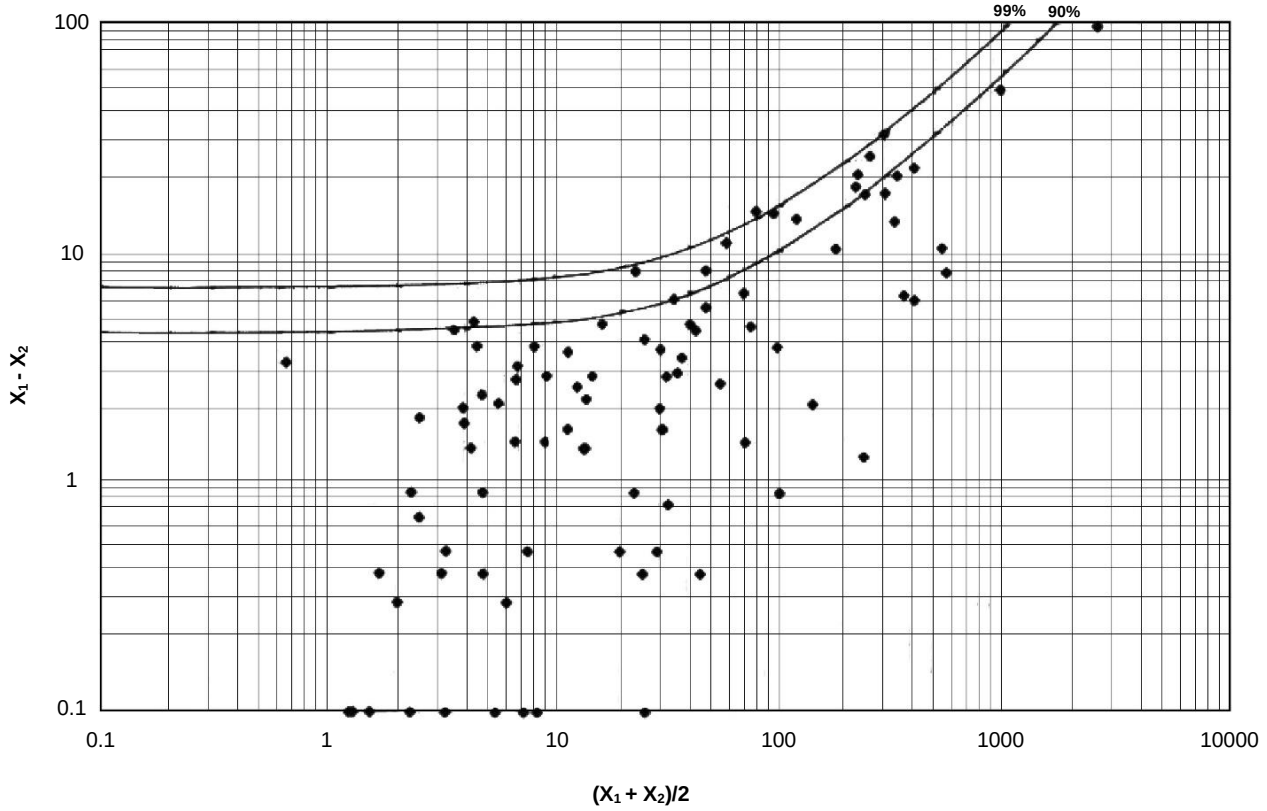

Figure 1. Arsenic duplicate analyses. Precision = 5%, DL = 4 ppm

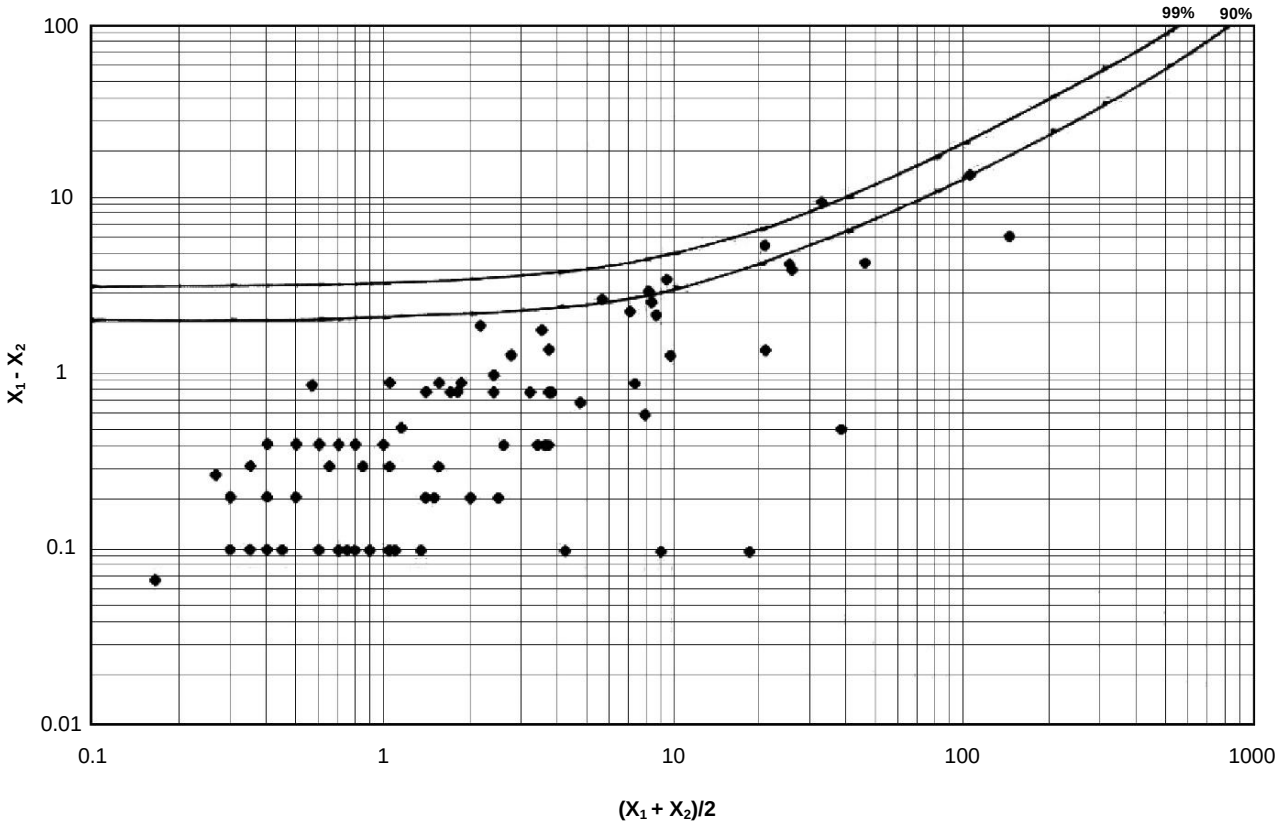

Figure 2. Antimony duplicate analyses. Precision = 10%, DL = 1.9 ppm

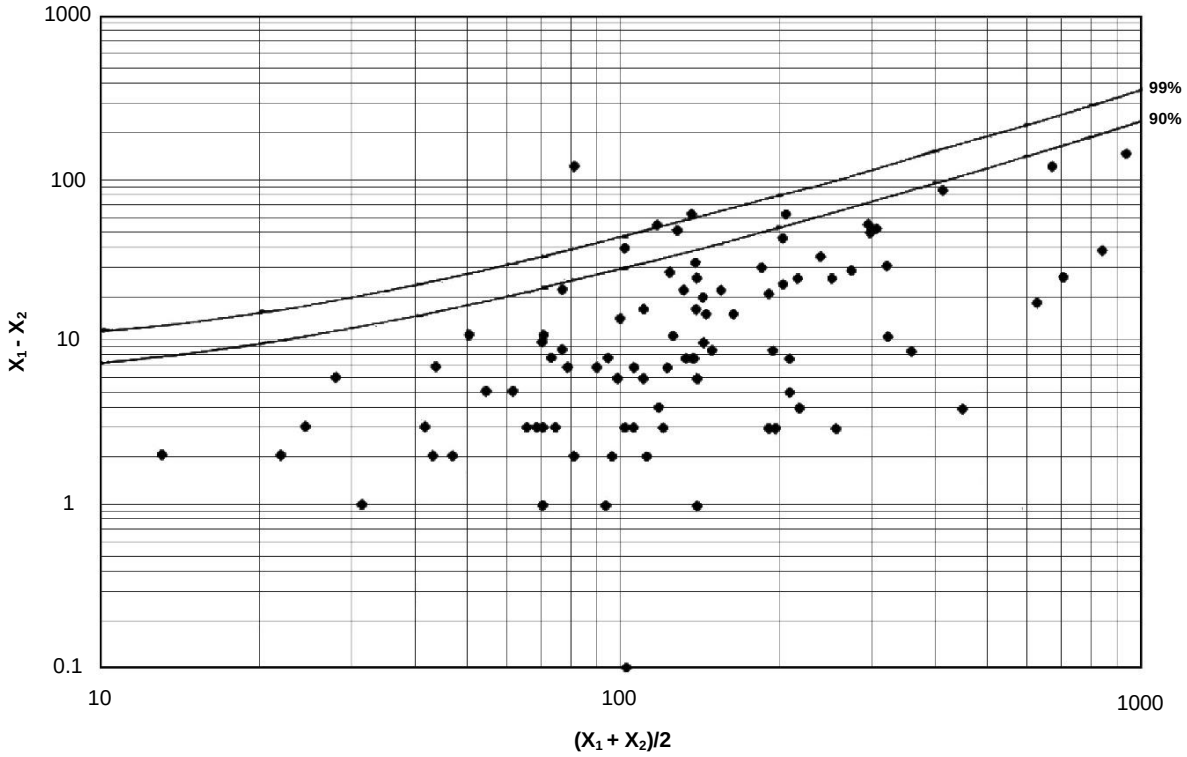

Figure 3. Barium duplicate analyses. Precision = 20%, DL = 5.4 ppm

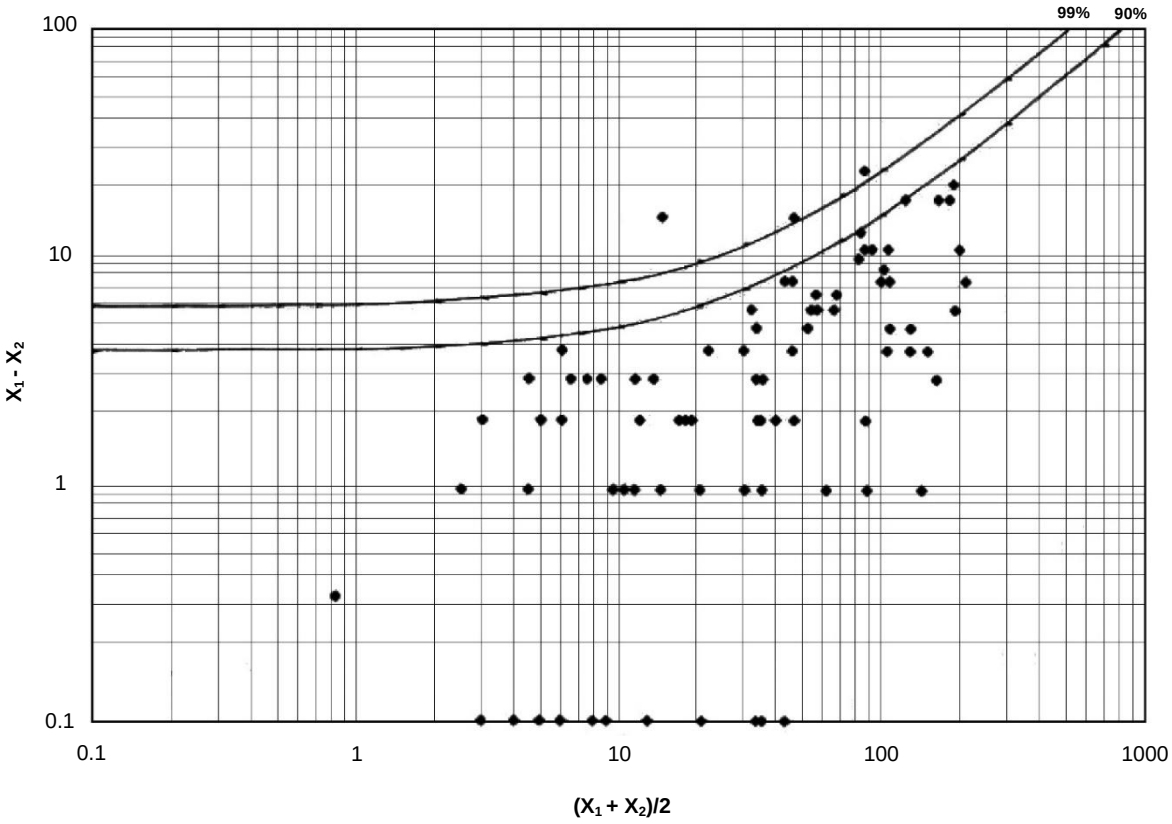

Figure 4. Chromium duplicate analyses. Precision = 10%, DL = 3.7 ppm

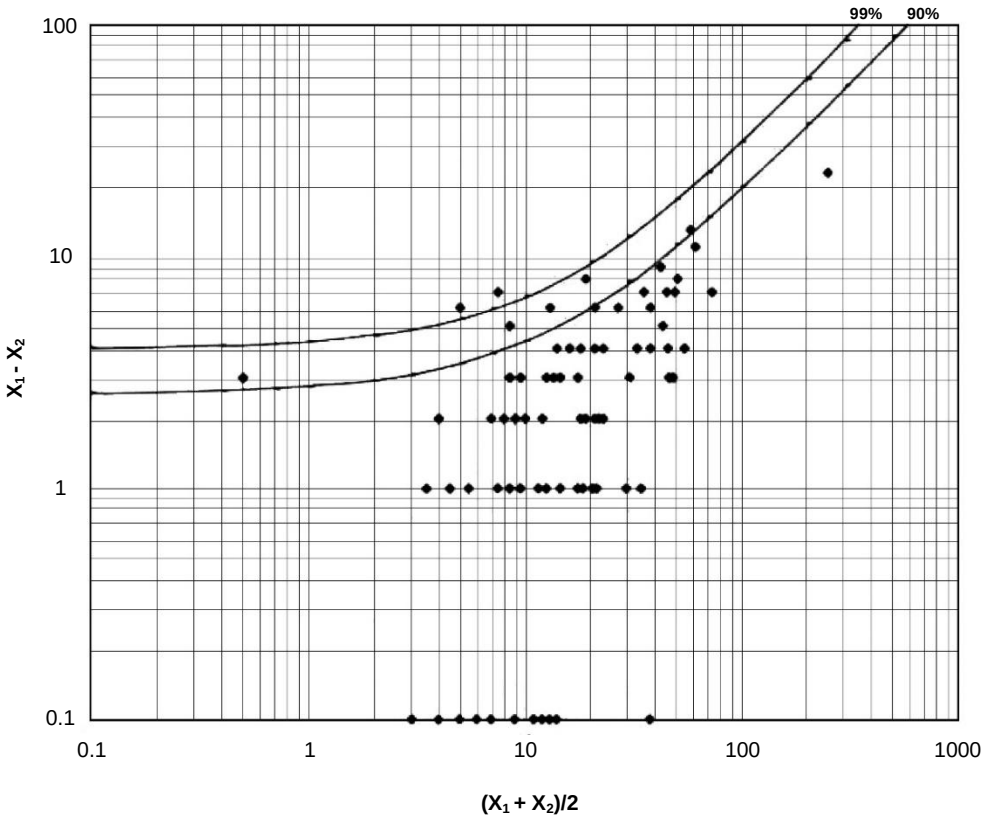

Figure 5. Cobalt duplicate analyses. Precision = 15%, DL = 2.6 ppm

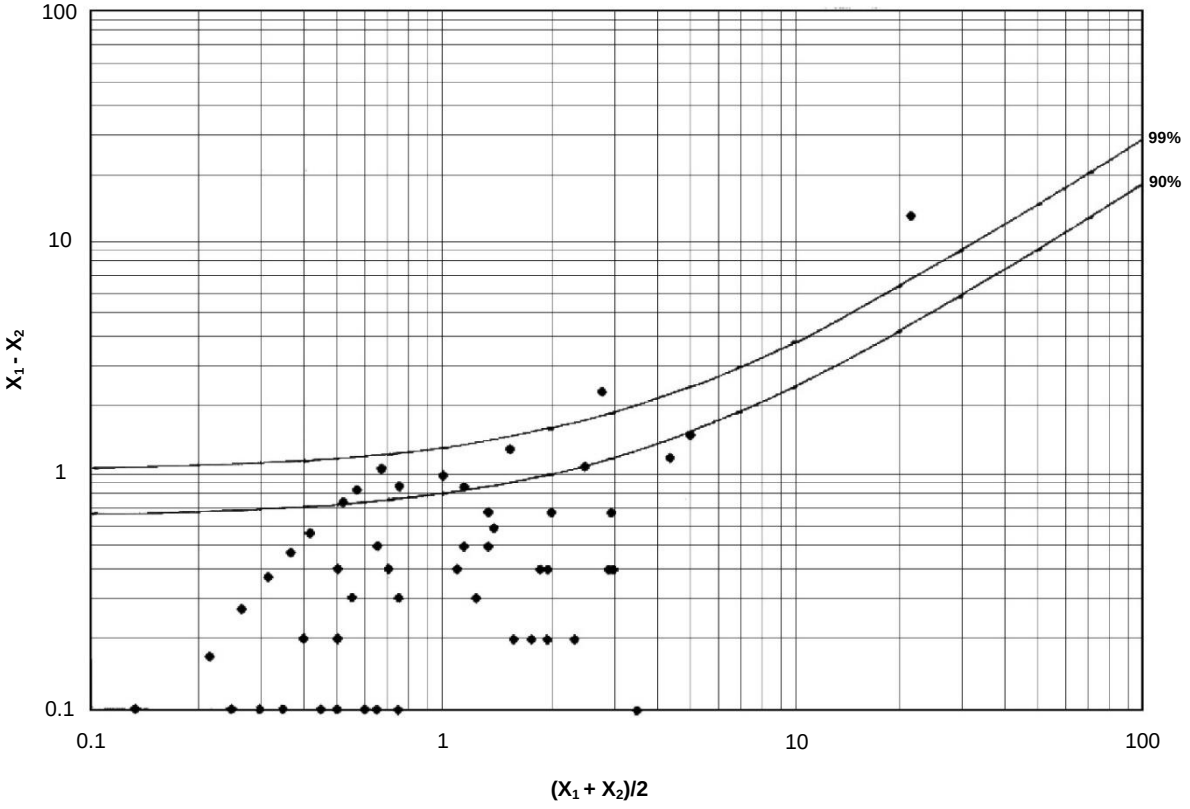

Figure 6. Cadmium duplicate analyses. Precision = 15%, DL = 0.67 ppm

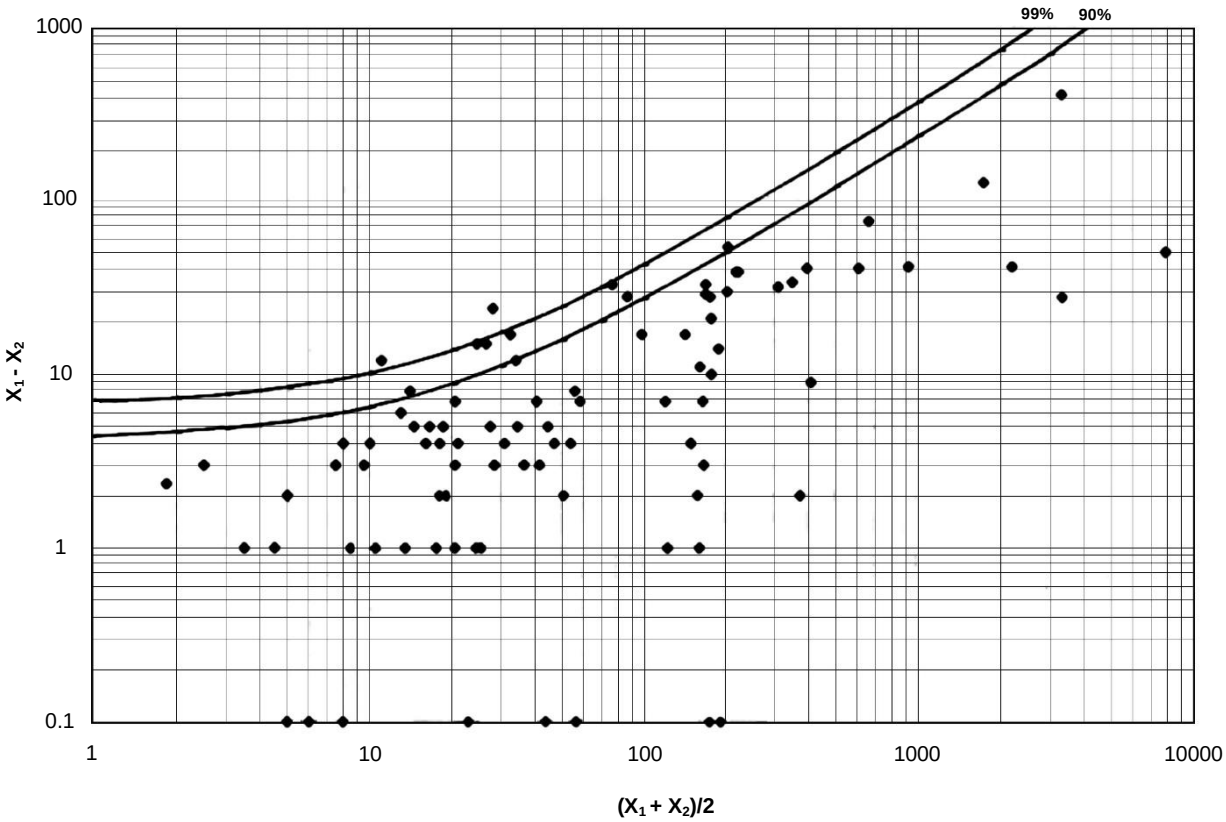

Figure 7. Copper duplicate analyses. Precision = 20%, DL = 4.5 ppm

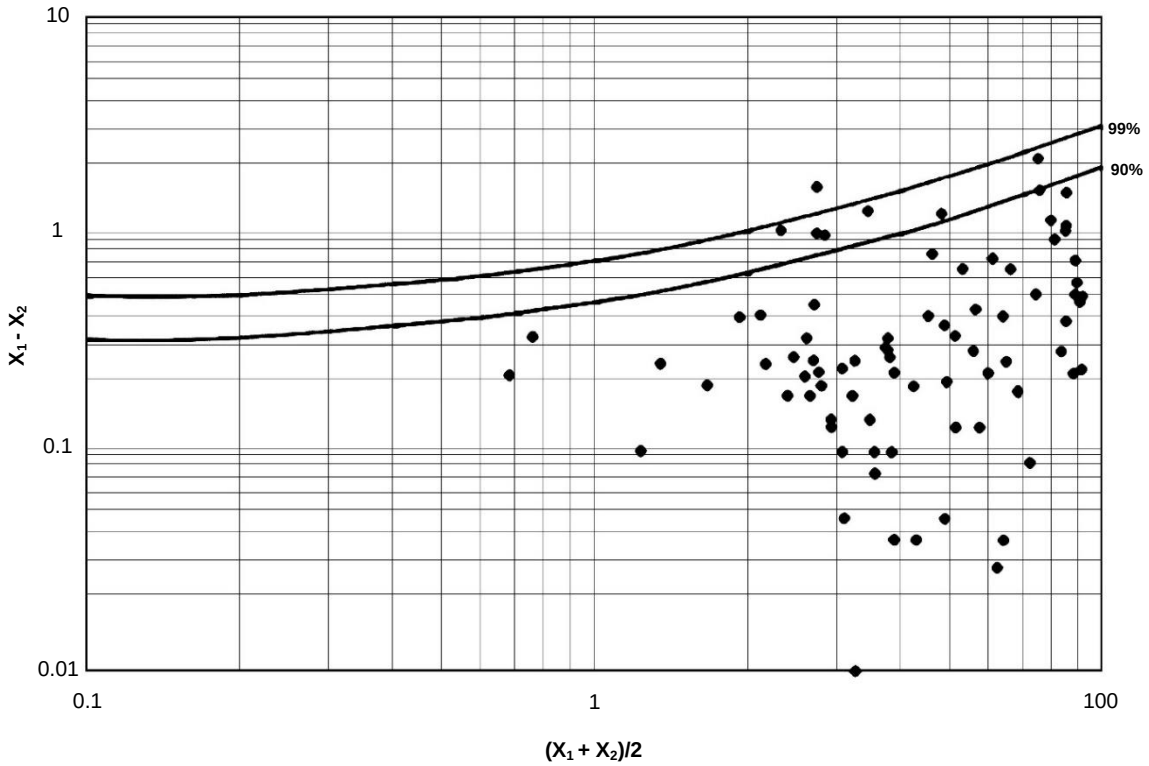

Figure 8. Iron duplicate analyses. Precision = 15%, DL = 0.3%

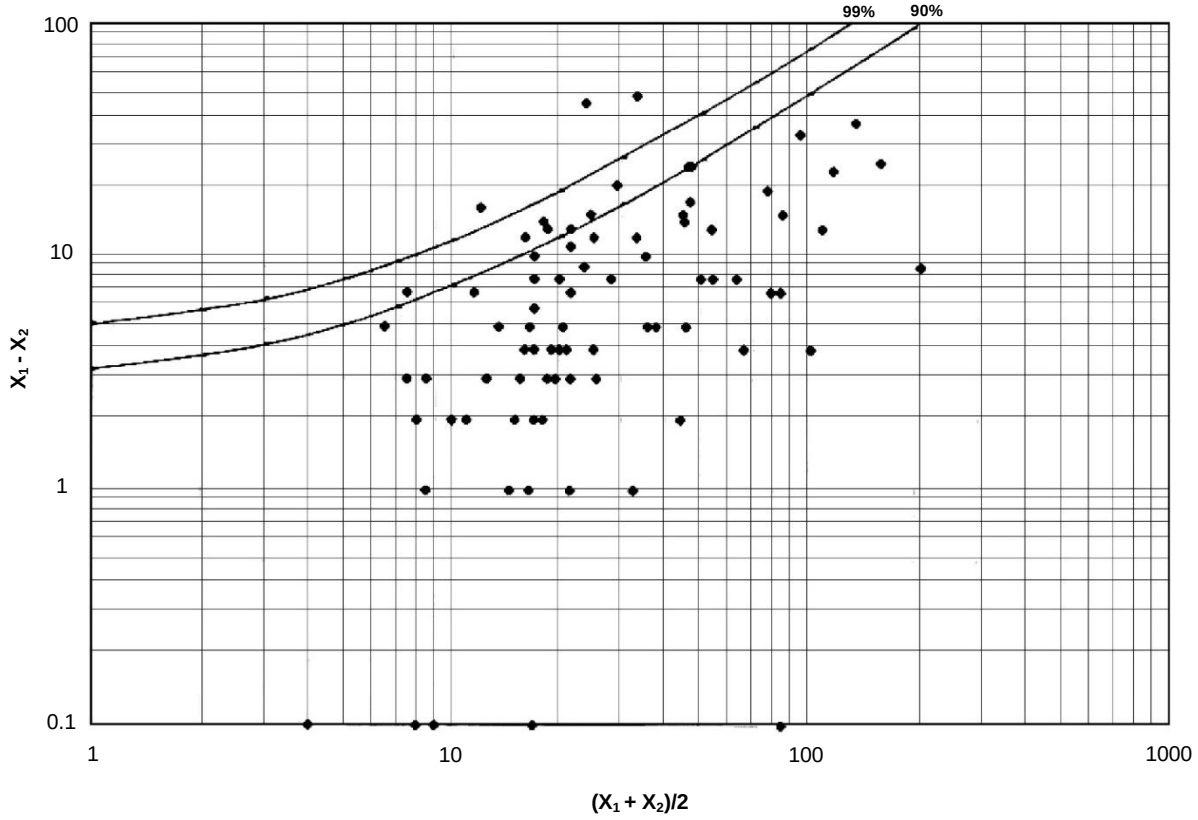

Figure 9. Lead duplicate analyses. Precision = 40%, DL = 4 ppm

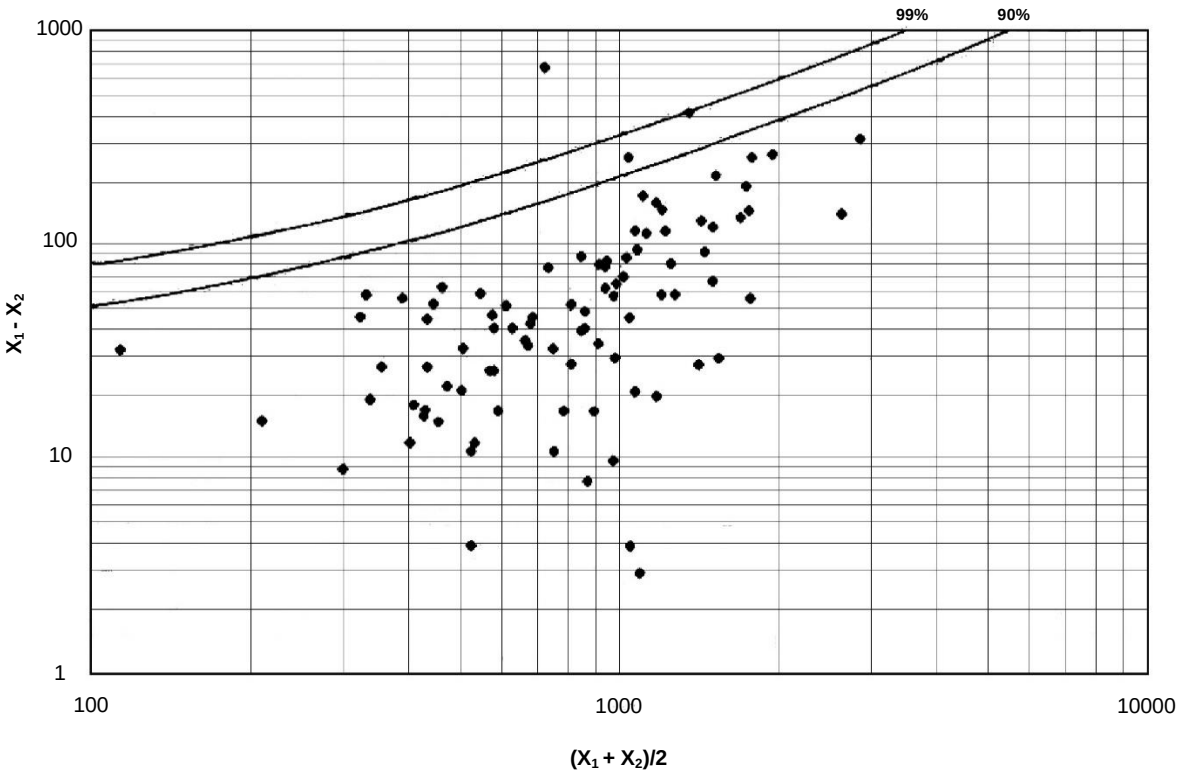

Figure 10. Manganese duplicate analyses. Precision = 15%, DL = 34 ppm

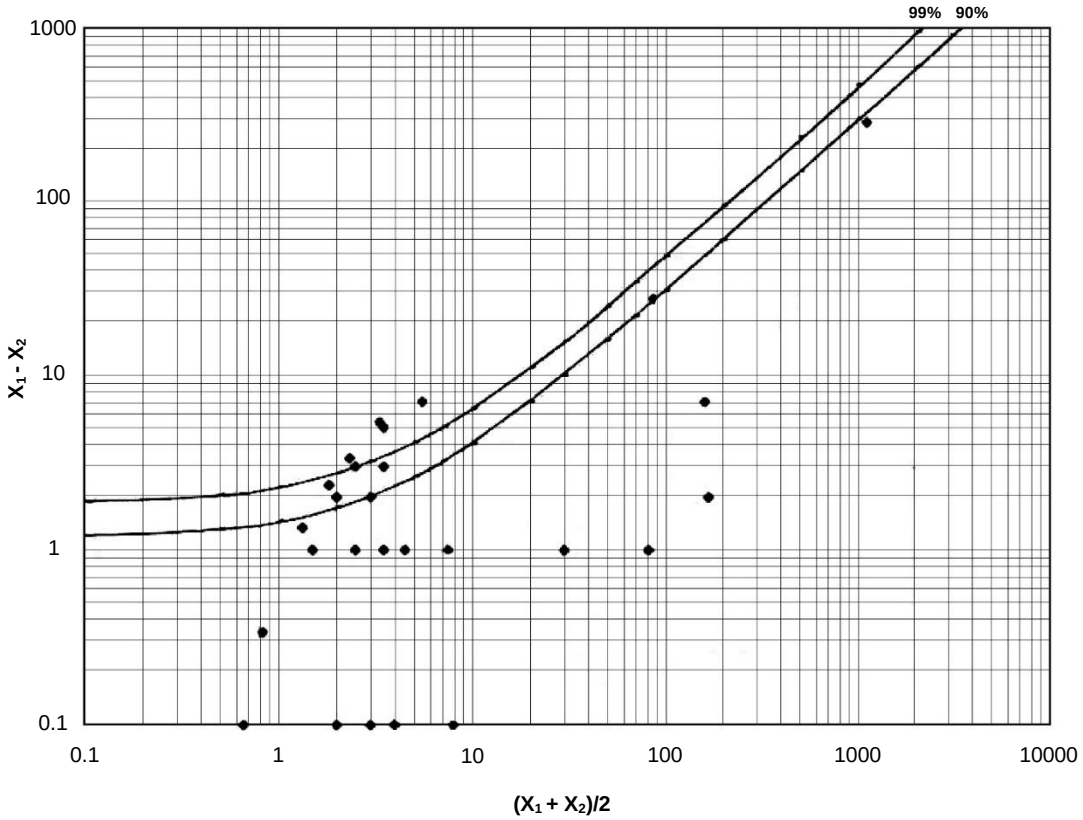

Figure 11. Molybdenum duplicate analyses. Precision = 25%, DL = 1.35 ppm

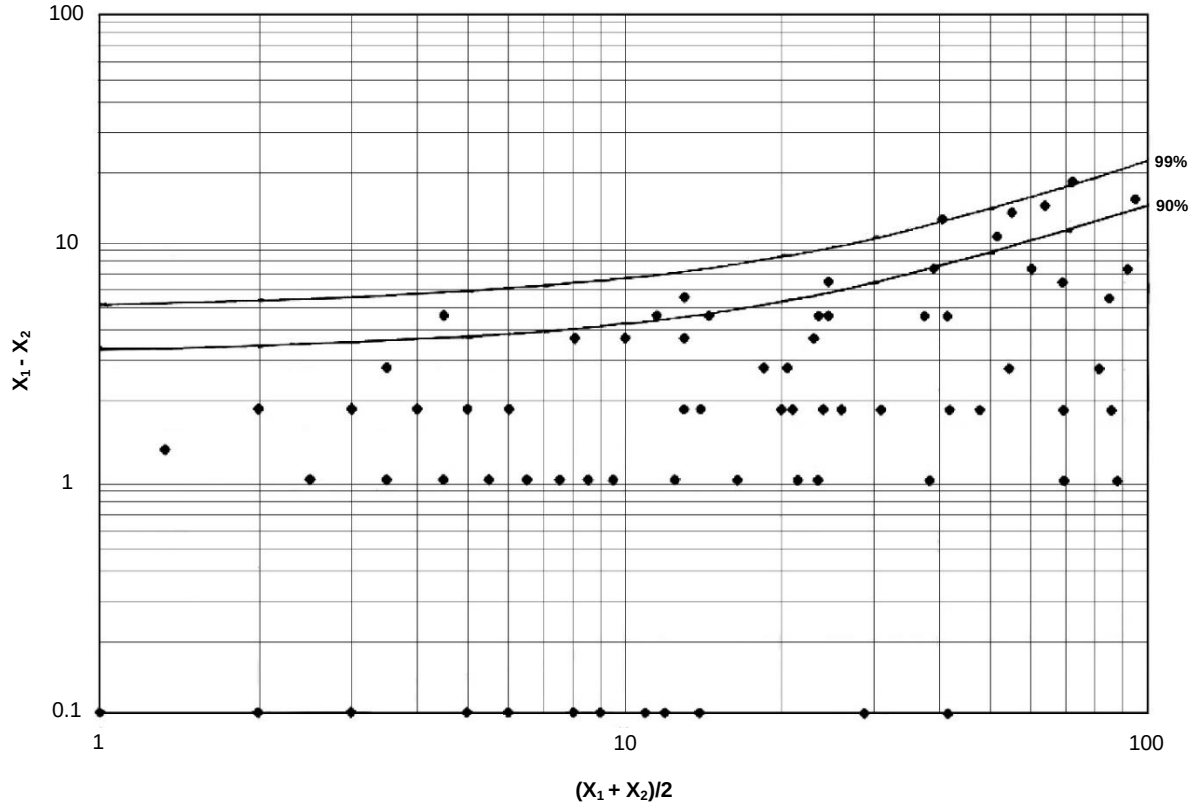

Figure 12. Nickel duplicate analyses. Precision = 10%, DL = 3.3 ppm

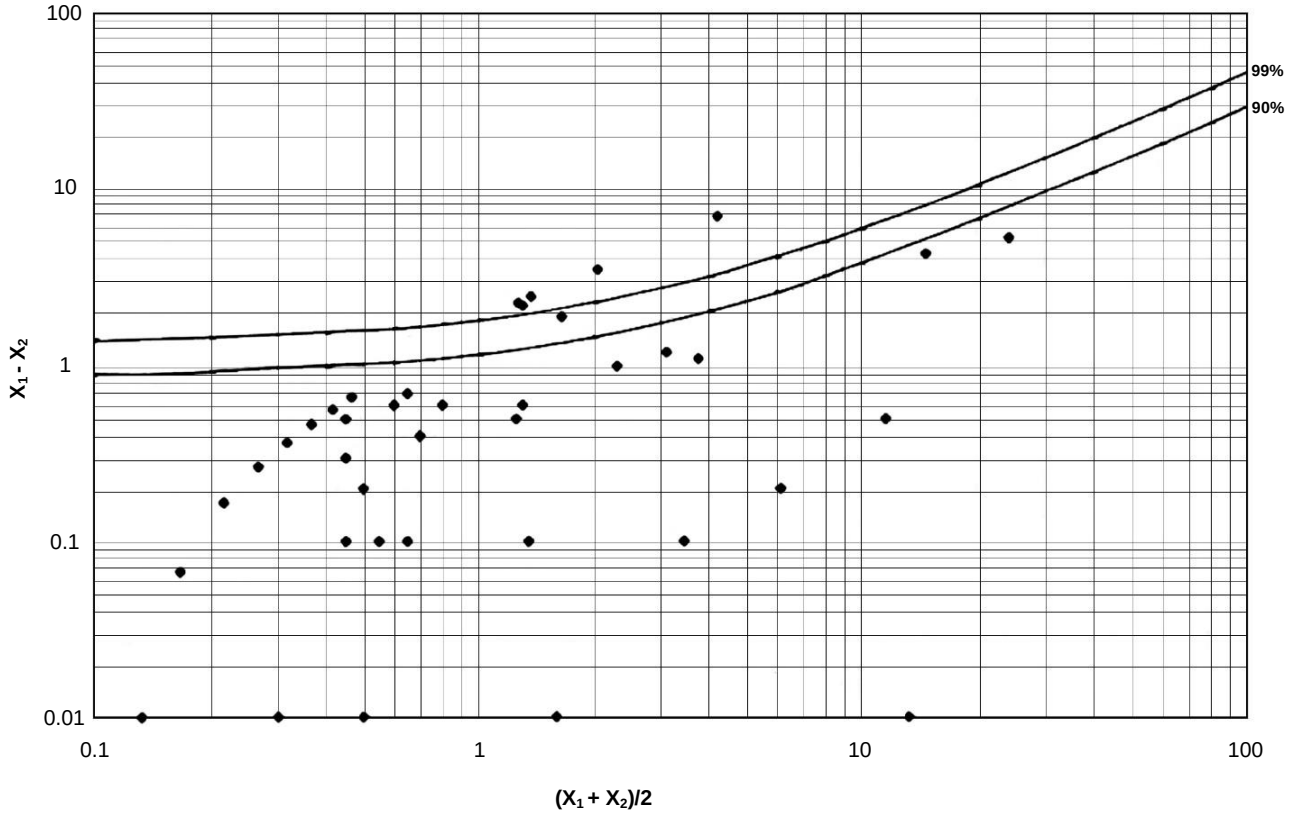

Figure 13. Silver duplicate analyses. Precision = 25%, DL = 1 ppm

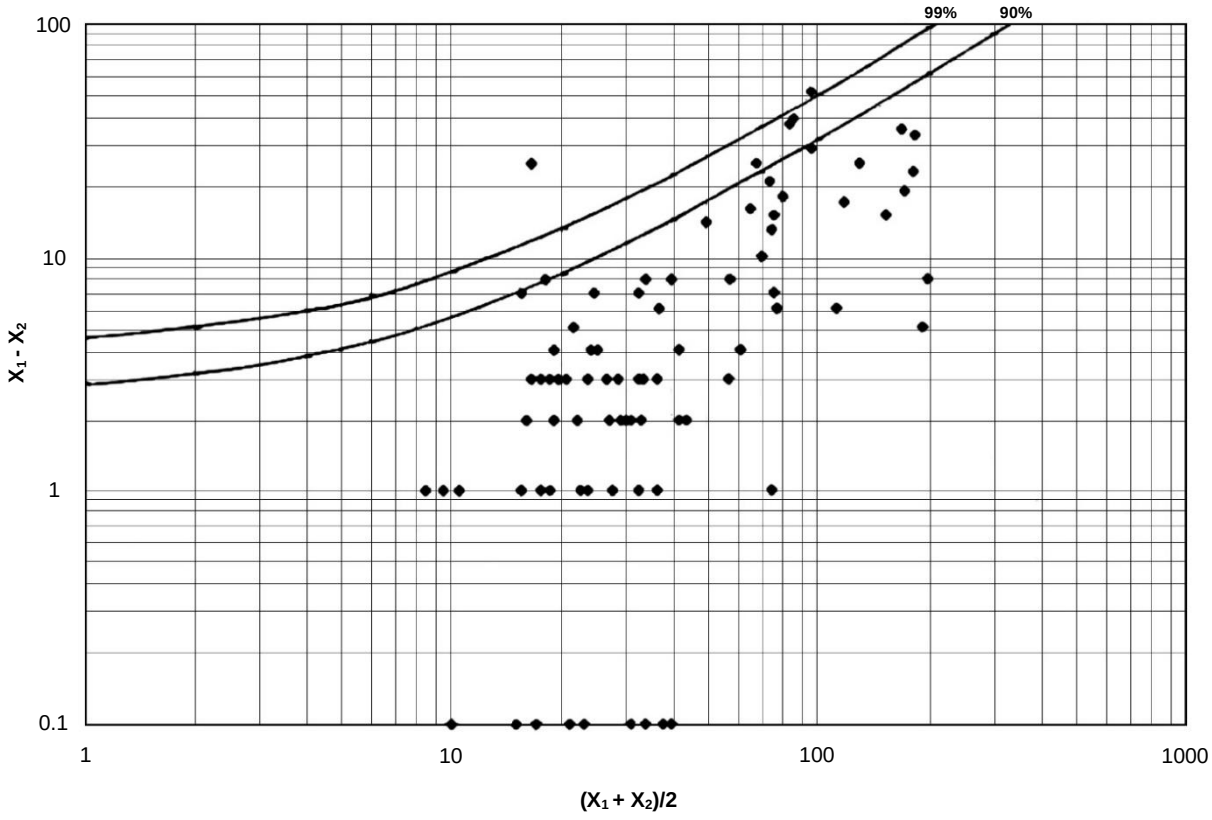

Figure 14. Strontium duplicate analyses. Precision = 25%, DL = 3 ppm

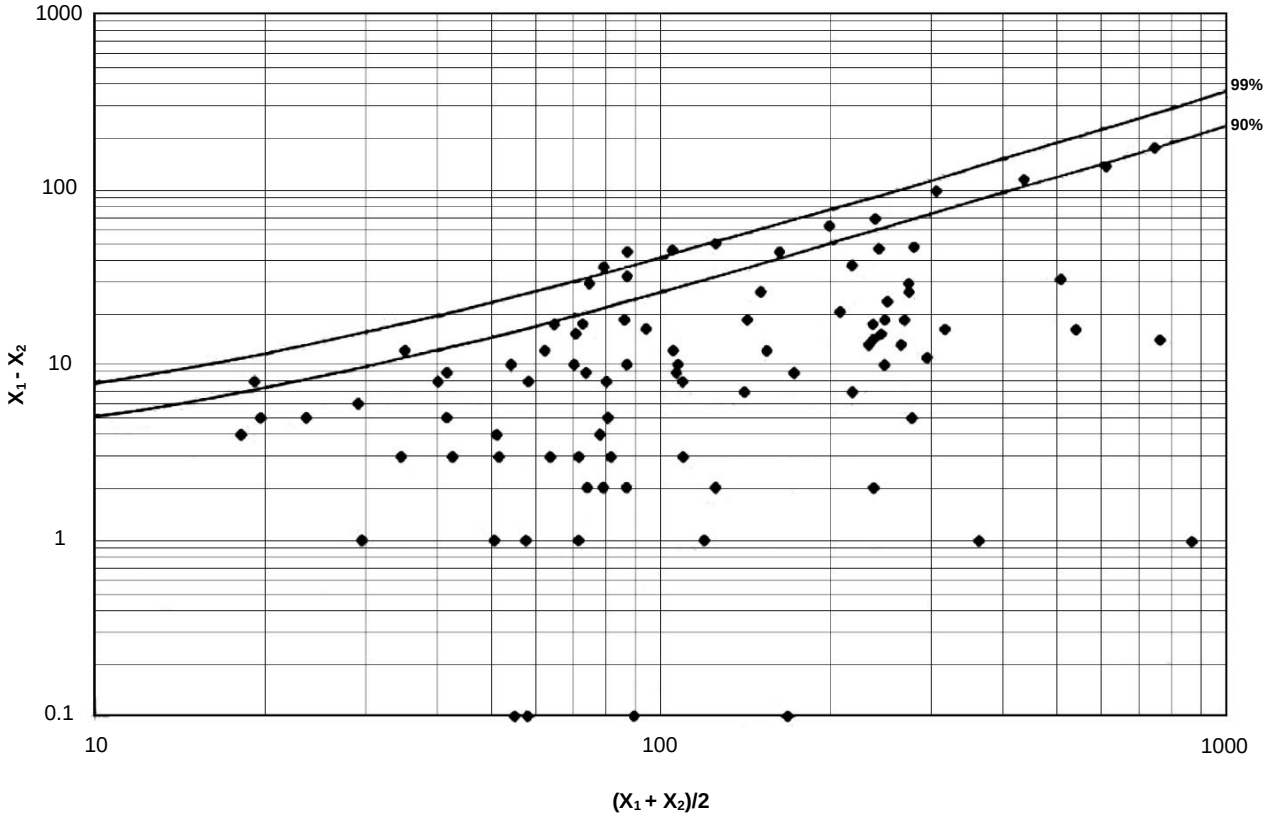

Figure 15. Vanadium duplicate analyses. Precision = 20%, DL = 3 ppm

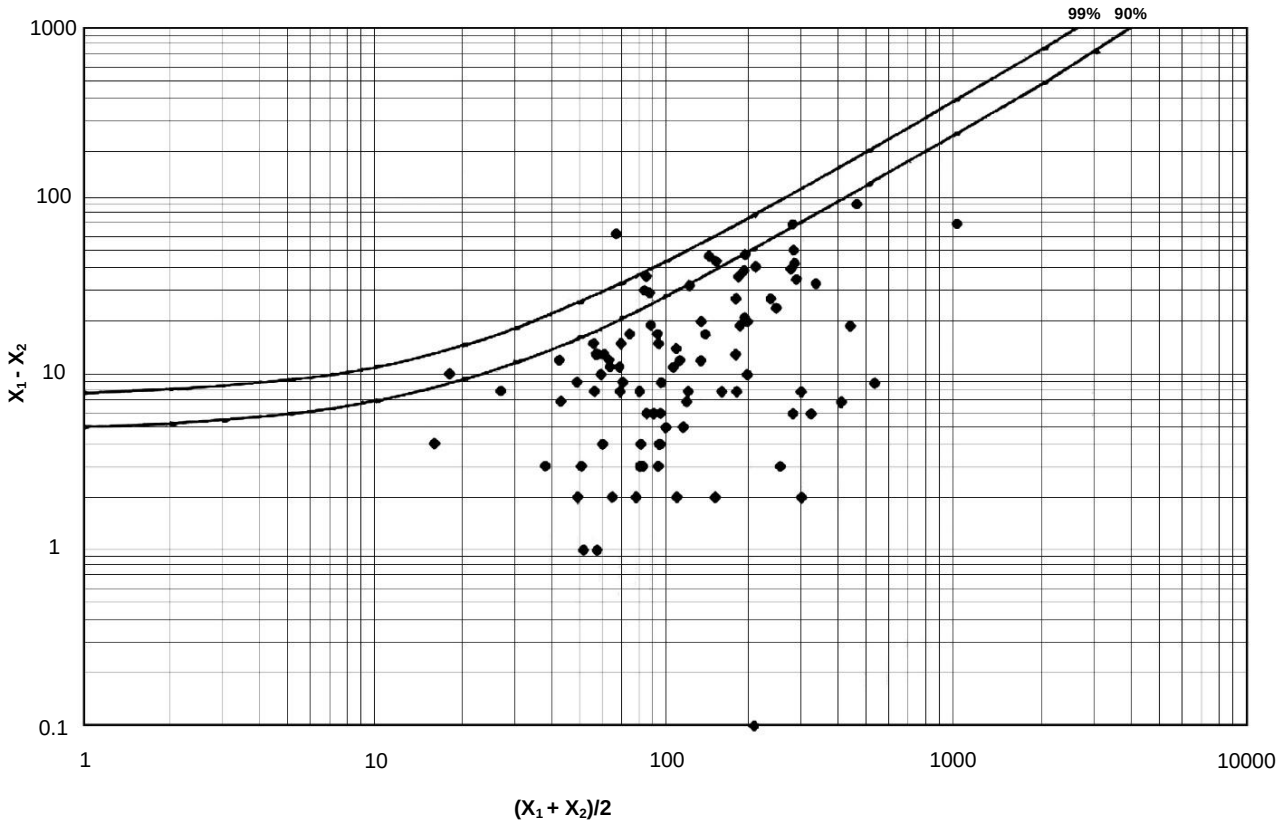

Figure 16. Zinc duplicate analyses. Precision = 20%, DL = 5 ppm

APPENDIX 2 OF REPORT:

GEOCHEMICAL RECONNAISSANCE SURVEY OF THE WESTERN CORDILLERA OF ECUADOR BETWEEN 2°00' AND 3°00' S

REPEAT ANALYSIS DATA

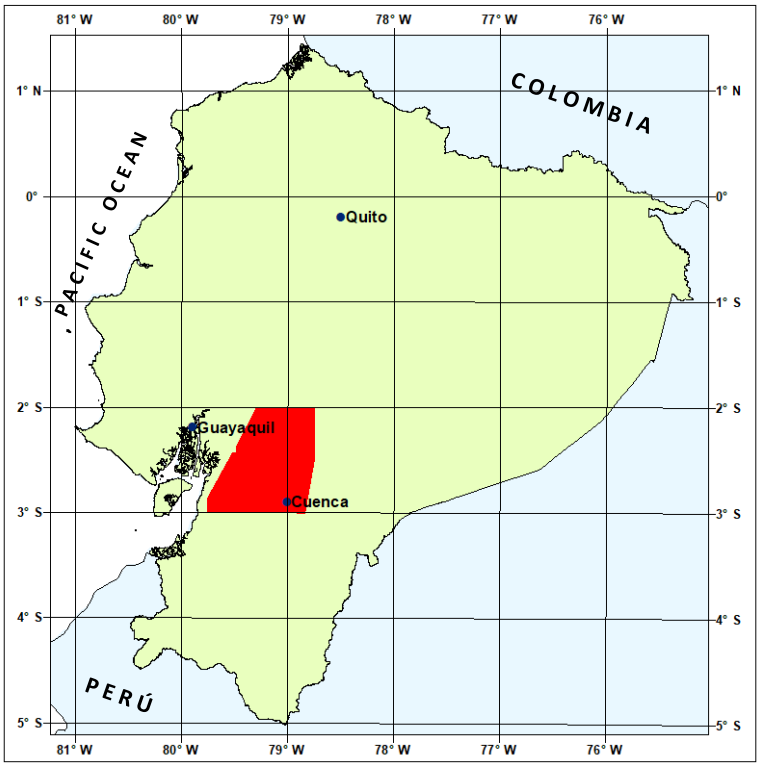

GEOLOGICAL INFORMATION MAPPING PROGRAMME
(LOCATION OF MAP 2 AREA)

QUITO, 1997

Repeat analysis data for control standards J-1, M-1, COR-1, CN, M-2 and PE submitted repeatedly during the analysis of field samples for the Cordillera Occidental, sector 2-3 °S. All data are quoted in mg/kg except for Fe for which values are given in %. The calculation of accuracy quotients (AC) was possible for standards J-1, M-1 and COR-1 only.

Table 1. Control standard J-1. Values below detection set to 2/3 detection limit prior to calculation of the mean, standard deviation and coefficient of variation.

J-1	Ag	Cu	Pb	Zn	Mo	Ni	Co	Fe	Mn	Ba	Cr	V	Sr	Li	As	Sb	Hg
	0.3	200	7	69	2	9	9	4.55	381	67	39	149	20	6	21.6	3.4	0.096
	0.5	207	8	74	2	9	9	4.79	393	69	41	158	21	6	16.6	5.2	0.029
	0.3	178	8	74	3	9	10	4.78	381	68	40	158	20	6	20.3	1.7	0.181
	0.6	188	7	70	1	9	9	4.39	392	71	37	145	21	7	15.4	1.9	0.051
	0.5	189	7	71	2	9	10	5.04	387	68	48	169	21	6	14.1	1.4	0.048
	0.4	179	7	71	1	9	9	4.72	381	68	40	156	20	6	14.3	1.9	0.056
	0.5	194	7	73	2	8	9	4.82	384	71	40	160	21	6	17.3	2.3	0.065
	0.5	163	7	77	1	9	9	5.08	389	63	43	168	19	6	12.4	2.9	0.049
	0.9	192	7	74	1	9	9	5.12	397	62	43	167	19	6	22	1.8	0.084
	0.4	174	7	70	2	9	9	4.64	371	61	39	153	18	6	15.7	2.5	0.082
	0.133	174	4	67	2	8	9	4.08	368	62	35	139	20	5	11.1	1.4	0.055
	0.133	162	3	67	2	8	9	4.36	361	63	39	153	20	5	13.2	2.2	0.112
	0.133	162	2	59	1	10	9	4.61	368	62	36	145	19	5	12.2	1.6	0.093
	0.133	175	4	62	0.66	10	10	5.03	388	64	39	158	20	6	14	2	0.071
	0.133	161	1	57	1	10	9	4.29	368	56	36	146	18	5	14.1	2	0.103
	0.4	174	2	60	0.66	10	9	4.85	387	60	38	153	20	5	16.4	4.2	0.074
	0.133	182	7	72	2	6	6	4.59	371	67	36	154	23	7	11	1.9	0.047
	0.133	191	7	68	2	6	7	4.92	376	63	39	166	23	7	18	2.8	0.051
	0.133	191	7	68	3	7	5	4.84	436	69	38	159	22	6	12.7	2.6	0.158
	0.133	195	6	71	3	6	6	5.14	437	67	42	169	21	6	11.2	2.5	0.102
	0.133	166	3	56	1	8	8	3.47	356	62	28	118	19	5	19.3	4.2	0.085
	0.133	166	3	61	0.66	9	9	4.43	375	58	37	152	20	5	16.4	1.8	0.062
	0.133	210	8	73	2	10	11	5.14	417	74	45	190	23	7	12.6	3.4	0.088
	4.7	187	9	72	2	11	11	4.59	408	73	40	169	23	7	13.5	2.9	0.094
	0.133	179	1.33	66	1	10	10	4.88	425	62	41	160	22	5	14.5	2.4	0.054
	0.3	181	4	68	1	9	9	4.73	432	68	39	162	23	6	16.2	1.5	0.049
	0.3	168	1.33	62	0.66	8	9	4.42	396	61	36	150	21	6	11	3.1	0.218
	0.4	192	1.33	64	0.66	9	9	4.78	416	61	41	164	21	6	10.7	6.6	0.194
Mean	0.45	181.43	5.21	67.71	1.55	8.71	8.82	4.68	390.75	65.00	39.11	156.79	20.64	5.89	14.92	2.65	0.09
SD	0.85	13.74	2.55	5.64	0.75	1.27	1.36	0.36	22.79	4.55	3.63	12.72	1.50	0.69	3.20	1.21	0.05
CV	187.91	7.57	48.99	8.32	48.55	14.60	15.44	7.77	5.83	6.99	9.29	8.11	7.25	11.63	21.45	45.56	54.02
AC*	2.27	1.04	1.49	1.11	0.97	0.83	0.82	0.96	0.83	0.88	0.88	1.05	0.72	1.00	1.19	0.80	1.75

AC* = ACCURACY QUOTIENT = MEAN/BGS CERTIFIED VALUE

Table 2. Control standard M-1. Values below detection set to 2/3 detection limit prior to calculation of the mean, standard deviation and coefficient of variation.

M-1	Ag	Cu	Pb	Zn	Mo	Ni	Co	Fe	Mn	Ba	Cr	V	Sr	Li	As	Sb	Hg
	0.5	87	8	67	1	14	12	6.99	362	60	60	253	30	6	11.5	1.0	0.040
	0.2	89	13	64	1	14	12	6.81	360	61	57	245	30	6	8.2	0.7	0.047
	0.5	81	16	61	1	12	11	6.13	333	53	50	218	27	6	12.4	2.4	0.043
	0.4	88	11	63	2	13	12	6.34	349	60	54	229	30	6	7.8	1.1	0.019
	0.5	85	7	66	0.66	13	11	6.52	355	57	56	234	30	6	8.5	0.9	0.027
	0.4	82	8	66	0.66	13	12	6.77	362	64	56	244	30	6	8.9	1.0	0.039
	0.6	76	10	66	0.66	13	11	6.34	352	53	53	223	28	6	10.5	0.9	0.043
	0.8	83	10	66	0.66	13	11	6.73	357	53	57	237	27	6	9.4	0.7	0.038
	0.6	79	7	65	0.66	12	11	6.20	339	52	52	220	27	5	8.1	1.2	0.036
	0.5	82	11	64	0.66	13	11	6.64	345	51	55	240	26	5	9.0	1.8	0.038
	0.133	80	4	61	2	13	11	6.44	341	51	52	218	26	5	7.8	1.2	0.037
	0.133	77	11	63	2	13	11	5.81	336	54	50	216	25	5	7.5	0.6	0.074
	0.4	76	2	58	0.66	15	12	7.88	358	55	58	263	29	5	7.9	2.6	0.038
	0.3	76	5	57	6	16	12	8.47	362	53	81	285	29	5	9.4	0.7	0.054
	0.2	85	1.33	58	0.66	14	12	7.38	385	50	63	272	29	5	9.0	1.3	0.035
	0.133	91	3	51	2	13	11	6.26	349	48	53	230	28	5	9.3	1.9	0.054
	0.133	89	7	66	4	10	7	6.94	344	60	56	257	36	7	14.7	1.5	0.030
	0.133	88	9	66	4	11	7	6.86	351	57	56	258	37	7	12.1	1.4	0.053
	0.133	86	9	70	4	8	7	7.32	422	63	58	265	36	7	6.4	0.9	0.030
	0.133	83	9	63	3	10	6	6.50	374	57	52	232	30	6	8.6	2.4	0.078
	0.2	69	2	53	3	18	11	6.37	336	46	61	235	26	5	10.6	1.2	0.015
	0.3	78	2	51	1	13	10	5.57	315	48	50	203	26	5	9.7	0.133	0.030
	0.133	79	7	57	0.66	13	12	6.45	359	62	55	253	31	7	7.7	1.2	0.025
	0.133	89	8	56	1	13	11	5.54	344	64	50	223	31	7	8.3	0.5	0.055
	0.2	75	1.33	57	0.66	13	11	6.44	372	51	56	230	33	5	9.1	1.0	0.026
	0.133	78	1.33	57	0.66	12	11	6.62	381	52	55	234	34	5	6.9	0.9	0.020
	0.3	85	1.33	55	0.66	13	11	6.45	359	55	53	236	31	5	8.2	1.4	0.016
	0.4	92	3	57	0.66	13	11	6.88	361	49	58	256	32	5	6.7	1.5	0.034
Mean	0.31	82.43	6.69	60.86	1.63	12.89	10.64	6.63	355.82	54.96	55.96	239.61	29.79	5.68	9.08	1.22	0.040
SD	0.19	5.68	4.05	5.22	1.42	1.83	1.70	0.62	19.86	5.17	5.95	19.09	3.21	0.77	1.86	0.58	0.020
CV	60.76	6.89	60.61	8.58	87.25	14.21	16.01	9.34	5.58	9.40	10.63	7.97	10.79	13.60	20.44	47.98	40.16
AC*	1.54	1.04	0.96	1.21	1.63	0.92	0.83	0.95	0.86	0.75	0.86	1.06	0.62	1.03	1.30	0.87	3.84

AC* = ACCURACY QUOTIENT = MEAN/BGS CERTIFIED VALUE

Table 3. Control standard COR-1. Values below detection set to 2/3 detection limit prior to calculation of the mean, standard deviation and coefficient of variation.

COR-1	Ag	Cu	Pb	Zn	Mo	Ni	Co	Fe	Mn	Ba	Cr	V	Sr	Li	As	Sb	Hg
	0.4	22	13	58	0.66	15	12	7.27	329	51	61	268	35	6	5.5	0.133	0.030
	0.4	29	10	59	0.66	16	12	7.60	335	50	61	279	35	6	5.9	0.3	0.023
	0.3	21	33	62	0.66	16	12	8.11	347	50	67	306	34	6	5.4	0.4	0.023
	0.2	22	8	66	0.66	17	13	8.43	355	56	71	317	36	6	7.0	0.3	0.014
		20	6	56	0.66	15	12	7.07	316	52	60	264	33	6	5.5	0.4	0.010
	0.3	21	11	63	0.66	16	13	7.88	336	53	66	297	36	6	5.9	0.3	0.090
	0.4	21	10	60	0.66	14	12	7.69	333	49	64	291	35	6	5.5	0.4	0.011
	0.3	22	8	58	0.66	15	12	7.34	330	52	61	277	35	6	5.0	1.4	0.018
	0.6	19	8	61	0.66	15	12	7.55	325	52	63	281	32	5	6.3	0.4	0.021
	0.5	19	8	60	0.66	15	11	7.21	310	49	62	269	30	5	5.1	0.6	0.010
	0.133	19	8	56	1	15	12	7.59	333	47	60	265	32	5	5.3	0.133	0.037
	0.133	19	4	61	2	16	12	7.23	334	46	66	282	31	5	5.4	0.2	0.023
	0.5	20	4	50	0.66	18	12	8.12	329	47	60	277	33	5	5.3	0.3	0.032
	0.4	20	17	54	0.66	17	12	8.52	329	47	62	292	34	5	4.9	1.0	0.027
	0.3	20	1.33	47	0.66	15	12	7.30	324	41	61	272	32	4	4.8	0.5	0.018
	0.3	22	2	51	0.66	17	12	7.72	341	46	66	295	36	5	5.3	0.6	0.026
	0.133	15	19	60	2	12	8	7.60	340	50	62	285	45	7	5.5	0.6	0.018
	0.133	12	6	49	3	10	7	6.56	279	49	54	253	36	6	4.2	0.4	0.01
	0.133	16	9	59	2	11	6	7.46	347	54	61	282	37	6	4.1	0.4	0.015
	0.133	29	9	57	4	12	7	7.26	351	54	60	274	39	6	1.2	0.4	0.015
	0.3	24	1.33	48	0.66	15	11	6.93	313	44	56	262	33	5	6.4	0.5	0.028
	0.133	22	5	51	0.66	16	11	6.88	323	43	57	264	34	5	6.5	0.133	0.017
	0.133	15	12	61	0.66	16	15	7.87	343	56	69	328	37	6	4.8	0.3	0.015
	0.133	27	13	51	0.66	16	13	6.86	312	53	61	290	32	6	4.7	0.3	0.06
	0.3	21	2	53	0.66	17	12	7.94	364	45	67	293	40	5	5.0	0.5	0.016
	0.2	22	1.33	55	0.66	17	13	8.83	372	43	74	330	39	5	5.4	0.4	0.017
	0.4	20	1.33	48	0.66	14	11	6.83	329	44	56	255	39	5	4.0	0.5	0.05
	0.4	21	1.33	52	0.66	16	12	7.44	347	47	61	282	40	5	4.3	0.5	0.053
Mean	0.29	20.71	8.27	55.93	1.02	15.14	11.39	7.54	333.07	48.93	62.46	283.21	35.36	5.50	5.15	0.44	0.03
SD	0.14	3.73	6.81	5.21	0.83	1.90	2.01	0.54	18.26	4.08	4.53	19.67	3.32	0.64	1.06	0.26	0.02
CV	48.40	18.01	82.35	9.32	81.34	12.54	17.61	7.20	5.48	8.34	7.26	6.94	9.40	11.61	20.54	58.79	69.30
AC*	1.43	0.90	1.65	1.30	2.04	0.62	0.77	0.93	0.89	0.76	0.76	0.96	0.58	0.92	1.03	0.73	2.60

AC* = ACCURACY QUOTIENT = MEAN/BGS CERTIFIED VALUE

Table 4. Control standard CN. Values below detection set to 2/3 detection limit prior to calculation of the mean, standard deviation and coefficient of variation.

CN	Ag	Cu	Pb	Zn	Mo	Ni	Co	Fe	Mn	Ba	Cr	V	Sr	Li	As	Sb	Hg
	11.3	400	127	74	47	3	15	8.58	311	155	26	128	9	6	381.6	293.2	0.422
	13.5	433	124	66	43	3	15	7.77	313	146	23	110	9	6	367.4	295.8	0.409
	17.0	402	128	67	44	3	16	7.87	295	149	24	109	9	6	363.5	262.5	0.429
	16.1	416	127	72	46	3	16	9.03	293	158	30	144	9	6	371.7	291.7	0.393
	13.9	363	117	67	41	3	15	7.90	285	152	24	116	9	6	366.3	281	0.365
	19.4	392	133	67	50	5	14	9.69	318	154	30	131	11	5	401.9	295.2	0.324
	28.8	434	142	77	57	7	16	9.85	340	163	29	129	11	6	404.6	273.1	0.297
	27.2	388	117	67	44	6	13	8.73	317	149	26	114	10	6	366.7	288.2	0.281
	11.2	377	123	60	46	5	13	8.86	296	146	28	119	10	6	375.9	307.4	0.357
	9.7		122	71	41	6	14	8.10	313	147	27	125	11	6	389.8	257.4	0.318
	5.6	371	125	66	46	4	18	7.49	269	172	28	124	9	6	413	291.7	0.345
	11.3	429	135	83	50	7	19	8.59	340	187	32	146	11	7	376	290	0.363
	8.8	342	146	64	42	5	15	8.54	280	165	27	123	9	6	389.6	304.7	0.487
	13.8	274	133	49	16	0.666		5.33		117	16	89	7	5	352.3	258.7	0.378
	33.4	386	120	59	43	5	15	8.75	256	136	27	126	9	6	375	276.9	0.413
	15.1	399	141	65	51	6	17	8.60	296	170	27	137	10	6	428.3	316	0.378
	17.4	379	123	61	42	4	19	7.78	269	170	29	127	10	6	399.1	244.2	0.375
	23.4	466	125	77	44	6	15	8.09	331	136	27	119	11	6	386.1	326.7	0.301
		372	100	57	38	4	15	7.34	263	152	19	98	9	6	398.7	294.5	0.288
	13.8	347	113	58	43	5	16	9.18	298	140	24	124	10	6	391.1	303.5	0.255
	10.6	419	129	73	44	4	18	8.89	315	164	29	134	10	6	389.6	274.5	0.362
	11.1	402	147		43	4	18	7.53	283	154	26	115	10	6	372.5	302.0	0.297
	10.9	404	113	61	42	6	13	8.48	295	144	23	120	9	6	378.3	321.3	0.289
	23	419	111	72	47	6	14	8.95	337	163	28	133	11	7	392.9	305.0	0.275
	13.9	398	146	65	53	2	15	8.40	284	141	28	122	9	6	396.9	296.5	0.279
	12.6	399	140	66	49	5	17	8.11	299	176	29	143	10	6	387.0	278.7	0.346
	13.3	464	128	73	51	5	15	9.30	350	151	31	144	11	6	405.9	299.0	0.398
	11.9	392	100	71	48	6	14	7.98	321	126	25	121	10	6	366.3	279.8	0.277
	10.8	405	117	73	48	6	15	9.38	343	149	30	144	11	5	398.1	308.5	0.286
	30.4	404	114	69	47	7	15	8.64	334	135	28	132	10	4	422.1	288.5	0.428
	13.5	403	114	70	43	5	15	8.34	289	130	26	128	10	3	400.0	328.3	0.350
	18.2	435	116	72	46	6	14	8.63	318	130	25	121	10	5	402.9	301.9	0.334
	16.3	406	108	65	48	6	14	8.47	336	139	26	124	10	6	399.1	290.9	0.299
	14	471	115	72	49	5	14	8.81	326	139	28	132	10	6	402.7	282.7	
	15.6	459	109	71	42	6	13	8.19	327	135	25	123	10	7	400.9	285.2	0.459
	7.1	381	125	69	39	5	15	7.18	282	141	23	105	10	6	387.5	276.0	0.449
	12.7	393	134	76	44	5	17	7.97	293	159	24	129	10	6	377.9	238.5	0.299
	28	448	121	71	48	8	15	9.24	325	137	29	139	11	5	406.5	288.0	
	14.9	429	112	69	47	5	15	8.80	350	144	27	127	10	5	394.3	254.7	0.289
	11.8	395	132	70	44	6	15	9.15	346	143	27	134	10	6	370.0	263.6	0.326
	14.2	418	112	70	46	4	17	8.68	305	136	24	122	10	6	364.2	265.1	0.337
	14.6	371	107	70	41	2	13	6.53	266	103	22	98	7	5	388.5	282.7	0.287
	18.5	369	117	70	39	1	15	7.33	275	119	26	118	7	5	375.0	274.1	0.302
	11.7	436	127	71	50	7	19	9.65	323	176	30	139	11	7	389.6	288.7	0.279
	11.2	390	136	66	46	5	16	9.08	298	164	27	134	10	6	375.5	284.9	0.390
	9.2	361	121	70	43	5	17	8.19	296	148	27	119	10	6	391.3	281.7	0.290
	7.7	405	124	67	51	5	17	7.89	286	149	23	109	10	6	412.0	312.0	0.298
	9.7	407	140	79	44	6	18	8.16	321	146	26	143	10	6	388.1	260.7	0.277
	12.7	375	122	76	48	6	17	8.38	298	127	26	144	10	6	358.6	266.2	0.312
	17.6	423	153	62	51	6	17	7.74	296	143	30	142	11	7	369.7	271.1	
	10.1	390	159	59	46	5	16	6.98	285	125	26	125	9	6	366.7	261	0.346
	24.9	381	131	62	43	6	16	8.30	271	152	27	129	9	6	385	314	0.314
	10	381	140	59	44	6	16	8.44	280	152	28	132	9	6	387	286.1	0.312
	7.6	414	138	66	45	5	17	8.79	307	170	28	146	11	7	399	296.1	0.281
	6.4	323	110	66	34	4	14	6.49	253	114	20	101	7	6	393.5	316.7	0.272
	15.2	407	109	61	45	6	18	9.34	320	170	30	140	10	7	359.6	328.8	0.322
	11.1	390	141	55	51	6	20	10	329	156	33	163	10	2	421	335.3	0.358
	9.3	404	117	81	42	5	14	8.45	329	140	26	127	10	7	381.1	327.4	0.341
Mean	14.514	398.965	125.103	67.842	44.914	4.977	15.684	8.361	304.807	147.483	26.534	126.534	9.759	5.845	387.152	289.114	0.337
SD	6.145	34.268	13.086	6.541	5.580	1.473	1.713	0.855	25.202	16.638	3.068	13.836	1.014	0.875	16.941	21.929	0.055
CV	42.046	8.589	10.460	9.641	12.423	29.606	10.922	10.232	8.268	11.281	11.561	10.935	10.392	14.964	4.376	7.585	16.389

Table 5. Control standard M-2. Values below detection set to 2/3 detection limit prior to calculation of the mean, standard deviation and coefficient of variation.

M-2	Ag	Cu	Pb	Zn	Mo	Ni	Co	Fe	Mn	Ba	Cr	V	Sr	Li	As	Sb	Hg
	3.2	362	56	82	13	14	18	8.09	332	78	50	222	23	5	462.8	61.3	0.197
	3.3	388	47	76	12	14	18	8.10	334	82	50	229	23	5	425.1	62.4	0.169
	1.9	367	65	84	13	14	19	9.28	350	75	56	253	22	5	462.2	71.6	0.141
	5.3	386	52	77	13	14	19	8.68	355	76	54	242	21	5	526.5	67.6	0.155
	2.4	365	48	72	12	13	18	8.31	323	74	52	231	21	5	430.2	66.0	0.126
		380	45	85	15	18	16	9.50	371	62	57	236	24	5	505.7	68.6	0.147
	3	398	38	80	14	17	16	8.96	351	65	56	228	24	6	505.9	76.5	0.111
	2	388	41	84	15	17	15	9.33	370	66	56	226	24	6	460.2	81.5	0.155
	2.5	391	44	78	15	16	18	8.75	362	67	54	214	24	6	483.0	75.5	0.145
	2.8	460	47	94	11	17	18	8.31	362	67	54	234	23	6	509.4	55.7	0.132
	3.1		41	82	12	15	15	7.50	326	60	49	220	23	6	482.1	59.4	0.135
	2.5	396	51	88	13	19	22	8.46	370	78	60	255	23	6	451.9	65.1	0.065
	2.2	381	43	88	15	18	22	8.28	376	76	60	250	23	6	418.9	78.3	0.102
	2.4	342	49	81	12	15	19	8.66	307	73	54	227	21	5	450.9	67.6	0.201
	2.7	330	50	83	12	15	19	9.28	304	67	59	254	22	5	476.4	77.4	0.207
	1.8	371	38	88	8		18	8.15	325	72	41	226	23	6	386.8	59.4	0.101
	2.7	404	61	84	9		18	8.50	334	74	48	235	23	6	445.0	66.1	0.118
	2.4	345	42	67	12	15	13	8.32	311	70	53	219	20	6	448.1	67.0	0.145
	2.3	352	48	73	11	16	18	8.69	299	64	53	228	19	5	509.6	66.3	0.139
	2.8	369	50	77	11	15	14	7.35	306	69	47	202	21	5	432.4	47.2	0.152
	2.4	361	41	69	13	15	13	7.15	331	70	45	198	22	5	419.4	67.6	0.125
	2.6	340	54	75	10	15	24	7.43	306	74	54	223	24	6	465.4	45.2	0.098
	2.8	334	46	89	10	15	22	8.11	308	74	56	243	21	5	530.6	49.1	0.114
	5.1	403	50	95	14	16	17	8.47	354	55	56	236	21	6	473.8	62.7	0.088
	2.9	404	42	80	13	16	15	7.57	346	59	51	210	23	5	422.1	67.5	0.103
	3.9	348	37	63	10	15	18	8.36	290	62	49	221	20	5	529.0	84.3	0.101
	6.8	307	44	66	11	15	21	9.33	325	64	50	235	21	5	455.1	80.5	0.107
	3.4	382	34	84	13	16	22	8.81	330	76	57	245	20	6	480.4	63.5	0.127
	8.8	384	36	81	11	13	20	8.85	322	64	51	232	19	5	507.4	65.6	
	2.4	397	52	55	12	16	22	8.82	351	79	62	251	25	6	484.6	81.7	0.132
	3.0	452	53	83	12	16	20	9.62	326	69	59	244	23	5	536.5	72.1	0.103
	2.8	384	41	76	10	17	14	8.47	324	64	46	216	23	5	461.2	69.9	0.129
	4.1	354	40	73	11	17	18	9.47	315	63	54	243	21	5	489.5	76.0	0.137
	2.3	361	44	85	13	17	16	8.83	389	63	56	231	23	4	488.0	70.9	
	4.1	426	38	92	12	18	17	8.82	380	61	56	241	23	5	451.6	76.8	0.123
	3.1	344	53	79	14	14	19	9.39	303	66	61	260	19	5	539.4	67.3	
	4.3	351	49	79	12	14	19	8.52	326	74	59	229	22	5	448.1	61.3	0.110
	2.9	360	56	73	13	17	20	7.97	334	77	58	254	22	6	464.4	65.4	0.106
	2.3	333	41	70	11	15	18	6.51	320	68	47	206	24	5	376.9	64.4	0.112
	2.8	443	45	93	11	18	18	10.0	412	65	66	295	26	5	482.1	73.6	
	2.2	333	43	76	13	16	20	9.22	316	67	55	235	21	5	435.3	61.8	0.161
	2.6	410	45	83	14	18	16	8.09	364	58	53	236	21	5	460.2	77.8	0.117
	2.2	410	38	81	11	16	16	8.13	340	63	54	236	22	5	460.2	69.4	0.109
	3.8	365	34	80	12	15	16	7.94	348	57	49	211	22	3	453.8	69.8	0.149
	5.7	355	43	75	12	15	17	7.69	331	55	49	213	21	3	456.5	73.1	0.160
	3.5	398	43	81	14	18	18	8.46	362	62	54	232	22	4	457.7	74.0	0.105
	8.8	413	42	80	12	18	17	8.78	377	61	55	238	22	5	466.7	73.5	0.115
	2.6	346	38	96	11	17	21	8.82	314	71	57	239	23	5	474.5	59.1	
	2.3	411	48	90	12	17	17	8.91	363	63	57	242	22	6	515.7	65.7	0.207
	2.3	357	49	86	10	17	19	8.37	304	65	60	243	21	5	535.8	67.9	0.142
	1.5	354	59	82	11	17	19	7.99	307	68	52	237	21	6	480.2	64.2	0.115
	7.2	401	42	93	15	17	17	8.73	382	66	54	236	23	5	448	53.9	0.119
	3.8	395	41	92	14	17	17	9.56	367	61	59	258	21	4	568.9	64.2	0.116
	2.8	350	50	84	13	17	17	8.82	336	64	52	237	20	5	470.9	68.2	0.151
	1.8	356	52	85	17	18	17	8.97	345	69	54	239	21	5	501.8	60	0.115
	2.7	322	38	73	9		17	7.06	297	60	51	190	14	4	473.1	62	0.103
	2.5	357	40	79	10	12	18	7.7	316	65	56	235	16	5	511	63.9	0.107
	4	368	54	90	13	17	21	9.84	366	78	58	266	23	6	524.1	74.1	0.183
	2.6	400	48	80	13	18	21	10	365	78	58	268	25	6	483.3	86.3	0.106
	1.2	350	41	83	12	17	20	8.53	325	65	56	235	22	5	497.1	76.5	0.122
	1.5	368	41	80	12	18	19	8.57	333	68	56	232	24	6	486.8	67	0.109
	2.3	348	46	96	11	17	22	8.55	344	68	54	278	22	6	491.5	63.6	0.127
	2	335	38	89	11	17	20	8.49	332	63	54	277	21	5	477.1	63.1	0.095
	2.3	401	56	87	13	16	20	7.47	334	66	57	256	23	6	449.7	58	0.137
	1.6	378	57	67	13	15	19	6.49	309	64	48	213	21	6	438	58.2	0.097
	4.3	351	59	83	12	18	20	7.84	316	75	59	252	22	5	484.3	88.9	0.129
	2.8	346	51	82	12	18	20	8.72	317	75	59	261	21	6	510.4	76.4	0.118
	2.3	399	46	78	14	17	22	9.44	353	71	64	312	24	6	526.9	76.9	0.108
	3.2	420	49	85	13	17	20	8.78	349	69	58	290	24	6	488.9	75	0.125
	2.4	353	37	71	12	17	21	8.51	331	72	54	229	23	6	413.2	69.8	0.105
	2.3	353	42	76	11	15	20	8.76	315	65	55	235	21	5	466.3	72.1	0.112
	4.9	355	45	81	12	18	22	9.98	357	78	60	272	24		420.4	72.2	0.122
	2.3	365	58	77	15	19	22	9.54	368	80	57	252	23		444.2	71.2	0.127
	2.7	404	41	88	14	18	17	9.20	381	70	58	255	25	6	458.8	71.6	0.149
	5.4	379	58	78	13	17	16	7.98	351	67	53	222	22	6	456.6	85.8	0.117
Mean	3.142	373.635	46.187	80.933	12.267	16.264	18.493	8.546	338.067	68.120	54.600	238.747	22.027	5.288	472.887	68.548	0.128
SD	1.483	30.562	6.935	7.892	1.622	1.520	2.350	0.754	25.429	6.335	4.466	21.503	1.889	0.697	36.487	8.614	0.028
CV	47.200	8.180	15.016	9.751	13.222	9.344	12.709	8.825	7.522	9.300	8.180	9.007	8.574	13.176	7.716	12.567	21.845

Table 6. Control standard PE. Values below detection set to 2/3 detection limit prior to calculation of the mean, standard deviation and coefficient of variation.

PE	Ag	Cu	Pb	Zn	Mo	Ni	Co	Fe	Mn	Ba	Cr	V	Sr	Li	As	Sb	Hg
	1.7	998	45	135	7	24	28	>10	395	63	61	231	4	4	1473.6	7.3	0.193
	2.2	1035	56	144	7	24	30	>10	415	64	64	239	4	5	1462.3	6.5	0.192
	1.3	1048	48	135	7	24	30	>10	413	65	62	236	4	4	1422	7.5	0.204
	1.5	1003	49	143	6	23	29	>10	392	63	61	235	4	4	1395.6	6.6	0.155
	1.3	1045	43	128	7	24	30	>10	403	67	63	238	4	5	1513.9	6.3	0.166
	0.133	1001	129	143	9	24	29	>10	382	64	64	241	4	4	1518.3	9.2	0.144
	2.1	1125	56	134	8	28	27	>10	405	50	62	217	5	5	1454.7	11.3	0.121
	2.4	1123	29	150	8	27	28	>10	435	52	64	217	6	5	1390.4	7.6	0.163
	0.7	1083	44	144	8	28	28	>10	440	53	63	213	6	5	1469.2	7.5	0.154
	2.4	1337	44	169	6	28	28	>10	440	51	62	227	6	5	1490.6	5.6	0.111
	1.7	1289	87	180			31	>10	393	53	72	248	1	3	1590.6	5.8	0.147
	0.4	1098	50	164	7	33	32	>10	454	69	76	263	6	5	1488.9	5.5	0.152
	1.6	921	56	145	6	26	30	>10	373	57	65	234	5	5	1374.5	6.5	
	1.3	1081	52	164	8		32	>10	398	61	58	240	6	5	1447.9	7.4	0.120
	2	985	43	141	5	27	25	>10	378	56	62	225	4	5	1425	9	0.176
	1.5	1024	48	138	5	28	23	>10	386	55	58	231	5	4	1583.9	4.6	0.187
	1.4	943	60	155	8	31	38	>10	383	66	69	251	6	5	1600	5.7	0.158
	1.9	1266	59	157	7	28	27	>10	444	50	66	235	5	4	1467.2	6.8	0.122
	1.8	918	42	119	5	24	28	9.68	365	53	56	211	5	4	1409.4	8.8	0.148
	1.7	867	47	130	6	26	33	>10	382	54	60	235	5	4	1492.5	10.1	0.111
	0.5	1035	61	141	5	26	35	>10	422	64	68	238	6	5	1445	7.4	
	1.3	1017	53	125	5	29	36	>10	440	67	74	246	7	5	1485.6	6.9	0.198
	1.4	1092	35	135	5	26	28	>10	377	55	56	220	5	4	1417.7	9.9	0.162
	1.8	1141	51	174	8	30	29	>10	463	54	69	246	6	5	1460.1	9.2	0.124
	1.4	1036	62	141	8	25	31	>10	397	66	72	243	4	5	1460.7	8.2	0.135
	1.3	1116	39	139	7	31	37	>10	467	73	73	258	6	6	1225.0	8.6	0.121
	1.3	1252	52	186	8	29	30	>10	471	50	71	264	6	5	1495.2	7.8	0.184
	1.4	1136	39	161	7	29	28	>10	465	54	67	241	5	5	1372.1	11	0.121
	1.8	1129	45	160	7	28	28	>10	450	51	68	250	5	4	1537.7	10.5	0.128
	2.7	1189	57	163	6	27	27	9.96	422	51	63	230	5	4	1553.9	7.9	0.169
	2.1	1274	52	173	9	30	31	>10	541	62	68	245	6	4	1323.6	9.3	0.125
	2.6	1153	33	154	8	27	27	>10	455	51	64	227	5	4	1279.6	8.3	0.154
	1.8	1199	48	179	7	29	29	>10	450	51	65	236	5	4	1488.2	7.9	0.164
	3.1	1160	42	171	7	30	29	>10	453	50	66	234	5	3	1429.6	8.8	
	1.8	1104	58	163	7	30	29	>10	420	54	67	237	6	5	1349.1	7.8	
	0.2	977	49	146	5	27	30	9.51	376	59	59	230	5	4	1541.2	11	0.171
	0.133	973	50	152	5	35	31	9.46	394	60	62	235	6	5	1338.5	8.8	0.136
	2.8	1161	47	163	8	28	28	>10	437	51	65	239	5	4	1477.4	10.7	0.144
	1.6	1175	42	154	10	29	28	>10	438	52	64	231	5	4	1502.0	11.2	0.080
	1.0	1005	58	134	8	29	28	>10	398	55	60	233	6	4	1571.2	13.3	0.152
	1.0	1008	41	143	8	30	30	>10	417	58	62	238	7	5	1547.1	6.5	0.119
	1.3	924	56	129	5	23	28	9.09	370	54	64	226	4	4	1503.8	7.5	0.135
	2.5	926	53	139	4	23	29	9.47	364	54	66	234	4	4	1632.4	7.8	0.121
	1.0	1119	56	158	7	29	34	>10	427	63	67	252	6	5	1642.6	8.2	0.141
	1.2	1139	54	153	6	30	33	>10	426	66	67	266	6	5	1511.3	9.1	0.146
	0.3	893	54	130	5	29	31	9.92	395	58	63	218	6	5	1589.2	13.2	0.147
	0.2	954	30	129	5	27	31	>10	366	53	60	220	6	5	1596.2	9.2	0.146
	1.2	947	49	154	7	29	32	>10	412	60	64	269	6	5	1357.4	7.1	0.169
	2.1	843	43	142	5	24	28	9.49	364	53	56	244	5	4	1523.4	7.2	0.105
	1.3	1132	55	141	6	26	30	8.71	404	55	63	246	6	5	1571.4	10.9	0.137
	1.2	967	63	151	5	24	28	7.96	357	48	58	216	5	5	1520.1	9.8	0.125
	1.5	981	49	136	6	31	34	>10	399	65	69	250	6	5	1581.4	9.5	0.131
	1.3	1024	48	151	6	30	30	9.96	391	62	67	244	5	5	1435.6	10	0.134
	1.2	1053	43	138	6	29	34	10	445	62	67	271	5	6	1368.6	10.9	0.145
	1.2	1021	53	171	5	27	33	9.97	435	56	67	273	5	5	1651	9.4	0.135
	1.6	1025	42	134	5	27	31	>10	368	56	66	247	6	5	1580.8	10.4	0.163
	0.6	995	48	136	6	32	36	>10	440	67	74	278	6	1	1485.6	9.3	0.228
	2.3	1174	73	166	10	29	29	>10	456	56	70	250	6	5	1324	10.2	0.160
Mean	1.484	1062.741	51.207	148.224	6.614	27.679	30.103		414.621	57.621	64.810	239.517	5.259	4.534	1476.307	8.557	0.148
SD	0.628	109.573	14.153	16.096	1.398	2.664	2.894		35.997	6.092	4.636	15.265	0.983	0.777	91.842	1.877	0.028
CV	45.986	10.310	27.639	10.859	21.143	9.623	9.613		8.682	10.573	7.153	6.373	18.700	17.140	6.221	21.930	18.696